

ABSTRACT

LIU, LU. Electrostatic Generation and Control on Textiles. (Under the direction of Dr. Abdel-Fattah M. Seyam and Dr. William Oxenham).

Static electricity has been a major problem for textile manufacturing as well as consumers, especially after the introduction of manmade fibers. Extensive research has been done in this field; however, there are still questions not answered, and drawbacks. For example, the accuracy of the measurement is questionable due to the manual transfer of samples to the measuring unit, the devices and procedures are complicated and the results are not reproducible.

The goal of this research was to gain a better understanding on the mechanism of static generation and dissipation and to find the effects of different parameters on electrostatic behavior of polymeric surfaces. To realize this goal, precise material handling/cleaning and testing procedures were developed and three automated devices for electrostatic measurement were used. The devices were a linear tester, a rubbing tester, and a contact tester. The description of the devices and the analysis of signal obtained are given in Chapter 4, 5, and 6. The charge generation and dissipation behaviors of different polymers were investigated and compared. The effects of different parameters, such as the rubbing speed, contact force, environmental conditions, and antistatic finishes, are analyzed, and suggestions are given to textile industries based on the studies.

In this dissertation, literatures are reviewed in Chapter 2. The objectives are given in Chapter 3. Chapters 4, 5, 6, and 7 were modified from four manuscripts, which had been submitted to journals. The overall conclusions and suggestions for future work are given in Chapter 8.

Chapter 4 discusses the electrification produced by running a yarn against a guide and it was found that charge could be effectively controlled by reducing the relative rubbing speed between two surfaces. For several applications in textile industry, it is suggested that rotating rollers would be better than fixed guides for electrostatic control.

Chapter 5 addresses research on rubbing electrification between finish free polymeric plates and stainless steel plate. It is shown that charge accumulates in repeating

rubbing and reaches the saturation after 2-3 cycles of rubbing PP and PTFE, while the charge reaches saturation after 40-50 cycles of rubbing nylon. This could be related to the difference of charge dissipation behavior of different polymers. The charge saturation is reached when the charge generation and dissipation are in balance. It is found that charge decays exponentially on nylon and the charge retained is about 60% or lower after 30 seconds, while, there is no decay on PP or PTFE during 30 seconds of observation.

Chapter 6 shows research on contact charging between polymeric plates. It is also shown that charge increases as the contact force increases. In addition, the tribo-electric series were found for nylon, stainless steel, PP, and PTFE by contact against each other.

Chapter 7 reports investigation in regards to contact charging and frictional charging on polymeric plates and yarns treated by antistatic finishes. It is found that ionic finish performs better than nonionic finish on both nylon and PP, and cationic finish works better than anionic finish due to difference in antistatic mechanism. From the observation of charge decay, it is found that there are two types of charge on nylon surface, which have different decay properties resulting from decay through air and spread on the surface.

In summary, systematic studies were conducted using newly developed automated devices, on finish free polymers and polymers with different antistatic finishes. From the experiments and analysis, the charge generation and dissipation on commonly used polymeric surfaces were better understood. Furthermore, suggestions were given to textile industry for reducing/eliminating static.

Electrostatic Generation And Control on Textiles

by
Lu Liu

A dissertation submitted to the Graduate Faculty of
North Carolina State University
in partial fulfillment of the
requirements of the Degree of
Doctor of Philosophy

Fiber and Polymer Science

Raleigh, North Carolina

2010

APPROVED BY:

Dr. Abdel-fattah Mohamed Seyam
Co-chair of Advisory Committee

Dr. William Oxenham
Co-chair of Advisory Committee

Dr. Thomas Theyson
Committee Member

Dr. Jacqueline Krim
Minor Representative

Dr. Kristin Thoney
Committee Member

DEDICATION

*Dedicated to my husband Li Yang
for his support and help in the whole process of my Ph.D. studying*

BIOGRAPHY

Lu Liu was born on July 13, 1983 in Hefei, China. She grew up in a family with a background of engineering and science. She received a Bachelor of Textile Engineering in 2005 from Dong Hua University in Shanghai, China. She joined the College of Textiles in North Carolina State University, in July 2005. She was awarded a Master of Textiles in 2008 and she is presently in the Ph.D. program of Fiber and Polymer Science.

ACKNOWLEDGEMENTS

The author wishes to express her appreciation to her advisors, Dr. Abdel-fattah Mohamed Seyam and Dr. William Oxenham, for the opportunity to work on this project and their guidance throughout the whole research. The author also wants to thank Dr. Thomas Theyson, who provided the materials for this research and gave extensive suggestions. The appreciation is extended to the other committee members, Dr. Jacqueline Krim and Dr. Kristin Thoney for their advice and help.

The author would like to thank Dr. Peter Castle of Western Ontario University, Canada, for his discussion and suggestions at the beginning period of this project. The author wants to thank Dr. Yiyun Cai of USDA for training on the use of equipments. The author also would like to thank Nguyen Dzung for help in modify and updating some devices. Additionally, the author extends her thanks to her partners and officemates, Vamsi Krishna Jasti, Tamer Hamouda, and Ahamed Hassanin for their support and help.

The author is also indebted to the National Textile Center for the financial support that enables the present research to be conducted.

TABLE OF CONTENTS

LIST OF TABLES	viii
LIST OF FIGURES	ix
1 INTRODUCTION.....	1
2 LITERATURE REVIEW.....	4
2.1 ELECTROSTATIC REGULATIONS.....	5
2.2 ELECTROSTATIC RELATED CHARACTERISTICS - RESISTIVITY AND CAPACITANCE.....	7
2.2.1 <i>Surface resistance/resistivity</i>	7
2.2.2 <i>Questions related to the resistivity of polymers</i>	10
2.2.3 <i>Capacitance</i>	14
2.3 MECHANISMS OF CHARGE GENERATION.....	15
2.3.1 <i>Contact charging</i>	15
2.3.2 <i>Frictional charging</i>	20
2.3.3 <i>Corona charging</i>	23
2.3.4 <i>Repeating contacts and separations</i>	23
2.3.5 <i>Ionic transfer mechanism</i>	26
2.3.6 <i>Bond-breaking mechanism</i>	27
2.4 MECHANISMS OF CHARGE DISSIPATION.....	29
2.4.1 <i>Charge decay of conductor</i>	29
2.4.2 <i>Charge decay of a non-conducting system</i>	31
2.4.3 <i>Charge decay through the air</i>	33
2.5 PREVIOUS EXPERIMENTAL STUDIES.....	35
2.5.1 <i>Sample preparation</i>	35
2.5.2 <i>Environmental chambers</i>	36
2.5.3 <i>Charge measurement on solids</i>	37
2.5.4 <i>Surface analysis</i>	39
2.5.5 <i>Effect of contact pressure</i>	39
2.5.6 <i>Effect of contact time</i>	42
2.5.7 <i>Effect of moisture</i>	42
2.5.8 <i>Effect of temperature</i>	45
2.5.9 <i>Effect of air pressure</i>	47
2.5.10 <i>Effect of rubbing speed</i>	48
2.5.11 <i>Effect of system shape</i>	51
2.5.12 <i>Effect of yarn blending</i>	52
2.5.13 <i>Effect of surface components and structure</i>	55
2.5.14 <i>Triboelectric series</i>	56
2.5.15 <i>Anti-static technology in textiles</i>	59
REFERENCES	61

3	OBJECTIVES	68
4	FRICTIONAL ELECTRIFICATION OF YARN AND PIN.....	72
4.1	INTRODUCTION	73
4.2	EXPERIMENTAL.....	75
4.2.1	<i>Equipment and test protocol.....</i>	75
4.2.2	<i>Materials and experimental designs</i>	77
4.3	CALCULATED RESPONSES	79
4.4	RESULTS AND ANALYSIS	81
4.4.1	<i>Experimental design-I.....</i>	81
4.4.2	<i>Experimental design-II.....</i>	93
4.5	CONCLUSION.....	98
	REFERENCES.....	98
5	FRICTIONAL ELECTRIFICATION OF POLYMERIC PLATES	101
5.1	INTRODUCTION	102
5.2	EXPERIMENTAL.....	104
5.2.1	<i>Charge generation/dissipation measurement device.....</i>	104
5.2.2	<i>Materials and experimental designs</i>	105
5.3	SIGNAL ANALYSIS	109
5.3.1	<i>Charge generation.....</i>	109
5.3.2	<i>Charge accumulation</i>	110
5.4	RESULTS AND DISCUSSION	112
5.4.1	<i>Experimental design I.....</i>	112
5.4.2	<i>Experimental design II.....</i>	119
5.4.3	<i>Experimental design III</i>	122
5.5	CONCLUSION.....	124
	REFERENCES.....	125
6	CONTACT ELECTRIFICATION OF POLYMERIC PLATES	127
6.1	INTRODUCTION.....	128
6.2	EXPERIMENTAL	129
6.2.1	<i>Contact device</i>	129
6.2.2	<i>Signal analysis.....</i>	131
6.2.3	<i>Sample preparation</i>	134
6.2.4	<i>Experimental design</i>	135
6.2.5	<i>Statistical analysis.....</i>	136
6.3	RESULTS	136
6.3.1	<i>Experimental design I.....</i>	136
6.3.2	<i>Experimental design II.....</i>	141
6.4	CONCLUSIONS.....	143
	REFERENCE	144

7 ELECTRIFICATION OF POLYMERIC SURFACES TREATED BY ANTISTATIC FINISHES	146
7.1 INTRODUCTION.....	147
7.2 EXPERIMENTAL	148
7.2.1 <i>Sample preparation</i>	148
7.2.2 <i>Experimental design</i>	150
7.3 RESULTS AND DISCUSSION.....	152
7.3.1 <i>Contact electrification</i>	152
7.3.2 <i>Rubbing electrification</i>	154
7.3.3 <i>Yarn rubbing electrification</i>	158
7.4 CONCLUSIONS.....	160
REFERENCES.....	161
8 OVERALL CONCLUSIONS	163

LIST OF TABLES

Table 1.1 Approximate value of charge potential generated in different situations (Welker, Nagarajan, & Newberg, 2006)	3
Table 2.1 ESD control requirements summary	5
Table 2.2 Classification of materials by their resistivity (unit: ohm)	9
Table 2.3 Dielectric constant of materials (Dielectric Constant Reference Guide)	15
Table 2.4 Work functions of polymers	19
Table 2.5 Order of magnitude of charge density observed on various materials after contact with metals..	20
Table 2.6 Penetration depths of charge from metal into polymers (Labadz & Lowell, 1986).....	25
Table 2.7 Indentation characteristics of polymers (Pascoe & Tabor, 1956)	41
Table 2.8 Effect of relative humidity on electrostatics	44
Table 2.9 Optimum fiber blend for staple yarn to minimize charge	53
Table 2.10 Intrinsic impurities for different structures (1980).....	55
Table 2.11 Fiber crystallinity (Morton & Hearle, 2008)	56
Table 2.12 Triboelectric series	57
Table 4.1 Experimental design-I	78
Table 4.2 Experimental design-II (D_{pin} : 25.4 mm, V_y : 100 m/min).....	79
Table 5.1 Experimental design I used to study the effect of contact force on static generation/dissipation of polymers after rubbing against stainless steel	108
Table 5.2 Experimental design II for studying the effect of rubbing speed on static behavior of polymers after rubbing against stainless steel	108
Table 5.3 Experimental design III for investigating static properties of polymers after rubbing against each other.....	108
Table 6.1 Experimental design I.....	135
Table 6.2 Experimental design II used to investigate the static generation of nylon, PP, stainless steel, and PTFE by contact against each other	136
Table 7.1 Components of model surface finishes.....	149
Table 7.2 Experimental design I.....	151
Table 7.3 Experimental design I.....	152

LIST OF FIGURES

Figure 2.1 Basic setup for surface resistivity measurement	8
Figure 2.2 Surface resistivity measurement configuration by concentric ring electrodes	9
Figure 2.3 Effect of relative humidity on resistance of yarn bundles made of different materials (temperature: 20°C) (Hearle, 1953).....	11
Figure 2.4 Effect of temperature on resistance of cotton yarn bundles (moisture contents were calculated by weighting dry samples and samples after conditioning under the testing relative humidity) (Hearle, 1953)	12
Figure 2.5 Effect of voltage on the resistance of cotton yarn bundles (moisture content: 6.8%, R_{100} : the resistance measured under 100 voltage) (Hearle, 1953).....	13
Figure 2.6 Charge transfer by making and breaking contacts (Taylor & Secker, 1994)	16
Figure 2.7 Charges recombine (left) and remain (right) (Taylor & Secker, 1994).....	16
Figure 2.8 Metal A and B of different work functions (b) Fermi level* of the two metals become equal after contact (Taylor & Secker, 1994)	17
Figure 2.9 Energy band for (a) intrinsic (b) n-type and (c) p-type semiconductor (Taylor & Secker, 1994) (E_c is energy level of conduction band, E_G is energy gap between the conduction band and the valence band, E_d is energy level of donors, E_F is the Fermi energy level, E_a is the every level of acceptors)	18
Figure 2.10 Asymmetric rubbing (Morton & Hearle, 2008)	22
Figure 2.11 Corona charging, V_a is applied potential and V_s is the surface potential (Taylor & Secker, 1994)	23
Figure 2.12 Charge backflow from insulator I to metal M (Lowell & Rose-Innes, 1980).....	28
Figure 2.13 Charge decay of a conductor characterized by its capacitance C and resistance R with respect to ground.....	30
Figure 2.14 Charge dissipation (Taylor & Secker, 1994).....	31
Figure 2.15 Charge decay of charged insulator resting on grounded plane.....	33
Figure 2.16 Charge decay of charge insulator resting on a grounded plane with a grounded plate placed parallel with the charged surface	33
Figure 2.17 Charged body in air with ions	34
Figure 2.18 Decay curves of charge on PET film (Ieda & Shinohara, 1967)	35
Figure 2.19 Diagram of apparatus for measurement of electrostatic charge	38
Figure 2.20 Deformation of OB hard elastic (diamond), OE soft elastic, and OI polymers (The full line represents the load-deformation curves (similar to stain-stress curve), and the dotted curves are pressure- area curves under constant loads. The intersection points indicate the equilibrium situation.).....	42
Figure 2.21 Effect of temperature on the amount of water in air ^(Wikipedia_Humidity)	47
Figure 2.22 Paschen curves obtained for Helium, Neon, Argon, Hydrogen and Nitrogen, using the expression for the beakdown voltage, V_B as a function of the parameters pd , where, p is the pressure (torr), d is the gap distance (cm) between two parallel paltes.....	48
Figure 2.23 Blends of nylon-Dacron polyester staple-charge developed against chrome-plated surface.....	54
Figure 2.24 Blends of nylon-Dacron polyester staple-charge developed against cotton	54
Figure 4.1 Linear Tester	77
Figure 4.2 Yarn/pin contact angle (same contact angle for pins of two sizes), $\theta=60^\circ$	77
Figure 4.3 Force diagram analysis on the yarn section contacted with pin when V_y was smaller than V_p (left) and when V_y was larger than V_p (right).....	80
Figure 4.4 Effect of yarn/pin relative rubbing speed on yarn surface potential measured by the probe-I (pin: stainless steel cylinder of 25.4 mm diameter, yarn: 420/72 nylon multifilament with anionic lubricant)....	82

Figure 4.5 Data of figure 4.4 corresponding to the speed of charge pin.....	82
Figure 4.6 Data of figure 4.4 corresponding to the speed of yarn	83
Figure 4.7 Effect of yarn/pin relative rubbing speed on yarn surface potential measured by the probe-II (pin: stainless steel cylinder of 25.4 mm diameter, yarn: 420/72 nylon multifilament with anionic lubricant)	83
Figure 4.8 Effect of yarn/pin relative rubbing speed on yarn output tension (pin: stainless steel cylinder of 25.4 mm diameter, yarn: 420/72 nylon multifilament with anionic lubricant).....	84
Figure 4.9 Effect of yarn/pin relative rubbing speed on contact force on yarn (pin: stainless steel cylinder of 25.4 mm diameter, yarn: 420/72 nylon multifilament with anionic lubricant).....	85
Figure 4.10 Effect of yarn/pin relative rubbing speed on friction force on yarn (pin: stainless steel cylinder of 25.4 mm diameter, yarn: 420/72 nylon multifilament with anionic lubricant).....	85
Figure 4.11 Effect of yarn/pin relative rubbing speed on yarn/pin coefficient of friction (pin: stainless steel cylinder of 25.4 mm diameter, yarn: 420/72 nylon multifilament with anionic lubricant).....	86
Figure 4.12 Correlation between yarn potential-I and yarn/pin friction force (pin: stainless steel cylinder of 25.4 mm diameter, yarn: 420/72 nylon multifilament with anionic lubricant).....	86
Figure 4.13 Pin vibration amplitude measured at different rotating frequency (pin: stainless steel cylinder of 25.4 mm diameter, yarn: 420/72 nylon multifilament with anionic lubricant).....	87
Figure 4.14 Vibration force calculated at different yarn/pin speeds (pin: stainless steel cylinder of 25.4 mm diameter, yarn: 420/72 nylon multifilament with anionic lubricant).....	88
Figure 4.15 Effect of yarn/pin relative rubbing speed on yarn surface potential measured by the probe-I (pin: stainless steel cylinder of 6.35 mm diameter, yarn: 420/72 nylon multifilament with anionic lubricant)	89
Figure 4.16 Effect of yarn/pin relative rubbing speed on yarn surface potential measured by the probe-II (pin: stainless steel cylinder of 6.35 mm diameter, yarn: 420/72 nylon multifilament with anionic lubricant)	89
Figure 4.17 Effect of probe-I to pin spacing (the spacing from the aperture of probe-I to the yarn/pin separation point) on measured yarn potential (the position of probe-II was fixed) (yarn: nylon with lubricant, pin: stainless steel cylinder of 25.4 mm diameter; $V_y = 100$ m/min, $V_p = 0$, input tension=50 cN)	90
Figure 4.18 Effect of yarn/pin relative rubbing speed on yarn output tension (pin: stainless steel cylinder of 6.35 mm diameter, yarn: 420/72 nylon multifilament with anionic lubricant).....	91
Figure 4.19. Effect of yarn/pin relative rubbing speed on yarn/pin contact force (pin: stainless steel cylinder of 6.35 mm diameter, yarn: 420/72 nylon multifilament with anionic lubricant).....	92
Figure 4.20 Effect of yarn/pin relative rubbing speed on yarn/pin friction force (pin: stainless steel cylinder of 6.35 mm diameter, yarn: 420/72 nylon multifilament with anionic lubricant).....	92
Figure 4.21 Effect of yarn/pin relative rubbing speed on yarn/pin coefficient of friction (pin: stainless steel cylinder of 6.35 mm diameter, yarn: 420/72 nylon multifilament with anionic lubricant).....	93
Figure 4.22 Effect of yarn/pin relative rubbing speed on finish free yarns' surface charge potential measured by the first probe (pin: stainless steel cylinder of 25.4mm diameter).....	94
Figure 4.23 Effect of yarn/pin relative rubbing speed on finish free yarns' surface charge potential measured by the second probe (pin: stainless steel cylinder of 25.4mm diameter).....	95
Figure 4.24 Effect of yarn/pin relative rubbing speed on yarn output tension (pin: stainless steel cylinder of 25.4mm diameter)	95
Figure 4.25 Effect of yarn/pin relative rubbing speed on yarn/pin contact force (pin: stainless steel cylinder of 25.4mm diameter)	96
Figure 4.26 Effect of yarn/pin relative rubbing speed on yarn/pin friction force (pin: stainless steel cylinder of 25.4mm diameter)	96

Figure 4.27 Effect of yarn/pin relative rubbing speed on yarn/pin coefficient of friction (pin: stainless steel cylinder of 25.4mm diameter)	97
Figure 4.28 . Charge potential-I on finish free yarns corresponding to the yarn/pin friction force	97
Figure 5.1 Rubbing tester	105
Figure 5.2 Charge potential on nylon in terms of time and locations of potential probe, rubbing head, and rubbing area at starting point (t = 0) and at reversing point (t = 1.2 second) in the first cycle	110
Figure 5.3 Charge accumulations in 50 cycles and charge decay on nylon surface	111
Figure 5.4 Charge accumulations in 50 cycles and charge decay on PTFE surface	112
Figure 5.5 Charge accumulations in 50 cycles and charge decay on PP surface	112
Figure 5.6 Effect of contact force on charge generated on polymer surfaces after the first cycle of rubbing against stainless steel (rubbing speed: 27 mm/sec)	114
Figure 5.7 Effect of contact force on charge accumulated on polymer surfaces after 50 cycles of rubbing/contact against stainless steel (rubbing speed: 27 mm/sec).....	114
Figure 5.8 Effect of contact force on charge retained on polymer surfaces after 30 seconds of decay time	115
Figure 5.9 Effect of contact force on normalized charge retained on polymer surfaces after 30 seconds of decay time.....	115
Figure 5.10 Charge potential of the first and second cycles of rubbing (contact force: 1N, rubbing speed: 47 mm/sec)	116
Figure 5.11 Exponential behavior of charge decay of nylon	117
Figure 5.12 Charge decay model of a charged polymeric rubbing plate	118
Figure 5.13 Effect of rubbing speed on charge generated on polymeric surface after the first cycle of rubbing or the first contact/separation against stainless steel	120
Figure 5.14 Effect of rubbing speed on charge generated on polymeric surface after 50 cycles of rubbing (99 strokes) or 99 contacts/separations against stainless steel.....	120
Figure 5.15 Effect of rubbing speed on charge retained on polymeric surfaces after 30 seconds of decay	121
Figure 5.16 Effect of rubbing speed on normalized charge retained on polymeric surfaces after 30 seconds of decay	121
Figure 5.17 Triboelectric series of nylon, stainless steel, PP, and PTFE.....	122
Figure 5.18 Charge potential on rubbing plate after the first cycle of rubbing against the rubbing head (rubbing speed: 47 mm/sec, contact force: 1N).....	123
Figure 5.19 Charge potential on rubbing plate after 50 cycles of rubbing against the rubbing head (rubbing speed: 47 mm/sec, contact force: 1N).....	124
Figure 6.1 A Diagram of the contact charge generation/dissipation measurement device	130
Figure 6.2 Image of the contact device.....	130
Figure 6.3 Typical static charge data of repeated contact test	131
Figure 6.4 Electrostatic charges of 50 cycles of contact.....	133
Figure 6.5 Experimental data of Figure 6.4 and derived exponential regression relationship of charge generated in terms of cycle number.....	133
Figure 6.6 Images and dimensions of contact heads	135
Figure 6.7 Charge generated on PTFE after the first contact against nylon	137
Figure 6.8 Charge generated on PTFE after 50 cycles of contacts against nylon.....	138
Figure 6.9 Charge generated on PTFE after 100 cycles of contacts against nylon.....	138
Figure 6.10 Charge generated on PTFE after 120 cycles of contacts against nylon.....	139
Figure 6.11 Charge generated on PTFE by repeated contacts/separations against nylon, at different contact force (temperature of 30°C and R. H. of 30%).....	139
Figure 6.12 Data of Figure 6.9 sorted by the relative humidity.....	140

Figure 6.13 Data of Figure 6.9 sorted by the temperature	140
Figure 6.14 Charge generated on PP after 50 cycles of contacts against nylon, stainless steel, and PTFE	142
Figure 6.15 Charge generated on PTFE after 50 cycles of contacts against nylon, stainless steel, and PP	143
Figure 7.1 Schematic of surface treatment by an air brush.....	150
Figure 7.2 Charge generated on PP after the first contact against stainless steel	153
Figure 7.3 Charge generated on PP after 50 contacts/separations against stainless steel	153
Figure 7.4 Surface charge potential of nylon after the first cycle and 50 cycles of rubbing against stainless steel.....	154
Figure 7.5 Experimental data of charge decay of blank nylon and nylon treated by nonionic finish after 50 cycles of rubbing against stainless steel and regression curves	156
Figure 7.6 Experimental data of charge decay on blank nylon and the regression curves	156
Figure 7.7 Experimental data of charge decay on nylon treated by 0.025% nonionic solution and the regression curves	157
Figure 7.8 Experimental data of charge decay on nylon treated by 0.05% nonionic solution and the regression curves	157
Figure 7.9 Surface charge potential of nylon yarns by moving over a chrome pin (surface concentration of active finish: 7 mg/m ² , nylon yarns: 200 denier/60 filaments, yarn speed: 300 m/min, yarn input tension: 20 gf, charging pin size: 2 cm in diameter, contact angle: 90°) (Goulston Technologies, Inc.).....	159

1 INTRODUCTION

Static charge has positive and negative attributes. On one hand, it is useful in electrets filters and the formation of textiles structures such as electro-spinning and flocking. On the other hand, it has negative impacts on processes and products. For example, charge accumulation during the processing of yarns, fabrics, or films may cause irregularity of textiles and low efficiency of manufacturing. Major issues to end users are related to static generation and discharge such as clinging of clothes and discomfort from static shock when walking on a carpet and touching a doorknob. More seriously, potential life threatening accidents may take place because of static generation and discharge such as initiation of major fires at gas stations and failure of a parachute to open. Table 1.1 shows the approximate levels of charge potential generated in different situations.

To minimize the impact of static electrification, it is necessary to obtain a better understanding of the mechanisms involved in static generation and dissipation. Electrostatic charge is generated by contact and separating two different surfaces (contact charging). When two different surfaces were contacted, charge would transfer from surface of high Fermi level to surface of low Fermi level. When the two surfaces are separated, the transferred charge would be recombined (metals contact/separation) or be trapped on the surface (insulators contact/separation), which is determined by the static properties of contacted surfaces. Charge generated by rubbing two surfaces (frictional charging) is more severe than the contact charging, which is more complex. It could be affected by the rubbing speed and local temperature of the surface. The mechanisms of electrostatics will be reviewed in section 2.3 and 2.4.

To eliminate the static generation, there have been different approaches, such as, applying antistatic surface finish, incorporating conductive fibers, increasing the relative humidity, using ionizing gas gun, and it is always suggested to ground the working table and machines. However, the difficulties are that, polymeric surfaces are hard to control, which are irregular, not 100% crystal, and usually have contaminations. The electrostatic properties of polymers can be very different when the surface is contaminated or just been touched. Therefore, a very careful and consistent handling process is required for electrostatic studies. In addition, very precise static detecting methods are required. Electrostatic charge has to be monitored in time and without touching, otherwise, the

reading would be very different. Extensive research has been done in this field, which is reviewed in section 2.5. However, there are still questions, and drawbacks. For example, the accuracy of the measurement is questionable due to manual transfer of sample to the measuring unit, the devices and procedures are complicated and the results are not producible. Therefore, a more critical study is required on the electrostatics in textiles.

Table 1.1 Approximate value of charge potential generated in different situations (Welker, Nagarajan, & Newberg, 2006)

Activity	Charge Generation (kV) at	
	20% R.H.	80% R.H.
Walking across vinyl floor	12	0.25
Walking across synthetic carpet	35	1.5
Arising from foam cushion	18	1.5
Picking up polyethylene bag	20	0.6
Sliding styrene box on carpet	18	1.5
Moving the Mylar [®] tape (PET) from PC board	12	1.5
Shrinkable film on PC board	16	3
Triggering vacuum solder remover	8	1
Aerosol circuit freeze spray	15	5

2 LITERATURE REVIEW

2.1 Electrostatic regulations

Worldwide, there are almost one hundred standards and testing methods associated with static generation and dissipation (1999). They are published by institutes such as:

- U.S. Military Department of Defense (DOD)
- American Society for Testing and Materials (ASTM)
- National Fire Protection Association (NFPA)
- Joint Electron Device Engineering Council (JEDEC)
- International Electro technical Commission (IEC)
- American National Standards Institute (ANSI)
- Institute of Electrical and Electronics Engineers (IEEE)
- Electronic Industries Alliance (EIA)
- ESD Association (ESDA)

Generally, the electrical resistance of an item is used alone or combined with the charge potential generated on the item to evaluate its electrostatic properties, though it is still questionable whether the resistance is necessarily correlated with the static generation or dissipation (Owen, 1990). Table 2.1 shows static control levels (as inferred from resistance) recommended by several standards. The testing methods are described in detail inside the standard.

Table 2.1 ESD control requirements summary

ESD Control Item	Recommended Range	Standard
Work surface	$<1 \times 10^9$ ohm and/or <200 Volts	ESD S 4.1
Wrist Strap Cord	0.8×10^6 to 1.2×10^6 ohm	ESD S 1.1
Footwear	$<1 \times 10^9$ ohm	ESD S 9.1
Flooring	$<1 \times 10^9$ ohm	ANSI ESD S 7.1
Seating	$<1 \times 10^9$ ohm	ESD STM 12.1

The charge potential generated on an item is also used for qualifying its electrostatic properties. For example, the Military Standard 883 classifies items as follows using the standard 100 pF, 1.5 K Ω human body model:

- Class 1: > 0 to ≤ 1999 V
- Class 2: > 2000 to ≤ 3999 V
- Class 3: > 4000 V and above

In industry, to evaluate whether a work area is safe from potential static hazards, the working areas are classified into three different levels characterized by the discharge time and the charge potential (Welker, Nagarajan, & Newberg, 2006):

- For critical ESD (electrostatic discharge) safe work areas, the float potential should be less than ± 20 V and the discharge time should be less than 20 seconds from ± 1000 V to less than ± 20 V.
- For highly sensitive but not critical ESD-safe work areas, the float potential should be less than ± 50 V and the discharge time should be less than 20 seconds from ± 1000 V to less than ± 50 V.
- For conventional ESD-safe work areas, the float potential should be less than ± 100 V, and the discharge time can be less than 45 seconds from ± 1000 V to less than ± 100 V.

In all the standards and testing methods, the sample conditioning and cleaning are emphasized, since static properties are dramatically sensitive to the surface conditions. The sample has to be stored in uncontaminated environment under constant ambient conditions (temperature and relative humidity). Even contact to another surface during a test can alter a surface and give non-reproducible results in subsequent tests. Additionally, it is stated in the ASTM D 4470-97, Standard Test Method for Static Electrification, that "Cleaning" of a surface with solvents rarely cleans the surface. It probably produces a uniform, reproducible, state of contamination, however. Thus, cleaning with solvents should be considered as a means of obtaining reproducibility in a test.

Charge generation varies widely with the moisture content of a material. The conditioning time required depends on the rate of adsorption of moisture and the thickness (or mass) of the specimen. Thick sheets, for example, it takes a much longer time to condition than thin films. For another example, materials with high affinity (or absorptive capacity) for water take longer to condition than those with low affinity. Since there is a hysteresis effect on conditioning of many materials, the moisture content of a specimen also depends on whether the material was wetter or dryer than the conditions of the test. It is required by ATMS 4470-97 that the specimens should be dryer than the specified test condition before conditioning and the specimens should be equally conditioned for at least 24 hours at the specified relative humidity before testing. Additionally, not only it is important to condition specimens properly at the required relative humidities prior to the test, but the test should also be conducted in the same conditioning environment.

Practical considerations favor conditioning in the following two environments: (1) preferably $20\pm 2\%$ relative humidity, $23\pm 2^\circ\text{C}$, (2) preferably $50\pm 2\%$ relative humidity, $23\pm 2^\circ\text{C}$. Other relative humidity may be adopted depending on specific end-use requirements. However, the relative humidity, temperatures, and the conditioning time are required to clearly state in the test results.

2.2 Electrostatic related characteristics - resistivity and capacitance

The resistivity and capacitance are important electrical characterizations of materials. Their definitions, testing methods, and how they are affected by other factors, like the relative humidity and temperature, are reviewed in this part.

2.2.1 Surface resistance/resistivity

The surface resistance is the resistance to the flow of electrical current across a surface, while the volume (bulk) resistance is the resistance to flow through the three-dimensional volume of a sample. Since static is considered to primarily be a surface phenomenon,

which is mostly determined by surface properties of materials, thus the surface resistance, instead of the volume resistance, is usually more important in studies of electrostatic.

Concepts of surface resistance and surface resistivity can be sometimes confusing. Definitions of both terms can be found in many book and standards. Surface resistance, R_s , is defined as the ratio of a DC voltage U to the current, I_s flowing between two electrodes of specified configuration (Figure 2.1) that are in contact with the same side of a material. The surface resistivity, ρ_s is determined by the ratio of DC voltage U drop per unit length L to the surface current I_s per unit width D (equation [1-1]). The surface resistivity is the intrinsic property of a surface, which is not affected by the measured surface area. The physical unit of surface resistivity is also ohm (Ω). In order to differentiate from the volume resistivity, the surface resistivity is expressed also in ohm/square (Ω/square).

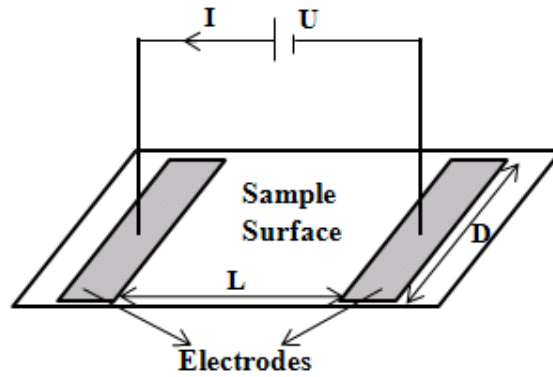


Figure 2.1 Basic setup for surface resistivity measurement

$$\rho_s = \frac{U/L}{I_s/D} \quad [1-1]$$

The testing method for measuring the surface resistivity using concentric ring electrodes is recommended in standards (AATCC 76, ASTM D257, IEC 93-IEC 60093 and JIS K6911). The sketch of equipment used by this method is shown in Figure 2.2. The inner top electrode is circular while the outer top electrode is annular. The sample area between the inner and outer electrodes is measured when voltage applied between

the electrodes. The electrical current flows from the inner electrode to the outer electrode through the sample surface.

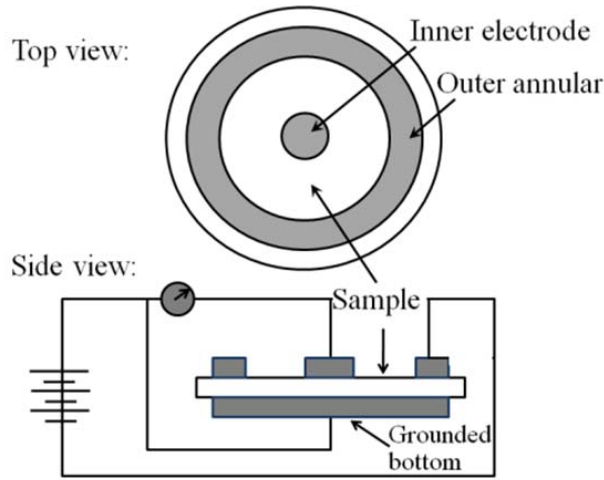


Figure 2.2 Surface resistivity measurement configuration by concentric ring electrodes

The resistance was used by standards to evaluate static properties of items as shown in Table 2.1. Furthermore, the surface resistivity and the linear resistivity (volume resistance per unit length, ohm/m) are often used to classify materials of isolative, antistatic, static dissipative, conductive, etc, as shown in Table 2.2. The term “static dissipative” is not synonymous with the term “antistatic”. The "static dissipative material" defines material on which charge can decay quickly, while the material's charge generation ability is not concerned. On the other hand, the "antistatic material" represents material that resists charging and produces minimal static charge generation.

Table 2.2 Classification of materials by their resistivity (unit: ohm)

Classification	ESDA Standards	Typical Vendor	Kanarek & Tan (1998)
Isolative	ND ¹	ND	ND
Antistatic	ND	10^{10} - 10^{14} Ω /sq	ND
Static dissipative	10^2 - 10^9 Ω /m 10^5 - 10^{12} Ω /sq	10^2 - 10^8 Ω /sq	10^5 - 10^{12} Ω /m 10^5 - 10^{12} Ω /sq
Resistive	ND	ND	ND
Conductive	$<10^2$ Ω /m	ND	$<10^2$ Ω /m

	$<10^5 \Omega/\text{sq}$		$<10^5 \Omega/\text{sq}$
Electrostatic shielding	ND	ND	$<10 \Omega/\text{m}$
EMI shielding	ND	$10^{-2} - 1.0 \Omega/\text{sq}$	ND

[†] ND: not defined

Besides the resistivity of materials, the conductivity is sometimes used to describe material electrical properties, which is the reciprocal of surface resistivity.

2.2.2 Questions related to the resistivity of polymers

There are mainly three questions raised from the literature review of surface resistivity of polymers.

- 1) Does the volume resistivity affect the surface resistivity?

Using the standard surface resistivity testing method, the electrical current will flow mostly along the surface, thus the surface conducting mechanism was dominant. However, the measurement of surface resistivity is affected by the volume resistivity (Taylor & Secker, 1994). For example, the charge conduction of fibers depends on the contacts between fibers surface as well as the fibers bulk, which is hard to separate.

- 2) Are the effects of different factors on the resistivity of polymers the same as that on the resistivity of conductors?

The resistivity of conductors has been well understood, for example, the resistivity of metals decreased as the temperature increased. However, the effects of different factors on the resistivity of polymers are not always the same as that for conductors. It is pointed out in the ASTM D257 that the resistance of insulators decreases both with increasing temperature and with increasing humidity. In addition, for polymers, the volume resistance is particularly sensitive to temperature changes, while surface resistance changes greatly and very rapidly with humidity changes.

Hearle (1953) tested the resistance of yarn bundles under different conditions, where the yarns were wound on a polythene film, and the two electrodes were set at two ends of the film. The study included the effect of different parameters on resistivity.

a) The effect of relative humidity

Testing environments of different levels of relative humidity were realized using saturated solutions of different salts inside testing jars. The results are shown in Figure 2.3, which indicates that the resistance of yarn bundles decreases as the relative humidity increases. This effect was explained as that the movement of ions and the dissociation are varying with the moisture content (Hearle, 1953).

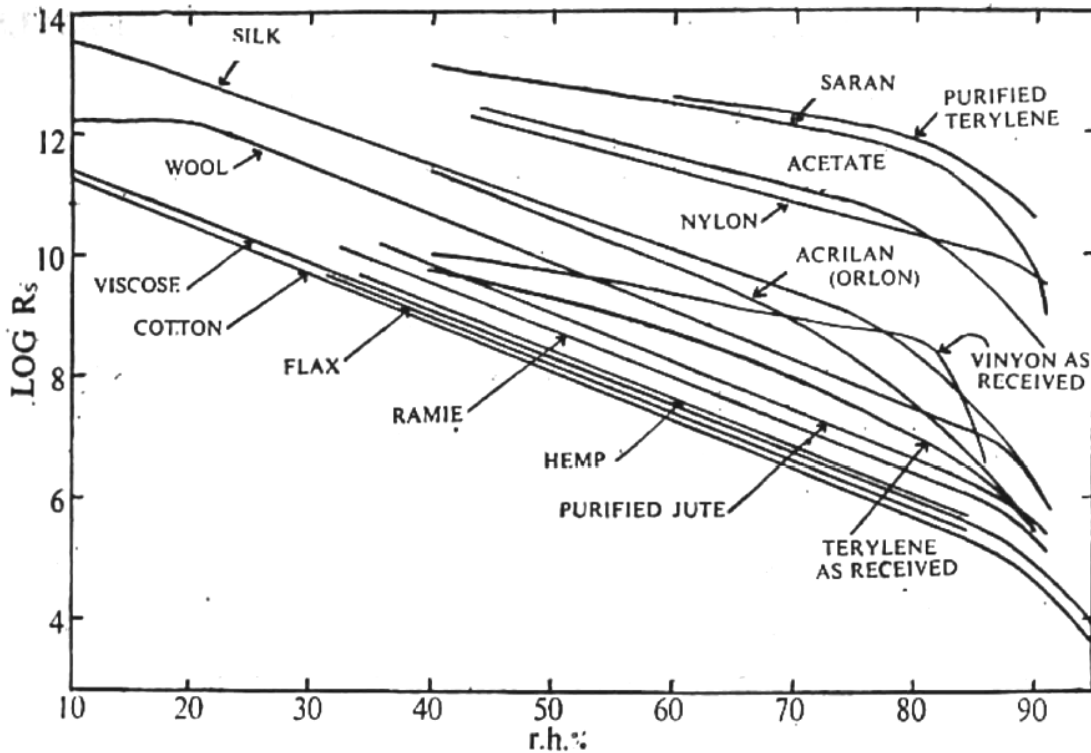


Figure 2.3 Effect of relative humidity on resistance of yarn bundles made of different materials (temperature: 20°C) (Hearle, 1953)

b) The effect of temperature

Experiments showed that, at each level of relative humidity, the resistance of cotton, silk, acetate rayon and wool yarn bundles all decreased as the temperature increased. Figure 2.4 shows the effect of temperature on resistances of cotton yarn bundles.

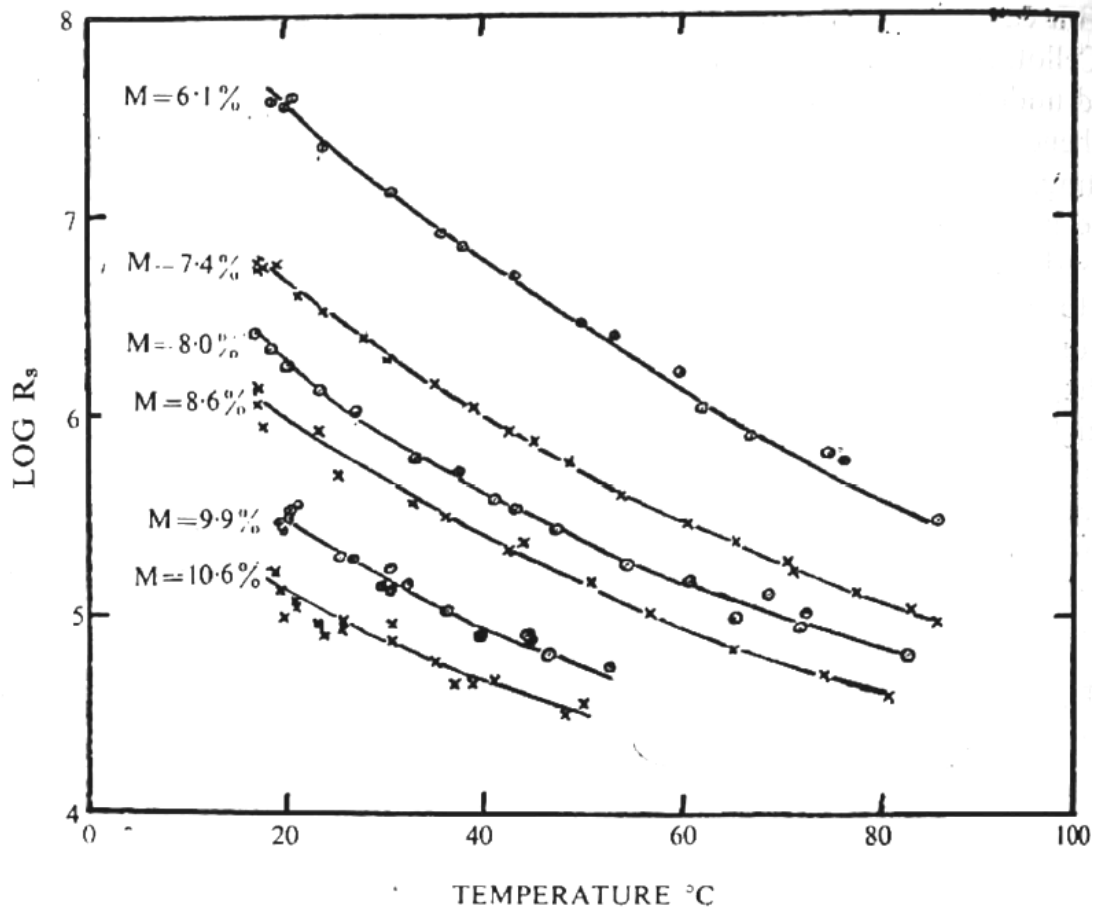


Figure 2.4 Effect of temperature on resistance of cotton yarn bundles (moisture contents were calculated by weighting dry samples and samples after conditioning under the testing relative humidity) (Hearle, 1953)

c) The effect of voltage

Experiments showed that, at low voltages, the resistance falls rapidly as the voltage increases, but the decrease in resistance became leveled at higher voltages, though there is still a slight trend of decrease from 50 to 400 Volts. Figure 2.5 shows the effect of voltage on cotton yarn bundles.

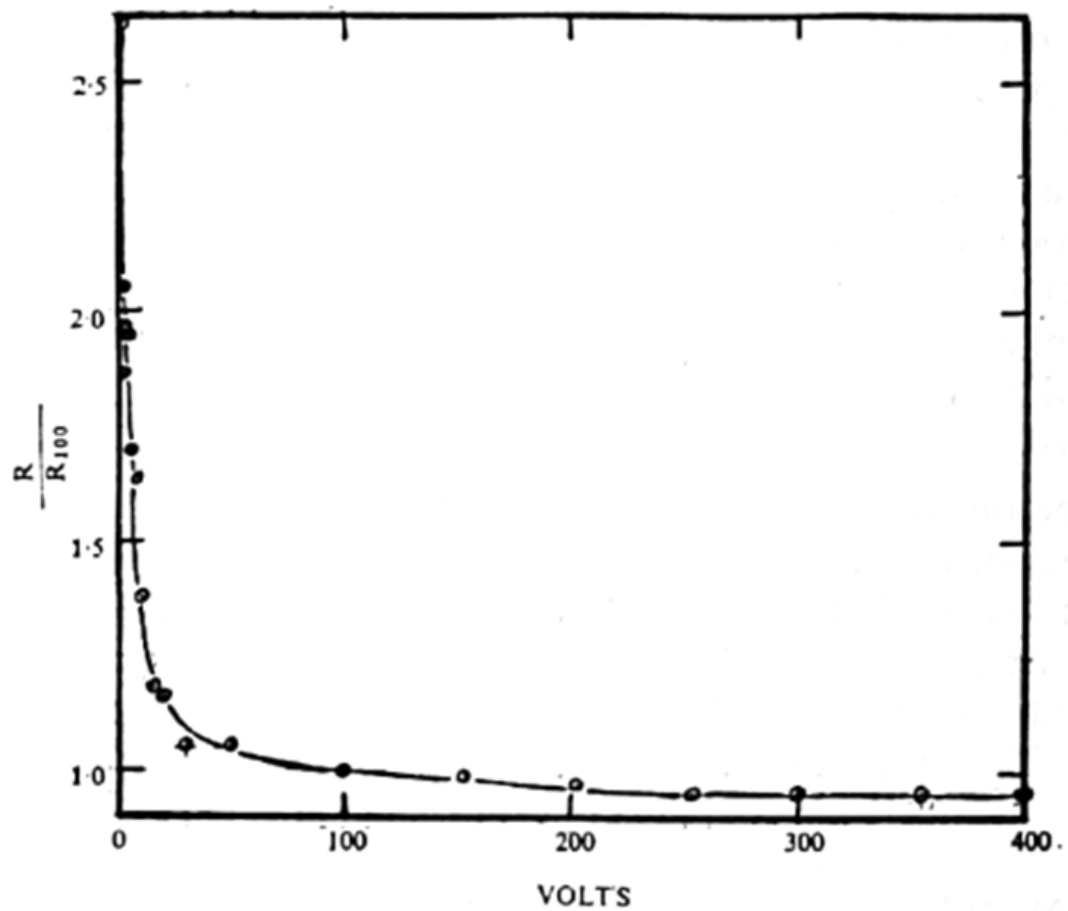


Figure 2.5 Effect of voltage on the resistance of cotton yarn bundles (moisture content: 6.8%, R_{100} : the resistance measured under 100 voltage) (Hearle, 1953)

d) The effect of the tension on the specimen

The effect of tension on the yarn resistance was investigated by hanging weights on two ends of the yarn bundles. For cotton, there was a tendency for the resistance to increase as the tension is increased, but for viscose rayon filament, the resistance decreases as the tension is increased. In both case, the change was very small.

3) Is surface resistivity a parameter of importance?

It is questionable that the surface resistivity may not necessarily correlate with the static phenomenon of the surface (Owen, 1990) and this need to be verified by further investigations.

On one hand, the mechanism of charge generation indicates that the amount of charge generated is determined by the difference of Fermi energy level of two contacted surfaces. There is no indication that surface resistivity is directly correlated to the charge generation. On the other hand, it is commonly considered that the charge decay would be affected by the surface resistivity, since the definition of surface resistivity is the resistance to the flow of electrical current across a surface. However, when the surface is not put between two electrodes, which is the setup of surface resistivity measurement, then the charge dissipation may be determined by the dielectric constant and the resistivity of the surrounding items, such as the atmosphere air and solids close to the surface (Niels, 1998).

2.2.3 Capacitance

The capacitance quantifies the ability of a system to store charge (Cardona, 2001). Its unit is Faraday, which is one coulomb per volt. If a charge is transferred from one surface to another, it produces a potential difference between them, then the capacitance of the system C can be given by equation [1-2]. For a parallel-plates capacitor, if the potential of the lower plate is zero, the system's capacitance can be given by equation [1-3].

$$C = q/V \quad [1-2]$$

$$C = \varepsilon \varepsilon_0 A/d \quad [1-3]$$

where q is the charge (Coulomb), C is the system capacitance (Faraday), V is the potential (Volt), ε_0 is the vacuum permittivity, ε is the media permittivity (relative dielectric constant), A is the surface area of the plates (m^2), d is the plates' separation (m) between plates.

The relative dielectric constant (relative permittivity) is defined as the ratio of the actual permittivity versus the permittivity of the vacuum media. The values of the relative

dielectric constants of materials used in this work are shown in Table 2.3. The charge dissipation may be affected by the relative dielectric constant of materials (Niels, 1998), which will be discussed in detail in section 2.4.

Table 2.3 Dielectric constant of materials (Dielectric Constant Reference Guide)

Medium:	Vacuum	Atmosphere	Cotton	Teflon	PP	PET	Nylon
ϵ :	1	1.00054	1.3-1.4	2.1	2.25	2.8-4.5	4-5

2.3 Mechanisms of charge generation

Charge generation can be classified into contact charging, frictional charging, and corona charging according to the mode of charge generation. The contact charging or frictional charging is composed of bond-forming and bond-breaking processes and charge is generated by contacting (bond forming) and breaking (bond breaking) two different surfaces. The bond-forming process is usually explained based on an electrons-transfer mechanism; however, it is also explained by an ions-transfer mechanism. The bond-breaking process can be combined with several complicated phenomenon, such as the back-flow and gaseous discharge. In addition, charge can accumulate by repeating contacts and separations. The mechanisms on all these aspects are reviewed and discussed in this section.

2.3.1 Contact charging

Taylor and Secker (1994) explained the contact-charging phenomenon from thermodynamic point of view: when two different surfaces get into contact, charges will transfer from one surface to the other in order to keep the thermodynamic equilibrium. When the two surfaces are separated quickly, the transferred charge may be kept on the other surface as shown in Figure 2.6. For conductors, the transferred charge will move rapidly and will recombine during the separation. However, for insulators, the transferred charges cannot move as freely because they are trapped inside the insulator surface,

which will remain on the surface and generate static (Figure 2.7). Therefore, static electricity is defined as the behavior of electric charges that rest on insulators or isolated conductors.

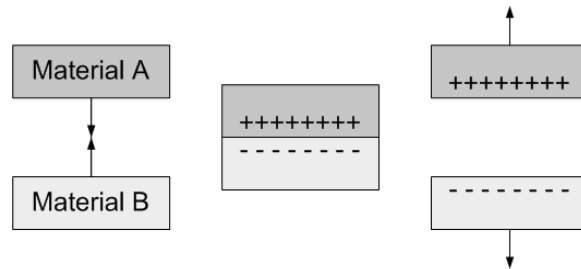


Figure 2.6 Charge transfer by making and breaking contacts (Taylor & Secker, 1994)

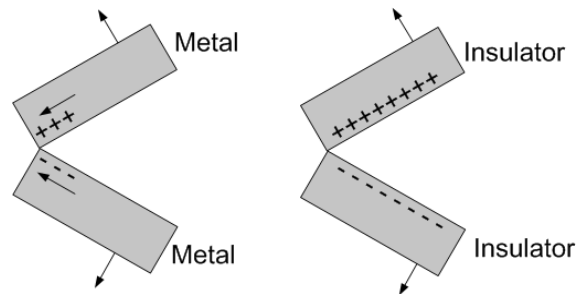


Figure 2.7 Charges recombine (left) and remain (right) (Taylor & Secker, 1994)

It is generally assumed that contact charges can be ignored for metals used in common industrial process because of charge backflow on separation. However, a series of experiments showed that charge did exist on metal balls rolling out of a metal tube into a Faraday tube Castle (2004). The possible hazards and the reason why it was not widely observed were analyzed.

Lowell and Rose-Innes (1980) reviewed researches on the contact electrification of different materials. The metal/metal case (charging by metal contacting against metal) was well explained by the electronic-transfer theory as introduced in next paragraph. Nevertheless, the explanations on metal/insulator case (charging by metal contacting

against insulator) and insulator/insulator case (charging by insulator contacting against insulator) remained unsatisfactory since the lack of knowledge on insulators' surfaces.

The theory of contact charging between metals was established in by Harper (1957). As shown in Figure 2.8, metal A has work function ϕ_A , and metal B has work function ϕ_B , where $\phi_A < \phi_B$ (the work function represents the minimum energy for an electron to escape from the metal). When the metal A and the metal B get into contact, electrons in higher energy state in metal A will transfer into unoccupied lower energy states in metal B until the surface potential is sufficient to cause the same work function for both surfaces (Taylor & Secker, 1994). The work functions of 94 elements can be found in literature (Welker, Nagarajan, & Newberg, 2006). The surface work function of most metal is about 4-5 eV.

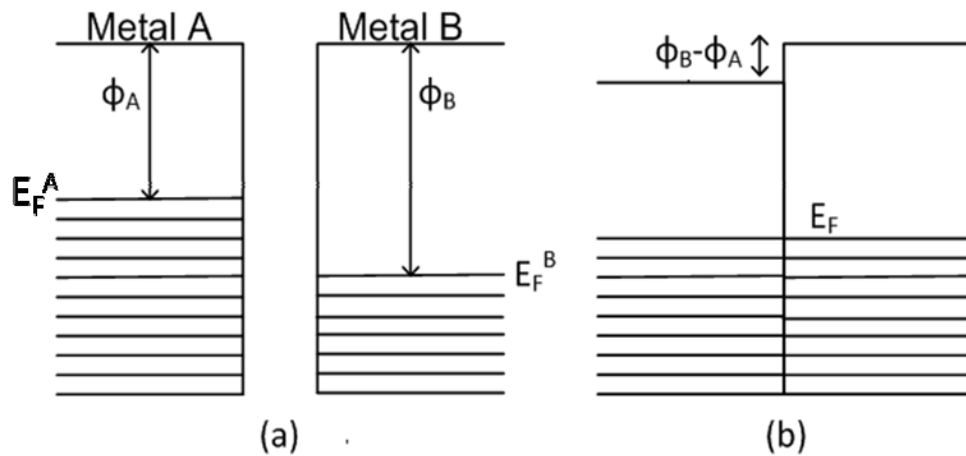


Figure 2.8 Metal A and B of different work functions (b) Fermi level* of the two metals become equal after contact (Taylor & Secker, 1994)

*In Quantum mechanism, solid surface is occupied by electrons in discrete energy states. For metals, electrons only occupied the states below Fermi energy, E_F . The energy interval, ϕ_W , from E_F to vacuum level (zero potential state) is the work function (Patterson & Bailey, 2007).

The surface energy states for semiconductor is similar to that for metal surface, but there exists a forbidden band, E_G , between the valence band and the conduction band as shown in Figure 2.9. The valence band of these materials is already fully occupied by electrons, therefore, the electrons cannot move freely in the valence band. However,

when they are excited, for example by thermal or optical excitation, then the electrons in the valence may jump across the forbidden band to the conduction band and the surface becomes conductive.

Intrinsic semiconductors are hard to be excited. Usually, the conductivity of semiconductors is caused by chemical impurities on their surface. Two models of semiconductors' surface were established based on the type of the impurities: “n-type semiconductor” and “p-type semiconductor” (Figure 2.9). For the “n-type semiconductor”, which has impurities like phosphorus (P_i) or arsenic (Se), the atoms of impurities provide donor sites centers below the conduction band. The electrons of these atoms can be thermally excited into the conduction band easier than the electrons from the valence band, therefore contribute to the conduction. For the “p-type semiconductor”, which is caused by impurities like boron (B), the impurities atoms can generate acceptors just above the valence band. Therefore, the electrons from the valence band can be thermally excited to these acceptor atoms easier, leaving charge holes unoccupied on the valence band, which contribute to the conduction (Taylor & Secker, 1994).

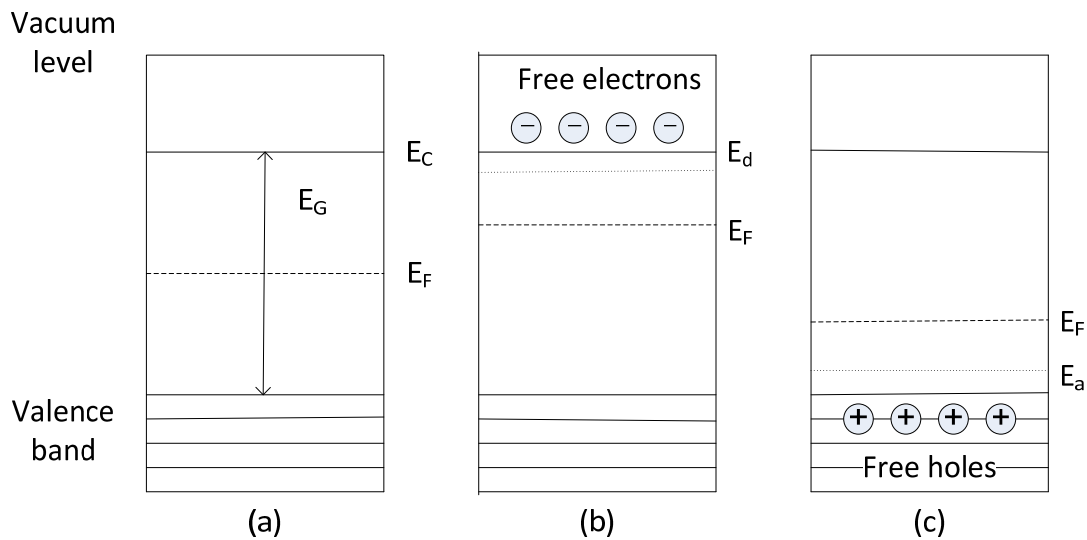


Figure 2.9 Energy band for (a) intrinsic (b) n-type and (c) p-type semiconductor (Taylor & Secker, 1994) (E_C is energy level of conduction band, E_G is energy gap between the conduction band and the valence band, E_d is energy level of donors, E_F is the Fermi energy level, E_a is the energy level of acceptors)

Insulators can be considered as semiconductors with wide forbidden energy gap, which is too difficult for electrons to escape. The surface work functions of a range of polymers are given below (Davies, 1978):

Table 2.4 Work functions of polymers

Polymer	Fermi energy (eV)
Polyvinylchloride	4.85
Polyimide	4.36
Polytetrafluoroethylene (PTFE)	4.26
Polycarbonate	4.26
Polyethyleneterephthalate	4.25
Polystyrene	4.22
Nylon 66	4.08

Based on the electronic-transfer theory, Cowley and Sze (1965) first gave an expression to calculate the charge transferred in metal/semiconductor contact, which is proportional to the different of surface work function, $\phi_A - \phi_B$. The calculating method was improved by Hays and Donald (1971), Krupp (1971), Bauser et al (1974), Davies (1970) (1967), and Hays (1974). In addition, it was pointed out that the charge transferred was proportional to $(\phi_A - \phi_B)^{1/2}$ (Chowdry & Westgate, 1974). However, usually, the calculated results were different from the experimental results (Castle P. G., 1997). There are several limitations for these calculating methods. For example, the fluctuation of insulator's work function is not considered, thus the work function is not quite precise (Fabish & Duke, 1977). For another example, the physical structure and the chemical reaction may affect charge exchange in practice, which were also not considered in the calculations. Lee (1978) found that polymers surface work functions changed due to surface oxidization and he proposed that the apparent work function under certain condition should be measured for a more accurate prediction.

Lowell and Rose-Innes (1980) reviewed the charge observed on various polymers after contacting with metals (Table 2.5). It is meaningless to compare the charge generated in different tests, since the real contact area could be different for different materials under different conditions. Lowell and Rose-Innes (1980) assumed that the real contact area is about half of the appearance contact area (geometric contact area), however, this is questionable and the real contact between two contacted surfaces is hard to be measured.

Table 2.5 Order of magnitude of charge density observed on various materials after contact with metals

Material	Charge density (pC/cm ²)	Condition
Polyethylene	500	Air, contact
	5000	Air, rubbing
	10000	Vacuum, rubbing
PTFE	3000	Vacuum
	7000	Air, rubbing
	20000	Vacuum, rubbing
	200000	Vacuum, rolling contact
Nylon	100000	Vacuum, contact
	100000	Vacuum, rolling contact
Polycarbonate	100000	Vacuum, rolling contact
Polyimide	300000	Vacuum, rolling contact

2.3.2 Frictional charging

The frictional charging is dynamic, involving friction between two surfaces. A difficulty for understanding the frictional charging is that the tribology phenomenon is complex. It is known that when two surfaces contact, real contact only occurs at the tips of their asperities. When sliding occurs, the real contact junctions will be sheared. The real contact area is related to the roughness of the surfaces and the deformation of asperities

(Howell, Mieszkis, & Tabor, 1959) (Gupta, 2007). As to the complex effect of speed on friction, it was found for example, that for lubricated yarns, the coefficient of friction increased when the rubbing speed increased. This is a practical example of the added complication introduced by additives (essentially deliberately applied “impurities”) which mean that some consideration must also be given to the influence of hydrodynamic factors (Lyne, 1955). Additionally, it is also interesting to note that friction could be reduced by modulating vibration (Armstrong-Helouvry, 1991), which is a factor that is of significance in a moving thread line. For those approaches that are applied to reduce friction, the ultimate goal is usually to control the electrostatic charging and reduce wear or surface attrition of the various component surfaces. While there is much work on friction and on static electrification, the correlation between these is still not well understood.

A commonly asked question is that whether rubbing charges different from charging by contact/separation. Experiments showed that charge transferred in a rubbing process was several orders of magnitude greater than in a simple contact, and it was easier for the frictional charging to reach the thermodynamic equilibrium than the repeating contact charging (Taylor & Secker, 1994). Experiments using the Van de Graff generator (Serway & Jewett, 2007) showed that charge increased as the rubbing speed (belt winding across rollers) increased. An obvious explanation of this phenomenon is that the sample length increased at higher rubbing speed, which gave more contact area for the charge generation. However, if the sample length was the same, the effect of rubbing speed on the charge generation is still unknown. It is also unknown that whether there is any more fundamental difference between rubbing charging and contact charging. If the process of rubbing were to influence the basic mechanism of charge transfer, in addition to the factor of contacting area, one would expect the velocity of rubbing to affect the charge (Lowell & Rose-Innes, 1980).

On one hand, a decrease of charge at high speeds could possibly be caused by heating, which would increase the conductivity of the polymer. On the other hand, it was expected that the charge would increase with speed increasing since charge tended to flow back to the rubbing metal. However, Ohara argued that charge back-flow is

probably not important for his samples. Ohara (1980) reported that the charge transferred to a polymer by a metal sliding on it increased at first with the speed of sliding, then decreased again at high speeds, in another word, there was a certain speed at which the transferred charge was maximum. He suggested that the peak is a consequence of thermal motion of the polymer segments (details introduced in following paragraphs). Zimmer (1970) found charge reversal phenomenon (charge polarity changed) when the rubbing speed increased. They proposed that as the high speed rubbing process caused the local temperature increased, therefore enhanced the diffusion of the electrons from the hotter part to the cooler part of the surface. However, there was no method to monitor the electrons diffusion on polymers surfaces. Cunningham showed that the electrification of a polymer sheet passing over a metal roller was much greater when slipping occurred than when the roller and the polymer sheet had the same velocity. However, it could be argued that the slipping merely increases the total area of contact. A variation of this kind has been reported several times (Hersh & Montgomery, 1956) (Lowell & Rose-Innes, 1980), but it is not certain whether it was caused by back-flow of charge or whether a more fundamental process was taking effect. More works will be reviewed in details in section 2.5.

In addition, usually, charge only transfers between two different surfaces, which have different surface work functions, however, in the frictional charging, if it is asymmetric rubbing (Figure 2.10), then charge could occur on surfaces of the same material (Morton & Hearle, 2008). This is because the asymmetric rubbing generates unequal heating on the two surfaces and therefore mobile particles will move from hot to cold, owing to the greater energy of the hot particles.

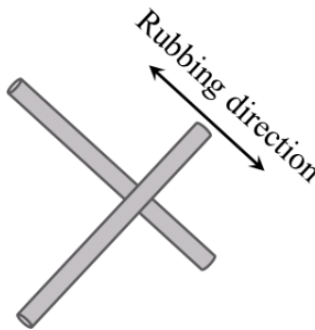


Figure 2.10 Asymmetric rubbing (Morton & Hearle, 2008)

2.3.3 Corona charging

Because the charge generation in the contact and rubbing processes are hard to control, (they are sensitive to the processing parameters, such as the contact pressure and the rubbing speed) corona charging is used for observing static behavior. As shown in Figure 2.11, the corona charging is a self-sustaining, partial breakdown of gas, which is subjected to highly divergent electric field (Taylor & Secker, 1994). It is often initiated deliberately for some application, such as for the precipitation of dust and smoke and for dry powder coating. There is significant information about the corona charging (Baum, Lewis, & Toomer, 1977) (Gas Gupta & Doughty, 1978) (Pethig, 1983). There is also research comparing the tribocharging and the corona charging (Chubb, 2002). However, corona charging is beyond the scope of this research work.

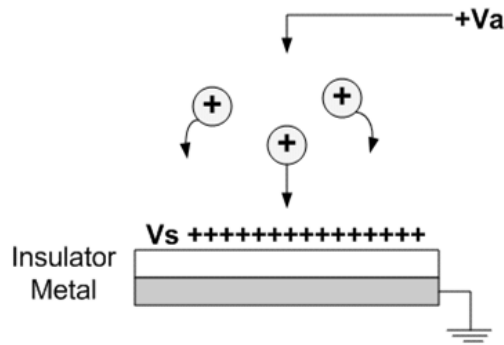


Figure 2.11 Corona charging, V_a is applied potential and V_s is the surface potential
(Taylor & Secker, 1994)

2.3.4 Repeating contacts and separations

Contact charging and rubbing charging are non-equilibrium bond-breaking and bond-building processes. For each contact/rubbing, new charge should be transferred from one surface to the other until equilibrium is reached. Although there is charge dissipation during each separation, usually the charge will accumulate in repeating contact. (Hays, 1991).

Previous researches on the contact electrification indicated that charge increased as the number of contact increased. The rate of increase of the charge decreased as contacts were repeated, and after many contacts, the charge appeared to saturate (Lowell and Rose-Innes, 1980). Why this happens is not, however, understood. Several explanations have been put forward, as discussed below, but each of these is applicable to only a certain kind of insulator:

1) The increase of charge with increased number of contacts may be explained by the suggestion that the charge transferred depends on the total time of contact.

This simple explanation is probably not generally correct. First, charge transfer seems to occur very quickly, in a period less than the duration of individual contact in most experiments (Lowell & Rose-Innes, 1980). Secondly, specific experiments on KCl, anthracene, and some polymers (Lowell & Rose-Innes, 1980) have shown that the increase in charge by repeating contacts cannot be explained in this way. In each case, N times of contacts, each of which had t seconds of contact, generated much more charge than a single contact with contact time of $N \times t$ seconds.

2) The increase of charge with number of contacts may be caused by the increase of real contact area, which is related to the visco-elastic deformation, by repeating contacts.

The visco-elastic increase of area seems to be ruled out by the following observations (Lowell & Rose-Innes, 1980). A series of contacts was made to the same position on the polymer. The charge increased rapidly at first, and then became almost constant. The charge was then removed by exposing the polymer to ionized gas and another series of contacts made to the same position. In this second series of contacts, the charge built up in much the same way as it did in the first series that the charge increased strongly initially. According to the visco-elastic hypothesis, however, the build-up of charge is due to a gradual increase in the total area of contact, and the fact that the charge eventually becomes almost constant must imply that that area of contact has almost ceased to change. The fact that in the second series of contacts, the charge increased strongly at first therefore contradicts the visco-elastic hypothesis.

3) The repeating contacts may be expected to increase the charge if the insulator is slightly conducting, because the charge tends to spread (under its own Coulomb repulsion) into the bulk, making room, for more charge to be deposited in the next contact (Harper, 1967).

Homewood and Rose-Innes (1982) used very hard crystalline insulators to study the charge accumulation, so that the surface relocation and the surface deformation in repeating contacts could be negligible. They found the charge accumulation began to happen after they added some additive to increase the surface conductivity. Therefore, they concluded that the charge accumulation was related to the surface conductivity. Between contacts, charge could leak from the contact point and be replaces on the next charging. Cunningham and Goodings (1986) observed charge accumulation a long time after the possible effect of plastic deformation has been eliminated. They assumed that the charge could penetration into the bulk, which depended on the surfaces boundary conditions. Other reserachers (Hays, 1991) (Lowell, 1984) (Labadz & Lowell, 1986) (Fabish & Duke, 1977) studied how charge is accumulated on an insulator and how deep the charge could penetrate. Their experiments indicated the repeating metal-polymer contact charging may involve the bulk states of the polymer, and they reported that the penetration depth is in micrometer range as shown in Table 2.6. In addition, Lowell (1967) pointed out that the charge penetration into the bulk of an insulator is caused by the thermal activation in the conduction band.

Table 2.6 Penetration depths of charge from metal into polymers (Labadz & Lowell, 1986)

Polymer	Penetration depth (nm)
Polyvinyl Chloride (PVC)	48
Polyimide	20
Polycarbonate	46

PTFE	13
Polyethylene Terephthalate (PET)	24
Polystyrene	43
Nylon 66	51

However, Lowell and Rose-Innes (1980) argued with this explanation. They pointed out that for polymers such as PTFE the charge is immobile. A spot of charge deposited on the surface remains virtually undiminished for several hours. Thus, for certain materials, it is unlikely that the increase in charge with repeated contacts is due to charge flowing away from the point of contact.

Mathematical methods and derived numerical techniques were used to predict the charge accumulation in repeating contact process, most of which were formulated by a function with a sum of exponential terms as shown in equation [1-4]:

$$y = y_{s1}(1 - \exp(-t/\sigma_1)) + y_{s2}(1 - \exp(-t/\sigma_2)) \quad [1-4]$$

Where, y is the saturation values of the whole process, which is a sum of y_{s1} and y_{s2} . σ_1 and σ_2 are time constants, respectively. In addition, a 3-exponential sum function was established by Gibbing (1975), which could fit the experimental curves better, but it became difficult to explain their physical meaning.

2.3.5 Ionic transfer mechanism

In early years, a number of authors (Henry, 1957) (Ruckdeschel & Hunter, 1977) have suggested that contact electrification may be caused by the transfer of ions from one surface to the other. It is possible that the ionic species can influence the charging mechanism, but the question remains whether it is correct to assume ions to be the charge carriers. However, the overall electrical effect of a positive ion being transferred from a surface cannot be distinguished from an electron transferred to that surface to neutralize the ion. In the case of metal-insulator contacts, at least, the latter is more plausible.

The ion transfer mechanism regained attention in recent years because in electrophotographic industries, the addition of some ionic CCA (charge control agents) has been shown to accelerate the charging process. Some additives, like organic pigments with NR_3 and NR_4^+ groups, are positively charged. Some substances with COOH , CONR_2 , SO_3 , SO_2NR_2 groups are anionic and negatively charged. However, their roles in contact electrification remain obscure.

Mizes et al. (1990) studied the contact charging between indium and polystyrene doped with some organic salt (cetyl pyridinium bromide). They observed the transfer of the bromide ions, and assumed the ionic transfer was the only mechanism for contact electrification. Dias et al. (1991) explained the charging results with pyridinium toluenesulfonate salts in terms of ionic transfer and pointed out the polarity and the magnitude of the charge is depending on the mobility of the cation and the anion.

Water is reported to influence contact electrification, which is related to the ionic-transfer mechanism (Field, 1946). When there was adsorption of moisture layer on a solid surface, ions were claimed to be the major cause of charging and charge transferring was seen as a redistribution of ions between the contacting surfaces. It is also claimed that the effect of water on contact electrification is to increase the conductivity of the insulator. The charge transferred in a single normal contact is unlikely to be affected, but if contacts are repeated, the enhanced conductivity of the insulator may help the charge build up to a large value and if sliding occurs, an increased conductivity may be expected to reduce the total charge transferred by enhancing back-flow. In summary, ion transfer between insulators is probably non-critical as well, though there is much less evidence in this case. The role of ions in a surface layer of water needs further investigation.

2.3.6 Bond-breaking mechanism

Both of contact and frictional charging are considered as two-step processes phenomenon consisting of instantaneous bond forming and bond breaking (1989). For the bond-forming step, electronic and ionic transfer mechanisms have been discussed. For the bond-breaking step, it may be combined with phenomenon like charge backflow, and air breakdown.

Backflow is the redistribution of charges due to the insulator's limited conduction (Lowell, 1991). As shown in Figure 2.12, when a metal rolls over an insulator, charge is deposited on the insulator. This charge tends to flow back to the metal and the extent depends on the insulator's resistance (Lowell & Rose-Innes, 1980). Castle (1997) pointed out the charge backflow was important and often caused the level of experimental charge data to be often well below theoretical prediction.

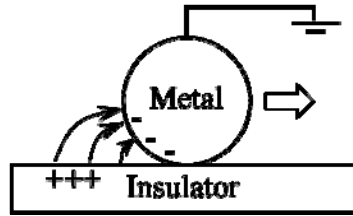
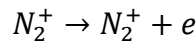


Figure 2.12 Charge backflow from insulator I to metal M (Lowell & Rose-Innes, 1980)

Gaseous discharge happens when the electric field near a charged object exceeds the breakdown strength of the ambient gas. The breakdown strength of dry air is approximately three MV/m (Taylor & Secker, 1994) (Tipler, 1987) (Rigden, 1996) (Yager, 1947) (Charles & Norbert, 1925) (Lewis, 1999). The exact value varies with the shape of the electrodes. Most polymer surfaces tend to reach a surface charge density of 3-5 nC/cm² before discharging (breaking the air strength) (Lee, 1994). During the discharging, the surrounding gases are activated (Kwetkus, Sattler, & Siegmann, 1992), for example:



Zimmerman et al. (1991) (1991) detected both electron emission (EE) and positive ion emission (PIE) for the air breakdown on polymer surface during the separation from a metal rod.

Gaseous discharge is dangerous in industry. Spark can happen on any conductor that is isolated from the earth when the voltage across two surfaces has been raised to the sparking voltage, which may initiate fire or explosion. Besides the spark discharging, there are also brush discharge, corona discharge, and propagating brush discharge. Brush

discharge happens between an earthed sphere and a suspended charged plate. The electric field between the sphere and the plate is not uniform. The spark is initiated at the sphere and then “fans” out into lots of small channels when approaching the plate surface. When the charged plate is put on the front of an earthed plate, the charge density on the charged plate will become significantly greater than the air breakdown limit. This is because the electric field density from the charge plate surface to the backing earthed plate will be much higher than that to the surrounding air. Now, if an earthed sphere approaches the charged plate surface, when the distance between the earthed sphere and the charged surface equal to the thickness of the charged plate, the charge flow direction will switch from the earthed bottom plate to the sphere and the propagating brush discharging will be initialized. The minimum charge required to initiate a propagating brush discharging depends on the plate’s thickness (Taylor & Secker, 1994).

2.4 Mechanisms of charge dissipation

The charge generated on a surface can move under the electric fields, spreading or neutralizing the charges and making the fields decay. In all kind of charge decay, some sort of conducting path, containing mobile charge carriers, has to be established from the location of the charge to the ground. The static decay can be classified to three types: 1) Charge decay of isolated conductors, 2) Charge decay of insulators, and 3) Charge decay through the air.

2.4.1 Charge decay of conductor

First, the charge might decay of an isolated conductor. For example, a conductor is insulated by a material has resistance R as shown in Figure 2.13. The capacitance of the conductor is C . When a charge q is plated on the conductor, then the conductor will be surrounded by an electric field E , giving an initial voltage V :

$$V_0 = q_0/C \quad [1-5]$$

A current, I , will flow to ground, making the charge decay at the rate:

$$I = -dq/dt \quad [1-6]$$

Since, $I=V/R$, and by substituting equation [1-5] into equation [1-6], the decay rate can be calculated by equation [1-7]:

$$-\frac{dq}{dt} = \frac{q}{RC} \quad [1-7]$$

The charge retained on the conductor after time t can be obtained by integral equation [1-7] from time 0 to time t as shown below:

$$\begin{aligned} \int_{q_0}^q -\frac{dq}{q} &= \int_{t_0}^t \frac{t}{RC} \\ -\ln q + \ln q_0 &= (t - t_0)/RC \\ q &= q_0 \exp\left(-\frac{t}{RC}\right) \end{aligned} \quad [1-8]$$

Therefore, the charge decay can be estimated follow the exponential relationship as shown in equation [1-8]. The value of RC is known as τ , which is called the characteristic decay time of the system. Figure 2.14 shows a typical charge decay curve, where RC is the initial slope on the decay curve.

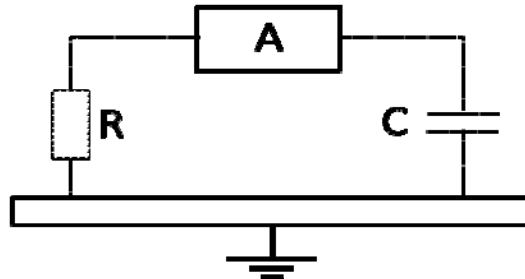


Figure 2.13 Charge decay of a conductor characterized by its capacitance C and resistance R with respect to ground

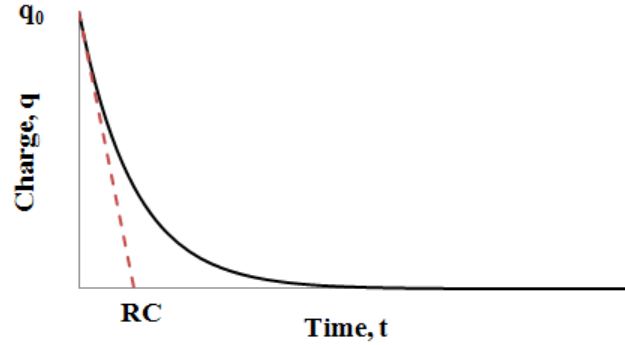


Figure 2.14 Charge dissipation (Taylor & Secker, 1994)

2.4.2 Charge decay of a non-conducting system

From the equation [1-8], the charge decay rate and voltage retained on the conductor can be calculated from the system's resistance and capacitance, which can be measured directly. However, for an insulator, the charge decay may depend on very complex geometrical, dielectric and resistive conditions of the system. For example, when an insulator of resistivity ρ and permittivity (relative dielectric constant) ϵ resting on a grounded plane, a charge q is distributed uniformly over the area A , then the surface charge density will be:

$$\sigma_0 = \frac{q_0}{A} \quad [1-9]$$

If there is no conductor surrounding the charge surface as shown in Figure 2.15, then the field from the charge will be directed toward the grounded plane and the charge will decay through the insulator itself. The charge density on surface after time t can be calculated by equation [1-10]:

$$\sigma = \sigma_0 \exp(-t/\rho\epsilon) \quad [1-10]$$

Where, σ is charge density on insulator surface after time t , σ_0 is the surface's initial charge density, ρ is the resistivity of the insulator, and ε is the relative dielectric constant of the insulator.

If there is a grounded plate placed parallel with the charged surface with distance x to the surface (Figure 2.16), then the electrical field will also direct from the charge surface to the grounded plate through the air. The charge density retained on surface after time t can be predicted by equation [1-11]:

$$\sigma = \sigma_0 \exp \left(-\frac{t}{\rho \varepsilon + \rho \varepsilon_0 \frac{d}{x}} \right) \quad [1-11]$$

Where, ε_0 is the dielectric constant of the air, d is the distance between the charged surface and the grounded plate, and x is the thickness of the insulator. Equation [1-10] indicated that the charge decay of an insulator is not only determined by the material parameters, but also by the geometry and dielectric and resistive properties of the surroundings. The charge decay can only be predicted in special cases like the model shown above, while, on the other hand, it can be much more complicated in practice. For example, when two different medium materials (e.g. insulator and gas) are present between a charged surface and the grounding point, the system's resistance and capacity need to be modified into a serial model. For another example, for insulators, volume and surface resistivity may be different and they have not been well separated. These can result in the decay characteristics of insulators departing significantly from the ideal exponential behavior expected.

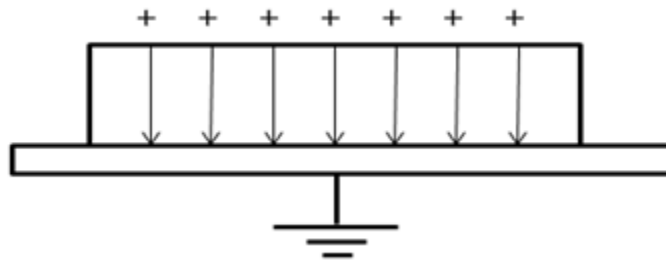


Figure 2.15 Charge decay of charged insulator resting on grounded plane

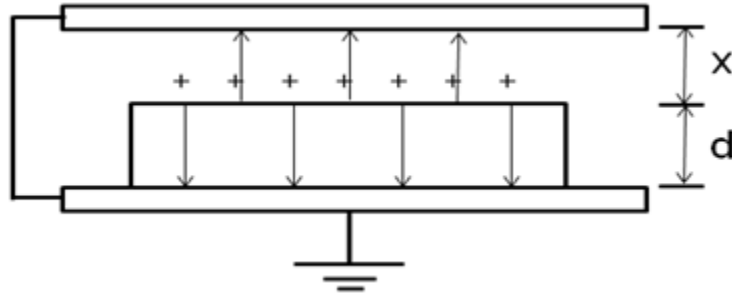


Figure 2.16 Charge decay of charge insulator resting on a grounded plane with a grounded plate placed parallel with the charged surface

2.4.3 Charge decay through the air

When a charge insulator is surrounded by the air, there is in principle no other pathway for the charge to be moved, and then the charge may be neutralized by oppositely charged ions attracted to the insulator surface. The decay rate is affected by the mobility, concentration, and charge carriers in the air. For example, as shown in Figure 2.17, a positively charged surface was surrounded by ionized air. The current of negative ions in the air will cause positive charge on the surface to decrease following equation [1-12]:

$$\sigma^+ = \sigma_0^+ \exp \left(-\frac{t}{\rho^- \epsilon_0} \right) \quad [1-12]$$

Where σ^+ is the surface charge density after time t , σ_0^+ is the initial value of the positive surface charge density, ρ^- is the polar resistivity of the ionized air, ϵ_0 is the dielectric constant of the air.

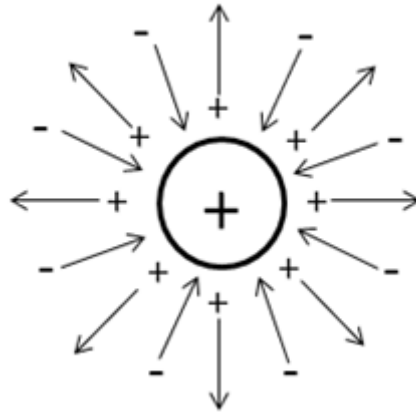


Figure 2.17 Charged body in air with ions

It worth mentioning that the characteristic decay time or the half decay time are often used for evaluating static properties of materials (Taylor, 1987, Kan, 2008) and these value are adopted by the industry. It has been documented by earlier investigation (Ieda & Shinohara, 1967) that the higher the charge generation the faster the charge decay. A material with low charge generation may take longer half decay time compared to another material with high charge generation. The latter may retain more charge than the former material as is demonstrated in Figure 2.18. The half decay time is therefore not a direct factor to be considered. The charge retained as a normalized value compared to the accumulated charge coupled with the actual decay behaviour (time versus charge level) provides better method to compare between materials.

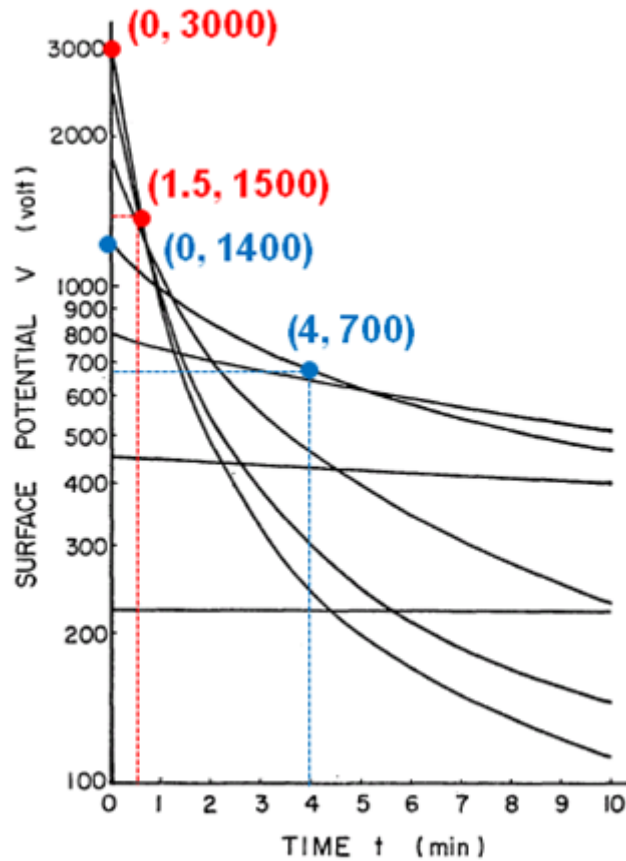


Figure 2.18 Decay curves of charge on PET film (Ieda & Shinohara, 1967)

2.5 Previous experimental studies

Previous researchers developed different methods for studying the triboelectric charging. The testing methods will be reviewed in this section, while the testing results will be reviewed in section 2.5.2.

2.5.1 Sample preparation

Extensive researches have shown that electrostatic properties of polymers were very sensitive to the sample surface condition, which includes surface chemical component, physical structure, or environmental conditions. To eliminate the variation of the surface

condition, different kinds of sample preparation methods were developed in previous studies. For example, in Medley's experiments (1954), petroleum ether and water were used to clean fibers, which could be distilled directly without exposure to the external air. The initial charge on fibers was discharged by β irradiation through an aluminum foil window on a sealed chamber, where all testing devices were enclosed. In the experiments of Kematsu et al. (2004), polymeric disks were cleaned by ethyl-alcohol and the initial charge was removed by spraying ionized air. In the experiments of Sereda and Feldman (1964), fabrics were washed in diethyl ether, ethyl alcohol, and distilled water in turn. After washing, part of the samples were dried over magnesium perchlorate and other part were centrifuged to a spin-dry condition. In the work of Homewood and Rose-Innes (1979), polymeric samples were discharged through a flow of ionized argon gas. Many researches also use coating method to get dense layer of desired molecular to make the tribo-electrification. For example, Ohara et al. (2001) used polymer films or LB (Langmuir-Blodgett) layers deposited on flat substrates to rub against each other. For another example, Robin et al. (1975) coated ions at two ends of pyroelectric materials (polarized in applied electric field) to investigate the effect of adsorbed ions in contact charging. However, until now, sample preparation remains one of the major difficulties of the static experiments. There is still accepted standard to what precision and cleanliness the surface should be prepared (2004).

2.5.2 Environmental chambers

For electrostatic tests, testing environment need to be controlled because electrostatic phenomenon can be affected by the environment parameters. For some static experiments, the purpose was to find the influence of relative humidity or temperature on the charge generation or dissipation, then the testing environment need to be adjustable to provide different levels of constant condition. To realize these experiment, sealed chamber were usually used in previous works, where the relative humidity was controlled. For example, in Medley's tests, all devices were enclosed inside a grounded metal chamber, where the relative humidity was controlled by solution. In the experiments of Hersh et al. (1956), parts of the devices (except cam, motor and electrometer) were placed inside a chamber

made of plywood and Lucite. The temperature was controlled by a heater and the humidity was controlled by saturated salt solutions contained in trays. Air –circulating fan was applied in most of previous work, which is also enclosed in their chambers. In the experiments of Sereda and Feldman (1964), two series of vacuum desiccators, containing sulphuric acid solutions adjusted to concentrations were used to give different levels of relative humidity conditions.

In addition, vacuum chamber and chambers filled with particular air were also used in previous work to study the static behavior in these environments. For example, vacuum bell jar and environment with Nitrogen gas of 50 KPa were also use in the experiments of Kematsu et al. (2004). For another example, the experiment of Homewood and Rose-Innes (1979) were carried out in a vacuum chamber.

2.5.3 Charge measurement on solids

Charge generated on small specimens can be measured by placing them into a Faraday cage. The Faraday cage is composed of two cups with a small opening on top of the inner cup and a lid, which can be closed on the top of the outer cup. The inner enclosure is electrically connected to an electrometer. It is insulated from the outer enclosure by rigid, very high resistance, insulator, such as the PTFE. The outer enclosure is connected to ground and serves to shield the inner enclosure from external fields, which could affect the measurement. Measurement of charge on large specimens, which cannot be totally enclosed by a Faraday cage, can be done using two concentric cylinders enclosing the part of the specimen to be measured. The outer cylinder should be longer than the inner cylinder to shield it from charge outside.

The electric field strength can be measured using a fieldmeter. When a charged specimen is placed in front of the sensing unit of the fieldmeter, the sensing unit will induce electrostatic charge. There are mainly two types of fieldmeter: 1) rotating vane fieldmeter, 2) vibrating plate fieldmeter.

For a rotating vane fieldmeter, the vane is rotating and a sensor plate is fixed. When the rotating vane covers the sensor plate, the induced charge in the sensor is small.

When the opening in the rotating vane is in the opposite position from the sensor, the induced charge in the sensor is a maximum. Thus, there will be a periodically AC signal on the sensor plate, which will be amplified, processed, and read by a display unit. For the vibrating sensor, there are a moving electrode and a fixed electrode (the two electrodes are called “folk”). As the distance between the two electrodes varied, the capacitance varies and electric charge is forced in and out of the capacitor. The AC signal produced is amplified and displayed as a voltage. As the probe moves away from the charged material, less charge is induced on the sensor, whereas as it moves toward the charged material, more charge is induced on the sensor. Thus, the distance between the sensor and the charged surface need to fix during the test.

Both the Faraday cage (charge measurement) and the fieldmeter (field measurement) are often attached by a cable to an electrometer, which is also called electrostatic voltmeter. Figure 2.19 shows the diagram of apparatus for measurement of electrostatic charge.

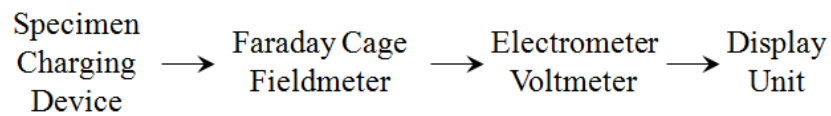


Figure 2.19 Diagram of apparatus for measurement of electrostatic charge

One of the drawbacks on charge measurement in previous researches is the manual moving of sample. For example, in the experiments of Sereda and Feldman (1964), after rubbing, the sample was lifted with insulated tongs and dropped into a Faraday tube. They announced that the variables caused by manual operation were not significant, however, there was no evidence and the limitation was obvious. Another drawback is that many researchers measured the charge on the other surface instead of the charge on the samples. For example, Robins et al. (1975) recorded the potential of metal ball before and after contacting with different polymeric surface and he stated that the charge on the insulator and the charge on the metal was equal and opposite. However, this assumption is questionable since the conductivity of two different contacted

materials are different and the distance from the measured surface to the grounding point are also different, both of which could cause different charge generated or measured.

2.5.4 Surface analysis

The most important surface analysis regarding electrostatic properties is the resistivity measurement, which has been introduced in section 2.2. Since the electrification is a surface phenomenon, therefore, different surface analysis techniques can be used to help understanding the electrification phenomenon. Briggs (1979) discussed the advantage and disadvantages of several types of methods and their use in the study of electrification phenomenon. Those techniques include photoelectron spectroscopy (PES), which is subdivided into ultraviolet (UPS) and x-ray photoelectron spectroscopy (XPS), electron spectroscopy for chemical analysis (EXCA), auger electron spectroscopy (AES), scanning auger microscopy (SAM), low-energy electron diffraction (LEED), secondary ion mass spectroscopy (SIMS) and ion scattering spectroscopy (ISS). For example, AES may damage the surface and may give additional charging onto the surface. In the work of Németh et. al., the XPS was used to investigate the elemental surface composition of film samples after charging. Beside this, solvatochromic measurements were also applied in their experiment, where proving molecules were used to display the polarity of surface after charging.

2.5.5 Effect of contact pressure

Since real bodies are never perfectly smooth, when two surfaces contact, the real contact only occurs at the tips of their asperities, which is affected by the surfaces roughness (crimp crowns in the case of woven fabric) and the asperities' deformation properties. The real contact area is defined as the regions of contact between two bodies through which mechanical actions or reactions are transferred. The apparent contact area is defined as the area of contact between two flat macroscopic bodies, which could be measured by measuring the length and width of the rectangular macroscopic contact region. The real contact area of

apparently flat materials is always less than the apparent contact area (ASTM D 4470-97 Standard test method for static electrification).

The real area of contact between two surfaces usually is not known, thus, the true charge density at the points of contact cannot be determined. Therefore, the questions are whether the real contact area is an appreciable fraction of the apparent contact area, and whether there is reason to believe that this fraction does not appreciably vary from one test to another under constant pressure. For example, Lowell and Rose-Innes announced that if a metal sphere about 1 cm in diameter contacts PTFE with a force of 0.1 N, then the PTFE plastically deformed indentation is about 0.5 mm in diameter. Therefore, he assumed that the true area of contact is about half the apparent area. In addition, the charge density averaged over the whole contact area (apparent contact area) may be used for comparison purposes.

During the electrification, charge only transferred at the points of real contact. Any parameters that may affect the real contact area between surfaces, such as the contact force, must be controlled. Slip between surfaces during the making or breaking of contact must be minimized or measured so it can be made reproducible. Roughness of surfaces can alter the real contact area and hence the charge transfer, so one must be careful to test surfaces of approximately the same roughness or under conditions (such as high pressure or long time of contact) where surface roughness has less effect (ASTM D 4470-97 Standard test method for static electrification).

For examples, Coste and Pechery (1981) found that the greatest charge transfer occurs when the surface roughness was the smallest by contact charging a series of PET film samples of various micro-roughness. Since larger contacting area provides more surface to participate in the charge transfer between two surfaces. For another example, Ohara et al. (2001) performed frictional charging on Langmuir-Blodgett film (LB film), and they found the charge magnitude increased as the roughness or the irregularity of the film decreased, also because less rough LB film provides bigger contact area in the rubbing process.

The surface deformation of a fiber compressed by a steel ball was studied (Pascoe & Tabor, 1956). They found the relation between applied force, the yarn diameter, and

the indentation diameter as shown in equation [1-13]. Some typical values of the index m in [1-13] are given in Table 2.7. The table also includes the value of the yield pressure of the polymer under specified conditions of deformation ($D=5$ mm, $d=1$ mm).

$$W = \frac{kd^m}{D^{m-2}} \quad [1-13]$$

W : load, D : fiber diameter, d : diameter of indentation, m , k : constant parameters (Pascoe & Tabor, 1956).

Table 2.7 Indentation characteristics of polymers (Pascoe & Tabor, 1956)

Polymer	m	Yield Pressure (kg/mm ²)
Nylon 6,6	2.7	7.32
PTFE	2.5	2.7
PP	2.7	1.27

* $D=5$ mm, $d=1$ mm

In addition, the relationship between material deformation and the truly contact area is shown in Figure 2.20.

Under contact force, in addition to the increase of contact area, some chemical bonds might be broken on polymers surfaces. These chemical segments can act as traps for electrons and promote the static generation. This phenomenon was observed when pressing polymers strongly against a metal and it was expected that the number of broken bonds correlated with the contact force (Rose & Ward, 1957).

Since polymers are a type of viscoelastic materials. Their viscoelasticity is the result of the diffusion of atoms or molecules inside their amorphous area (Morton & Hearle, 2008). Thus, there can be certain amount of chemical bonds breaking under compression and therefore affect the surface static behavior.

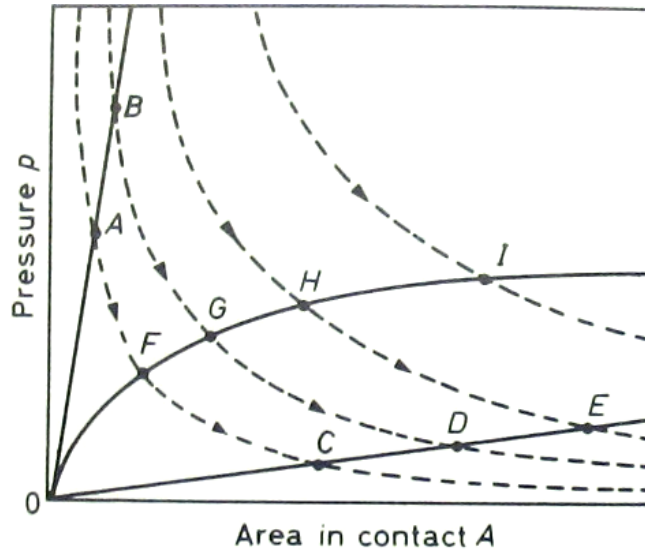


Figure 2.20 Deformation of OB hard elastic (diamond), OE soft elastic, and OI polymers (The full line represents the load-deformation curves (similar to stain-stress curve), and the dotted curves are pressure-area curves under constant loads. The intersection points indicate the equilibrium situation.)

2.5.6 Effect of contact time

Polymers surface deformation is a time dependent process (Morton & Hearle, 2008). As the contact time increases, the true contact area should increase within certain range, therefore, the charge transferred will also increase. This is verified in the work of Homewood and Rose-Innes (1979). They modified a microscope to contact a PTFE film by the lens of the microscope. The image of contacted surface was monitored after 3 s, 100 s, and 1000 s. They found the contact area was about 30% of the geometrical area after 3 s, and increased to about 40% after 1000 s contact. They concluded that the contact area increases with the contacting time, but the rate varies with different material.

2.5.7 Effect of moisture

Charge generation varies widely with the moisture content of a material. Generally, the moisture tends to increase the charge conductivity along polymers surface, as well as the

charge dissipation to the surrounding air. Therefore, it was believed that the static decreases as the relative humidity increases (Greason, 2000). However, it was also found that below certain level of relative humidity, the moisture contributes ions on polymers surfaces, which helps charge transfer (Nemeth, Albrecht, & Schubert, 2003) (Nemeth, Albrecht, & Schubert, 2003). Moreover, for hydrophilic fibers, the water absorption may cause swelling, which alters the stiffness and surface area of fiber, yarns or fabrics (Morton & Hearle, 2008), therefore, more chemical bonds in the microstructure of the surface may break and contribute to the charge exchanging. Considering effects from these aspects, people have determined the moisture level at which electrostatic reaches the maximum. Their results are shown in table 2.8.

Medley (1950)(1954) studied the charge behavior of Nylon film rubbing against a metal wire. He found the maximum charge occurred at 70% R.H., and assumed this was related to the air breaking strength (charge reaches the maximum value before break the air). This conclusion was supported by the test in air saturated with carbon tetrachloride (increase air breaking strength), which resulted in higher maximum charge.

Sawa and Calderwood (1971) investigated the corresponding increases in insulator's surface conductivity with water sorption. They conclude that the effect of humidity is to increase the mobility of the surface-charge carrier. However, the lack of knowledge of the depth of the surface layer prevents the determination of the exact calculation.

Awakuni and Calderwood (1972) found the effect of humidity for Teflon surface was much less than the effect for oxidized polyethylene. From their report, the surface conductivity of Teflon increased exponentially with water adsorption. This conductivity remained low until the first monolayer of water was complete. They concluded that, water molecules become mobile only when a first monolayer of water is complete.

Sereda and Feldman (1964) proposed a mechanism to explain the relation between the relative humidity and the charge saturation or discharge (saturation point exceeds the air dielectric strength). They assumed each water molecule occupies an area of 10.8 \AA^2 . Combined with the materials' sorption isotherms, they concluded "a maximum in electrostatic potential is attained when a monomolecular layer of water is complete".

The moisture on fiber surface contributed to the surface static generation by contributing hydrogen ions to the metal or by allowing a more effective transfer of electrons from the metal. A maximum electrostatic potential is attained when a monomolecular layer of water is developed where the leakage of charge becomes significant and this limits the value of the maximum charge that can be retained on the insulator.

Table 2.8 Effect of relative humidity on electrostatics

Reference	Conclusion
Medley (1950)(1954)	“On Nylon film surface, charge density is almost independent of humidity below 70%. At 70% charge reaches a maximum, and at higher humidity it fell rapidly to zero.”
Sawa and Calderwood (1971)	“Effect of humidity is to increase the mobility of the surface-charge carrier.”
Awakuni and Calderwook (1972)	“Surface conductivity of Teflon increased exponentially with water adsorption. This conductivity remained low until the first monolayer of water was complete.”
Sereda and Feldman (1964)	“Charge maximum occurred at 17 to 18% relative humidity for cotton and wool fabric. For Nylon Taffeta, the maximum occurs at 21% relative humidity. And for propylene fabric, the maximum charge occurs at a relative humidity of about 50%.”
Greason (2000)	“At a given temperature, an increase in the relative humidity causes a decrease in the net charge generated due to tribo-electrification. “
Erno, Victoria, Gert, and Frank (2003)	“Formation of water-containing layers is connected with an introduction of ionic species, increasing the surface conductivity that promotes tribo-electric charging.”

Greason (2000) found the increase in the relative humidity (from 10% to 70%) caused a decrease in net charge generated between a stainless steel ball and different insulators (glass, PTFE, acrylic, polycarbonate, and nylon). He assumed this decrease could be related to a decrease in the volume and surface resistivity of insulators caused by the increase in relative humidity.

It was pointed out that water adsorption influences the charging mechanism (Nemeth, Albrecht, & Schubert, 2003). Several polymers showed an increased uptake of water, which forms adsorption or swollen layers, with increasing the atmospheric humidity. The incorporation of water into polymer's surface introduces ions in the systems. These ions can be formed by the auto-dissociation of water. Furthermore, water molecules are able to initiate the dissociation reactions of surface groups (e.g. carboxyl groups). In addition, impurities may be solvated and mobilized by the water molecules.

2.5.8 Effect of temperature

In the energy states model for semiconductors or insulators' surfaces (section 2.3.1), the electrons cannot jump across the forbidden band to escape the surface until there are thermal or optical excitations, so temperature increasing will help the electrons transfer between two surfaces (Taylor & Secker, 1994). Besides the energy states theory, it is realized that molecular thermal motion increases as temperature increases, therefore, more molecules can be brought to the surface to participate in true (molecular) contact. There is microbrownian motion of polymer chains and some deformed polymer segments may relax from the main chain as temperature increases (Ohara K. , 1980). It is easier for frictional charging to reach the thermodynamic equilibrium because there is more heat generated in the rubbing process than in the contact charging (Lee, 1994).

Ohara (1980) investigated the relationship between frictional electrification and the molecular motion of polymers at different temperature. He used polycarbonate films (30 μm thickness) to rub against a spherical steel tip (5 mm in diameter) at chamber temperature ranging of 10 to 100 $^{\circ}\text{C}$. Peaks of output voltage appeared at 40, 50 and 70 $^{\circ}\text{C}$ and friction speeds of 0.065, 0.41 and 3.6 mm/s, respectively. For the former two cases, the charge began to increase again from 60 and 90 $^{\circ}\text{C}$, respectively. They predicted

there could be another peak at about the glass transition temperature (149 °C) of polycarbonate. These results were interpreted in terms of the molecular motion in the polymer chains and the relaxation of deformed molecules. The effect of temperature was considered as be related with the rubbing speed, because the charge transfer was affected by the frequency of thermal motion of the chains, and affected by the frequency of mechanical contact and separation.

From the contact tests between stainless steel and insulators (glass, quartz, PTFE, acrylic, polycarbonate, and nylon), Greason (2000) found that at a given relative humidity, an increase in the temperature (from 10 °C to 30 °C) caused a decrease in the average charge measured for all six insulators. He assumed this was ascribed to a decrease in the volume and surface resistivity of insulators by an increase in environmental temperature (the samples resistivity not measured in his work). This interpretation is questionable because the data analyzed were the average value from six different materials. Nevertheless, the effect of temperature on different materials may various largely.

Additionally, Greason (2000) found the interaction between the effect of relative humidity and temperature on contact electrification. At a high temperature, the effect of relative humidity was more distinct (charge decreases as relative humidity increased), and when the relative humidity was at a higher level, the effect of temperature on static generation was enhanced. The reason was not explained in his paper, but this could be due to the fact that, as there was more water vapor in the air at higher temperature when the relative humidity percentage is the same (Figure 2.21). Therefore, the effect of moisture was stronger under lower temperature.

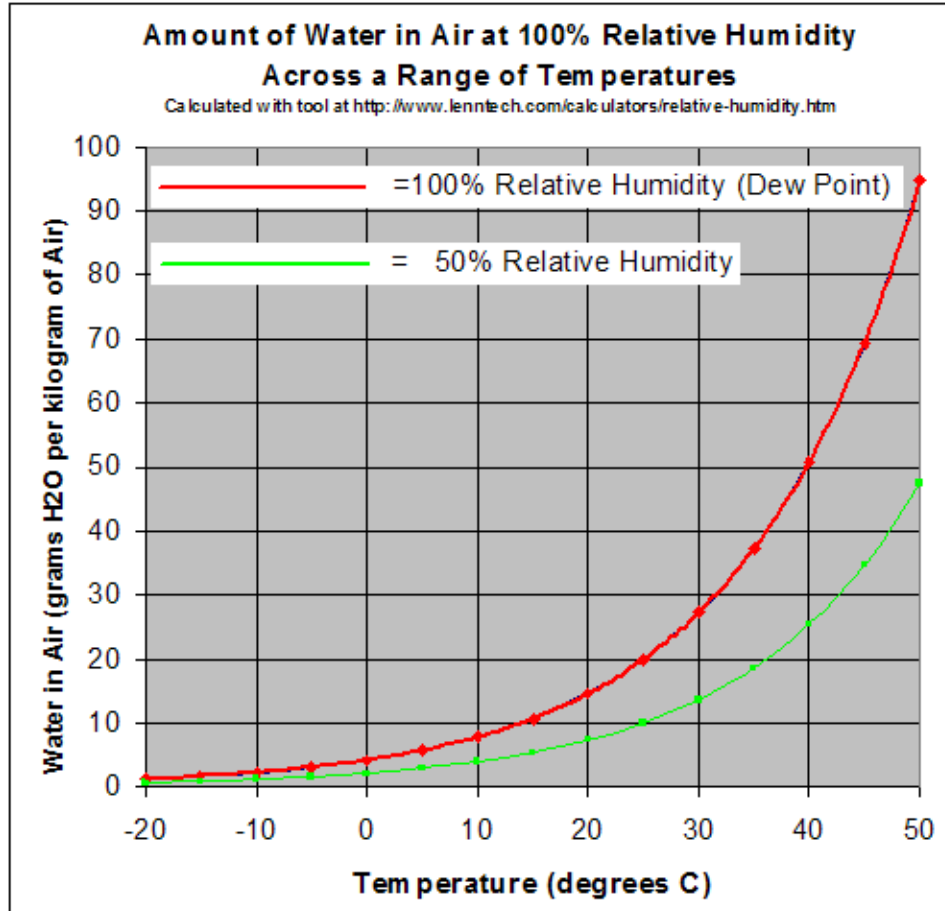


Figure 2.21 Effect of temperature on the amount of water in air ^(Wikipedia_Humidity)

$$RH = \frac{p_{(mixed)}}{p_{(saturated)}} \times 100\%$$

RH is relative humidity of the mixture $p_{(mixed)}$ is the pressure of water vapor in the mixture, and $p_{(saturated)}$ is the saturated vapor pressure of water at the temperature of the mixture

2.5.9 Effect of air pressure

Keiji Ohara (1988) studied the potential on a steel ball in repeating contact with a polymethyl methacrylate plate. He observed the saturation value at four different atmospheric pressures, and found it is the minimum at 1×10^3 Pa. This agreed with the “Paschen’s Law” (Figure 2.22), which studied the breakdown voltage of parallel plates in

a gas as a function of pressure and gap distance. The voltage necessary to arc across the gap decreased as the pressure was reduced. As the pressure was reduced below a torr, the curve of breakdown voltage versus pressure reaches a minimum, and then as the pressure is further reduced, rises steeply again (Paschen, 1889).

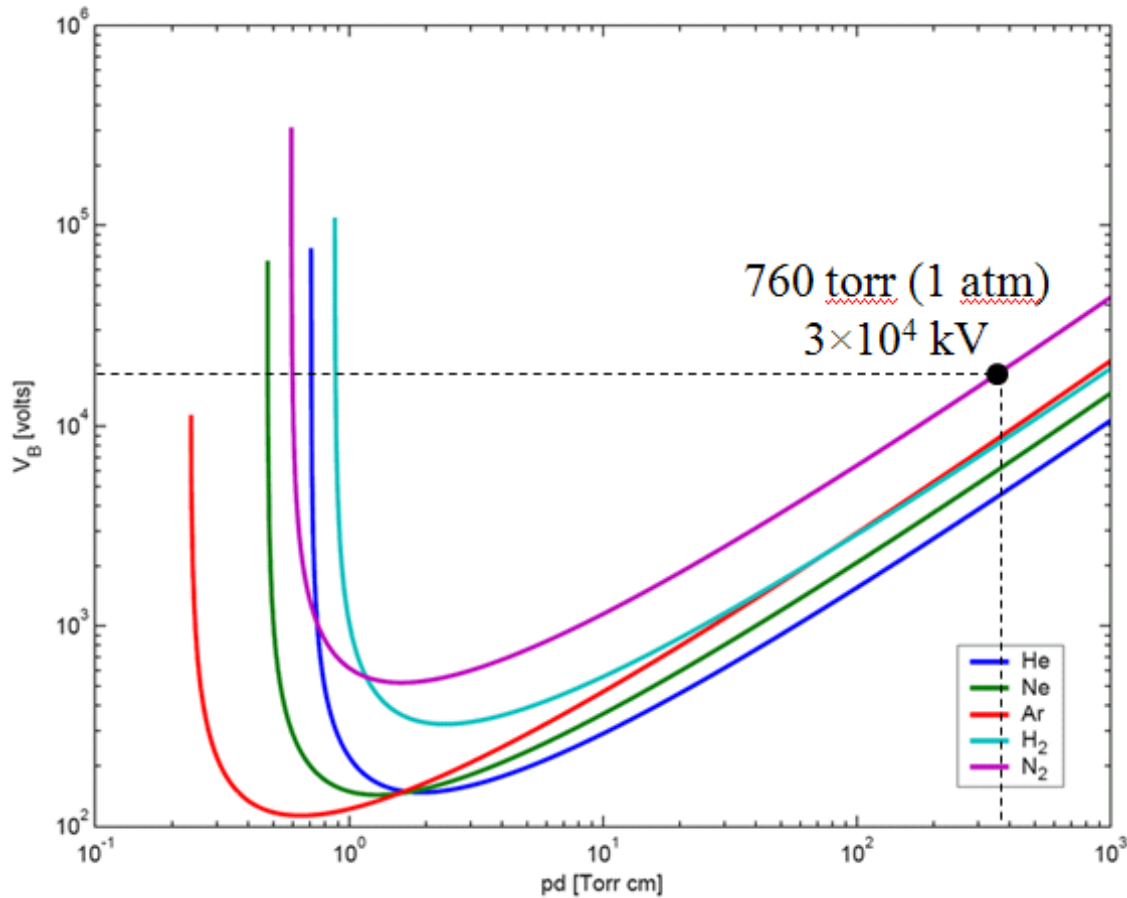


Figure 2.22 Paschen curves obtained for Helium, Neon, Argon, Hydrogen and Nitrogen, using the expression for the breakdown voltage, V_B as a function of the parameters pd , where, p is the pressure (torr), d is the gap distance (cm) between two parallel plates.

2.5.10 Effect of rubbing speed

The effect of rubbing speed on charge generation has been reviewed in section 2.3.2. In this part, the experimental results of some previous work will be introduced.

- 1) Frictional charging between yarn sections

Hersh and Montgomery (1955) investigated the influence of speed on yarns' tribo-electrification by rubbing yarns (viscose, nylon, cotton, polyethylene, polyvinyl chloride) against each other and by rubbing yarn against metal wires (aluminium, stainless steel, magnesium, and platinum). In their experiments, a top yarn or wire moved over a fix bottom yarn at different levels of speed. The rubbing motion direction was 45° to both yarns, therefore, fresh surface is always contacting fresh surface, which was called "symmetric rubbing". The bottom yarn together with other elements were enclosed in a Faraday cage, so that the charge generated on the bottom yarn was measured by a electrometer at about 90% resolution. It was found that for yarns other than polytetrafluoroethylene (PTFE), the charge was independent of speed when they rubbed against each other. When PTFE rubbed against other yarns, the charge was increasing with velocity sometimes. For all other yarns except PTFE rubbing against metals, the charge was found to increase linearly with velocity until a threshold value was reached, and then to remain constant. When PTFE and metals were rubbed together, the charge increased linearly with velocity without reaching a maximum. All their tests were conducted inside a chamber, where the temperature and humidity was simply controlled by enclosed heater and solutions.

2) Frictional charging between continuous moving yarn and stationary pin

Another study on the effect of rubbing speed was conducted by London (1966) by transporting continuous filament yarns over a stationary guider at different levels of speed inside a chamber. It was observed that charge increased with an increase of yarn speed for polypropylene and polyester over stainless steel or aluminium guides. However, the effect of yarn speed was a decrease in charge generation with an increase in yarn speed for all other combinations (polypropylene or polyester against ceramic guide, acetate or fibreglass against stainless steel, aluminium, or ceramic guides). Furthermore, they observed an increase in yarn speed for nylon on aluminium and stainless steel yielded a decrease in negative charge, a shift of sign, and an increase in positive charge generation. Their testing temperature and humidity are kept "constant" by continuous air feed and return. The cleaning of guiders was not mentioned in his procedures or not

conducted. From these previous works, the effect of speed on yarns' electrification is not consistent and there has been no universal agreement on the effect of speed on tribo-electrification.

3) Frictional charging between polymeric film and substrate cylinder

Ohara (1980) investigated the tribo-electrification by rotating a metal cylinder at different levels of rubbing speed and environmental temperature against a stationary polycarbonate film wrapped over the cylinder. The surface potential of the film was measured by an electrometer fixed inside the metal cylinder with a hole on the cylinder's surface, which allowed the electrode to detect the charge on the polymer film surface covered on the cylinder. The experiments were conducted inside a temperature and humidity regulated chamber. The electrification showed a maximum value and then decreased as the rubbing speed increased. It was pointed out that the electrification on polymers' surfaces was related to the relaxation process of the deformed molecular chains. He proposed that charge reached a maximum value when the frequency of appearance of polymer segments to the surfaces by thermal motion (temperature dependent) coincides with the frequency of surfaces mechanical contact/separation.

Ohara (1980) studied the dependence of rubbing speed and temperature in frictional electrification. He found the charge kept decreasing with the increasing friction speed in the range of 0.001 to 100 mm/s (very low speed range) when the temperature was 30 °C. Moreover, the charge had peak values at 0.02, 0.069 and 3.6 mm/s when the environmental temperatures were 45, 60 and 80 °C, respectively. Further, the charge kept increasing with the increasing speed at 100 and 110 °C, which suggested that the peaks might exist above their speed limit. Therefore, they concluded that the peak shifted to a higher friction speed region with increasing temperature. The peak position was explained as when the in/out frequency of polymer surface segments by thermal motion coincided with the contact/separation frequency of surfaces mechanical friction, the probability of molecular contact became largest and the number of transferred charges became largest.

4) Frictional charging between rotating polymeric disks

Komatsu (Komatsu, 2004) conducted asymmetric rubbing between eight different polymers, which were prepared in plastic disk shape. The electrostatic was generated by rotating two disks side by side at two different rotational speeds. Charge generated on each disk was monitored by a surface electric potential sensor with 1.5-2 mm spacing to the edge of each disk. They found that when positively charge was generated on the slow rotating disk, its charge magnitude was larger than that generated on the other disk. This was explained by the thermal diffusion of electrons due to a temperature gradient, because the temperature of slow rotating disk should be higher than that of the faster rotating disk. However, this rule could not be applied to the cases in which the slow rotating disk was negatively charged. They could not explain the instability. Their experiments were conducted in different conditions, vacuum, Nitrogen gas, and atmospheric air, all of which gave the similar results except the charge diffusion seemed larger in normal air.

From these previous works, the results about effect of rubbing speed on yarns' electrification were not consistent. This might be caused by some limitations in their equipments and measurements. First, the surfaces cleaning and conditioning procedures were not emphasized, which were a key factor for the electrification. Secondly, the charge measurements were questionable. The devices (e.g. the Faraday cage and the Field mill) calibration was not mentioned and the relative position between these devices and the charged surface had to be kept precisely constant. Third, the environments were all controlled by chambers, which might not be reliable. Last but not the least, the devices and procedures were complicated. These could have caused the issue of measuring not accurate and not repeatable.

2.5.11 Effect of system shape

Static phenomenon can also be affected by the shape of charged surface and the arrangement of nearby conductors. For example, the electrical field outside a yarn is $4\pi\sigma$ (σ is charge density), if gaseous discharging happen, it requires $4\pi\sigma=30$ KV (dielectric strength of air). Therefore, the discharging requires σ to be 8 e.s.u./cm². However, this

calculation has error in experiment, because usually the field force lines are not uniform in one direction. If the electrified surface has a small radius of curvature, the emerging field force line will diverge rapidly and the field will fall rapidly with distance from the charged surface, which reduce its ability to break the air. Therefore, the required charge density for air breaking should be higher than the calculated value. Medley ⁽¹⁹⁵⁴⁾ predicted the charge distribution around a yarn section, which was close to the contact/separation point with a metal roller. He summarized that the charge distribution was related to the shape of charged surface and the placing of nearby conductors. In the present work, static generation and dissipation on the same polymer but different shapes will be investigated and compared. On the other hand, the nearby conductors may affect the field distribution. The static can adjacent to nearby surface electrodes even without contact ^(Baum, Lewis, & Toomer, 1977). Therefore, in the present work, the bodies of static generation apparatus are all well grounded and their structures are kept consistent for each test.

2.5.12 Effect of yarn blending

It has been proved that a judicious combination of fibers from the triboelectric series can effectively reduce the static problem (Ballou, 1954). This was first noticed in textile processing that static was influenced by the blend ratio of different fibers. Then spun yarns of different compositions of nylon and Dacron were tested on purpose by rubbing against chrome-plated surface. It was found that no net charge observed somewhere between 40% and 50% nylon content as shown in Figure 2.23. Even though there are a large number of positive and negative charges, the blend is essentially static-free. This phenomenon was also seen when rubbing the same yarns against cotton and around 75% nylon is required for neutrality as shown in Figure 2.24. It was explained by the reason that, in the electrostatic series, cotton has a position in between nylon and Dacron, which means that some blend composition of nylon and Dacron should be neutral to cotton. This was also observed that none of the compositions of nylon and Dacron polyester could be neutral to wool because wool is even above nylon in the series. Table 2.9 summarized the yarn components, rubbing materials, and the optimum fiber blend when

the neutral point was achieved. In addition, knit fabrics behaved similar to the yarns when rubbing against chrome-plated surface, with neutrality requiring 40%-50% nylon.

It was pointed out that the most satisfactory blend is the one in which the fiber are mixed as intimately as possible, such as occurs in staple blends. Yarn blends, made by plying two different yarns, or weave blends, made by using one yarn as a filling and one as a warp, would be much less satisfactory. However, no evidence was shown and it is questionable. For example, when 50% of nylon was blended in a picker, as the method used in the work of Ballou, the percentage of nylon fiber on the yarn surface might not be 50% any more due to the spinning process, while static phenomenon is generally surface phenomenon and mainly due to the surface component. Therefore, blending in the intimate process may not give the accurate result of an optimum composition.

Table 2.9 Optimum fiber blend for staple yarn to minimize charge

Fiber A	Fiber B	Rubbing Material	Blend (A/B)
Nylon	Dacron Polyester	Chrome	40/60~50/50
		Cotton	70/30
		Wool	100/0
	Orlon acrylic	Chrome	20/80
		Cotton	70/30

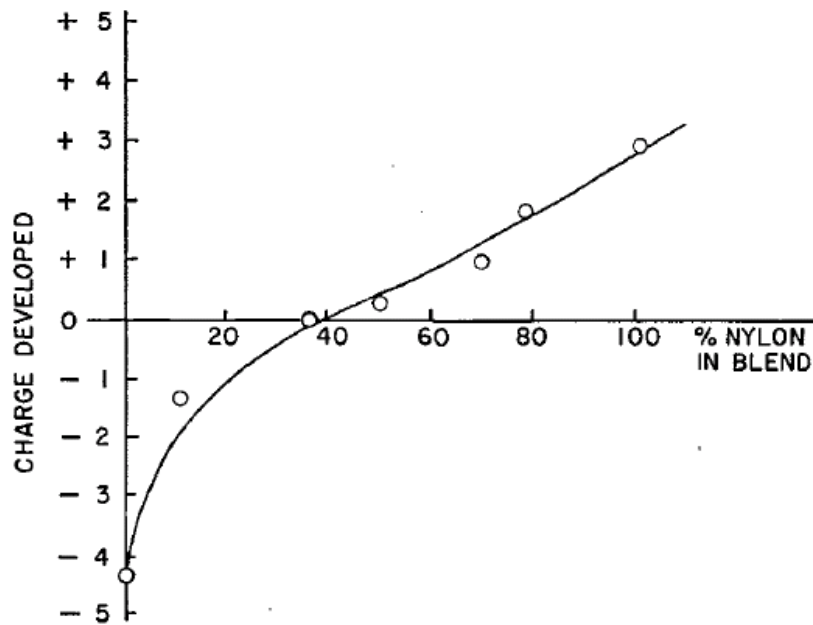


Figure 2.23 Blends of nylon-Dacron polyester staple-charge developed against chrome-plated surface.

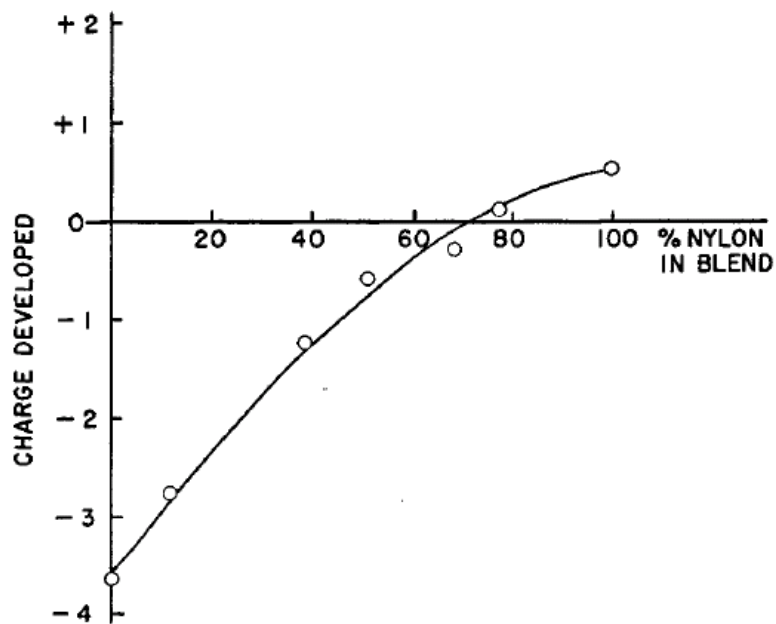


Figure 2.24 Blends of nylon-Dacron polyester staple-charge developed against cotton

2.5.13 Effect of surface components and structure

The electrostatic properties of polymers are decided by their surface chemical components. The Xerox Corporation investigated the static polarities of series of substitute styrene and n-butyl methacrylate copolymers. They found chemical groups, like NH_2 , OCH_3 , CH_3 , C_2H_5 , OH , H , are electron repelling, which causes the surface be positively charged. Some chemical groups, like Cl , Br , I , COCH_3 , NO_2 , are electron attracting, which made the surface charged negatively.

Many works have been done in this field, for example, Hays ⁽¹⁹⁷⁴⁾ found the contact charging between polyethylene and liquid mercury increased a lot when it was exposed to ozone. For another example, Lowell and Brown (1980) found polyvinyl alcohol was charged positively in contact with metals. However, after the surface OH group was converted to halogen (F , Cl , Br , and I), it was negatively charged under the same condition. Furthermore, Gibson et al (1979) found a linear relationship between the charging amount of polymer and the mole percent conversion to its substituted version.

In addition to the surface's chemical components, their structures are also important, which governs whether it is easy for the chemical segments to break to participate in the charge exchanging. As mentioned in electronic transfer mechanism, the surface impurities proved donor or acceptor energy states for the electron exchanging. Some of impurities come from the environment; some of them are intrinsic, which are segments loosed from the polymer chains. Lowell and Rose-Innes (1980) gave the sources of intrinsic impurities for different structures as shown in table 2.10.

Table 2.10 Intrinsic impurities for different structures(1980)

Structure	Intrinsic Impurities
Covalently bonded crystals	Dangling bonds
Ionic crystal	Perturbed orbital isolated ions
Molecular solids	Weak molecular interactions

In the present work, it is considered that polymer surfaces are typical molecular solids composed of irregular crystalline and amorphous area. It is much easier for the segment to break in the amorphous area than in the crystalline area. Therefore, polymers

structures of more amorphous area may have more intrinsic impurities on their surface, which make them easier to be charged, vice versa. The general agreement of the materials' crystallinity used in the present work is shown in Table 2.11. The static accumulation on these polymers will be observed to find the effect of their structure.

Table 2.11 Fiber crystallinity (Morton & Hearle, 2008)

Material	Crystallinity (%)
Nylon	40
PET	40
PP	80

2.5.14 Triboelectric series

Despite the complicated effects, it is possible to arrange materials in a “triboelectric series” from rubbing plants of materials against each other. With the triboelectric series, it is easy to figure out the charge polarity in contact or rubbing with another material. Materials at the top of the series (positive end) will charge positively when rubbed against those lower (negative end) in the series. Table 2.12 shows triboelectric series developed by different researchers, where the series established by Hersh and Montgaomery was cited in literatures most frequently.

Most of the work for determining the electrostatic series was made by asymmetric rubbing rather than by contact (Lehmicke, 1949) (Ballou, 1954). There are a few conflicts between different people's series, for example, the sequence between wool and nylon, but most of the results agreed with each other. One thing need to be noted is that fibers containing amide groups, for example, wool, nylon, and silk, are at the positive end of the series, and hydrocarbons and halogenated hydrocarbons, such as polyethylene and Saran (PVC) are at the negative end. Wool, silk, and nylon have significantly higher dielectric constants than that of polyethylene and Saran.

Most of the triboelectric series only gave the information on charge polarity, but did not conclude on the difference of charge magnitude when rubbing against different materials. However, it is mentioned in some research (Welker, Nagarajan, & Newberg, 2006) that, if two materials were contact and separated, the charge magnitude would

probably be greater if two materials are farther away from each other in the triboelectric series.

Table 2.12 Triboelectric series

Smith, East, Brown and Wake(1988)	Tsuji and Okada (1985)	Hesh and Montgomer y (1955)	Coehn (1898)	Henniker (1962)	Adams (1987)	Diaz and Felix- Navarro(20 04)
Wool*	Glass	Wool	Nylon 6.6	Silicone elastomer	Air	Poly(vinyl- 2-pyridine)
Hercosett wool	Nylon 6.6	Nylon	Cellulose	Voroslicate glass	Human hands	Nylon 6.6
Nylon 6.6	Nylon 6	Viscose	Cellulose acetate	Window glass	Asbesto s	Polyvinyl alcohol
Nylon 6	Wool	Cotton	Polymethyl methacrylate	Aniline- formol resin	Rabbit fur	Polycinyl acetate
Silk	Silk	Silk	Polyacetate	Polyformalde hyde	Glass	Polymethyl e methacrylat e
Regenerated cellulose	Viscose	Acetate	Poly(ethylene terephthalate)	Polymethyl methacrylate	Mica	Polycarbon ate
Cotton	Vynylon (PVAlc)	Lucite (PMMA)	Polyacylonitrile	Etylcellulose	Human hair	Polystyrene
Poly(vinyl alcohol)(PVAI c)	Acrilan (Acrylic)	PVAIc	Polyvinyl chloride	Polyamide 11	Nylon	Polypropyle ne
Chlorinated wool	Steel	Dacron (Polyester)	Polybisphenol carbonate	Polyamide 6.6	Wool	Polyimide
Cellulose triacetate	Cotton	Orlon (Acrylic)	Polychloroether	Rock salt (NaCl)	Fur	Polyethylen e terephthalate
Calcium alginate	Orlon (Acrylic)	PVC	Polyvinylidene chloride	Melaime formol	Lead	Polyvinyl chloride
Acrylic	Acetate	Dynel (VC/AN)	Poly(2,6- dimethy polyphenylene oxide	Wool	Silk	Polytetraflu oroethylene
Cellulose acetate	Dynel (VC/AN)	Velon (VDC/VC)	Polystyrene	Silica	Alumin um	

Table 2.13 Continued

Polytetrafluoroethylene (PTFE)	Saran (PVDC)	Polyethylene	Polyethylene	Silk	Paper
Polyethylene	Rhovyl (PVC)	Teflon (PTFE)	Polypropylene	Polyethylene glycol succinate	Cotton
polypropylene	Rubber			Cellulose acetate	Steel
Poly(ethylene terephthalate)				Polyethylene glycol adipate	Wood
Poly(1,4-butylene terephthalate)				Polydiallyl phthalate	Amber
Modacrylic				Cellulose acetate	Sealing wax
Chlorofibre				Sponge	Hard rubber
				Cotton	Nickel, Copper
				Polyurethane elastomer	Brass, Silver
				Styrene-acrylonitrile copolymer	Gold, Platinum
				Styrene-butadiene copolymer	Sulfur
				Polystyrene	Acetate, Rayon
				Polyisobutylene	Polyester
				Polyurethane sponge	Styrene (Styrofoam)
				Borosilicate glass	Orlon
				Polyethylene glycol terephthalate	Saran
				Polyvinyl butyral	Polyurethane

Table 2.14 Continued

Formo-phenolique	Polyethylene
Eposide resin	Polypropylene
Polychlorobutadiene	Vinyl (PVC)
Butadiene-acrylonitrile copolymer	Silicon
Natural rubber	Teflon
Polyacrilonitrile	
Sulfur	
Polyethylene	
Polydiphenylol propane carbonate	
Chlorinated polyether	
Polyvinyl chloride	
Polytrifluorochloroethylene	
Polytetrafluoroethylene (PTFE)	

2.5.15 Anti-static technology in textiles

An antistatic agent is a compound used for treatment of materials or their surfaces in order to reduce or eliminate buildup of static electricity generally caused by the triboelectric effect.

While there has been considerable discussion concerning the controlling of static through the use of ionizing atmosphere or through air conduction, the most prevalent approach for the static controlling in fibers and plastics is to modify the surface. There are mainly two methods: treatment by antistatic agent and incorporating with conductive fibers. For the antistatic agents, they can reduce the static by being conductive themselves,

or by absorbing moisture from the air. Most of the antistatic agents are kinds of surfactants, which are composed of hydrophilic and hydrophobic parts. The hydrophobic side interacts with the surface of the material, while the hydrophilic side interacts with the air moisture and binds the water molecules to improve the static dissipation. If the introduction of agents is by chemical bonding, it requires the modification should not affect the original property of the material. If the introduction is just coating without chemical reaction, it needs to be strongly attached on the surfaces (Holme, McIntyre, & Shen, 1998).

Conductivity of a fibrous assembly can be improved by incorporating conductive fibers such as carbon, copper, steel, silver, etc. or using fibers, which have been “treated” with metallic salts (Holme, McIntyre, & Shen, 1998). A recent alternative is the use of bi-component fibers where one component is conductive (Bharat, 2005) and there is currently a lot of interest in the use of fibers containing carbon nanotube (Puetz & Aegerter) (Lo, Li, Yeung, & Yuen, 2007).

Plasma treatment can be used to improve the anti-static property of textiles. After the plasma treatment, people have found the polyester surface was seriously etched, which provided more capacity of the surface to capture moisture and hence to increase the static dissipation. Moreover, because oxygen-containing polar groups were introduced by plasma treatment onto the surface, which could incorporate with moisture through hydrogen bonding and help moisture penetration, therefore, enhanced electrostatic dissipation (Kan & Yuen, 2008). The antistatic mechanism of plasma treatment is very different from the agents coating or conductive fiber blending. It is environmentally friendly, but it is higher cost now.

There are specialized anti-static performance apparel products. The static on human body is especially dangerous because the high conductivity of body and the large capacitance of clothing-body system. Therefore, most of the antistatic apparels are grounded by electrical continuity across all fabric panels, which are connected to a ground cord (Bharat, 2005). Kowalski et al. summarized some principles of static protection, and different evaluation systems and standards (Kowalski & Wroblewska, 2006).

The study of conductive fibers or plasma treatment for static control is not within the scope of the present work. However, when considering the effect of topical applied agents, though it has been widely recognized that minor changes in the composition can lead to significant changes in the static accumulation, there have been no systematic studies in this topic. The present project will apply non-ionic, cationic, and anionic agents on polymer surfaces at different concentration to observe their static phenomenon, which can provide constructive suggestions for the industry cooperators and may open the possibility of completely new approaches to the control of static in fiber processing environment.

REFERENCES

- Anti-Static Technology in performance Apparel. (2005). *Technical Textile Markets* , 4.
- Armstrong-Helouvry, B. (1991). *Control of machines with friction*. Norwell: Kluwer Academic Publishers.
- ESD association standard for the development of an electrostatic discharge control program for - protection of electrical and electronic parts, assemblies and equipment*. New York: Electrostatic Discharge Association.
- ASTM D 4470-97 Standard test method for static electrification. (n.d.).
- Awakuni, Y., & Calderwood, J. H. (1972). Water Vapor Adsorption and Surface Conductivity in Solids. *J. Phys. D: Appl. Phys.* , 5, 1038.
- Ballou, J. W. (1954). Static Electricity in Textiles. *Text. Res. J.* , 24 (2), 146-155.
- Baum, E. A., Lewis, T. J., & Toomer, R. (1977). Decay of Electrical Charge on Polyethylene Films. *J. Phys. D: Appl. Phys.* , 10, p. 487.
- Bauser, H. (1974). Static electrification of organic solids. *Dechema Monograph* , 72, 11-28.

Briggs, D. (1979). The Role of Modern Surface Analysis Techniques in Understanding Electrification Phenomenon. In D. Briggs (Ed.). The Institute of Physics.

Cardona, P. Y. (2001). *Fundamentals of Semiconductors (3rd Edition ed.)*.

Castle, P. (2004). Contact Charging between Metals Revisited. *40* (5).

Castle, P. G. (1997). Contact Charging between Insulators. *Journal of Electrostatics* , *40-41*, 13-20.

Charles, D. H., & Norbert, A. L. (1925). *Handbook of Chemistry and Physics 10th Edition*. Cleveland, OH: Chemical Rubber Publishing Co.

Chowdry, C. R., & Westgate, A. (1974). The Role of Bulk Traps in Metal Insulator Charging. *7*, 713-725.

Chubb, J. (2002). New Approaches for Electrostatic Testing of Materials. *54*, 233-244.

Clark, T. D., & Feast, J. W. (1978). *Polymer Surfaces*. New York: John Wiley & Sons.

Coste, J., & Pechery, P. (1981). Influence of Surface Profile in Polymer-Metal Contact Charging. *10*, 129-136.

Cowley, A. M., & Sze, S. M. (1965). Surface States and Barrier Height of Metal-Semiconductor Systems. *Journal of Physics* , *36*, 3212.

Cunningham, S., & Goodings, A. (1986). Plastic Deformation and the Transfer of Electrostatic Charge between Metals and Polymers during Repeating-Contact Experiments. *J. Electrostatics* , *18*, 103.

Davies, D. K. (1978). Corona Charging and the Piezoelectric Effect in Polyvinylidene Fluoride. *J Appl Phys* , *49*, 4601-4603.

Davies, D. K. (1967). The Examination of the Electrical Properties of Insulators by Surface Charge Measurements. *44*, 521-524.

Davis, D. K. (1970). Charge Generation on Solids. *Adv. Static Electricity* (1), 10.

Diaz, S., Fenzel-Alexander, D., Wollmann, D., & Eisenberg, A. (1991). Effect of Ionomer Ion Aggregation on Contact Charging. *J. Polym. Sci. Polym. Phys.* , *29*, 1559.

Dielectric Constant Reference Guide. (n.d.). Retrieved from http://www.clippercontrols.com/info/dielectric_constants.html#P

Fabish, T. J., & Duke, C. B. (1977). Molecular Charge States and Contact Charge Exchange in Polymers. *J. Appl. Phys.* , 48, 4265.

Field, R. F. (1946). The Formation of Ionized Water Films on Dielectrics under Conditions of High Humidity. *J. Appl. Phys.* , 17, 318.

Gas Gupta, K. D., & Doughty, K. (1978). Corona Charging and the Piezoelectric Effect in Polyvinylidene Fluoride. *J Appl. Phys* , 49, pp. 4601-4603.

Gibbings, J. C. (1975). On the Fitting of Exponential Curves to Experimental Results. *Journal of Electrostatics* , 187-192.

Gibson, H. W., Bailey, F. C., Mincer, J. L., & Gunther, W. H. (1979). Chemical Modification of Polymers: XII Control of Triboelectric Charging Properties of Polymers by chemical Modification. 17, 2961-2974.

Greason, W. D. (2000). Investigation of a Test Methodology for Triboelectrification. *Journal of Electrostatics* , 49, 245-256.

Gupta, S. B. (2007). *Friction in textile materials*. London: Woodhead.

Hanton, W. A. (1924). *Mechanics of Textile Machinery*. Manchester: Longmans.

Harper, W. R. (1957). The generation of static charge. *Advances in Physics* , 6 (24), 365-417.

Hays, D. A. (1974). Contact Electrification between Mercury and Polyethylene: Effect of Surface Oxidation. 61, 1455-1462.

Hays, D. A. (1991). *Fundamentals of Adhesion*. New York: L.H. Lee Ed. Plenum Press.

Hays, D. A., & Donald, D. K. (1971). *Effect of an Electric Field on the Contact Electrification of Polymers by Mercury*. Conference on Electrical Insulation and Dielectric Phenomena.

Hearle, J. W. (1953). The electrical resistance of textile materials: I.the influence of moisture content. *Journal of the Textile Institute Transactions* , 44 (4), 117-143.

Hearle, J. W. (1953). The electrical resistance of textile materials: II.the effect of temperature. *Journal of the Textile Institute Transactions* , 44 (4), 144-454.

Hearle, J. W. (1953). The electrical resistance of textile materials: IV.theory. *Journal of Textile Institute Transactions* , 44 (4), 177-198.

- Henry, H. P. (1957). Overseas conference-static electricity in textiles. *Journal of Textile Institute* , 48 (1), 4-122.
- Hersh, S. P., & Montgomery, D. J. (1956). Static Electrification of Filaments-Theoretical Aspects. *Text Res J* , 26, 903-913.
- Holme, I., McIntyre, J. E., & Shen, Z. J. (1998). Electostatic Charging of Textiles. *Textile Progress* , 28 (1), 1-84.
- Homewood, K. P., & Rose-Innes, A. C. (1979). The Effect of Contact Time on the Electrification of Polymer by Metals. 48. Inst. Phys. Conf. Ser.
- Howell, G. H., Mieszkis, W. K., & Tabor, D. (1959). *Friction in textiles*. New York: Textile book publishers in association with the Textile Institute.
- Ieda, S. M., & Shinohara, U. (1967). A Decay Process of Surface Electric Charges Across Polyethylene Film. *Japanese Journal of Applied Physics* , 6, 793-794.
- Intelligence, T. (2005). Anti-Static Technology in Performance Apparel. *Technical Textile Markets* , 4.
- Kan, C. W., & Yuen, C. W. (2008). Static Properties and Moisture Content Properties of Polyester Fabrics Modified by Plasma Treatment and Chemical Finishing. *Nuclear Instruments and Methods in Physics Research B* , 266, 127-132.
- Kanarek, J., & Tan, W. (1998). A primer on static control plastics-part 1. *Wescorp Corporation Newsletter* . Wescorp World.
- Keijo, O. (1988). A Method of Exponential Function Analysis of Contact and Frictional Electrification Curves. *Journal of Electrostatics* , 319-326.
- Komatsu, T. S., Hashimoto, M., Arakawa, I., & Nasuno, S. (2004). Static Electrification by Asymmetric Rubbing. *Applied Surface Science* , 235 (1-2), 60-64.
- Kowalski, J. M., & Wroblewska, M. (2006). Premises for Practical Evaluation of the Anti-electrostatic Properties of Protective Garments. *Fibers and Textiles in Eastern Europe* , 14 (5), 59.
- Krupp, H. (1971). Physical Models of the Static Electrification of Solids. *IOP Conf. Ser.*
- Kwetkus, B. A., Sattler, K., & Siegmann, H. C. (1992). Gas Breakdown in Contact Electrification. *J. Phys. D.: Appl. Phys.* , 25, 139.

- Labadz, A. F., & Lowell, J. (1986). Contact Charge Density and Penetration Depth. *J. Electrostatics* , 18, 103.
- Lee, L. (1994). Dual Mechanism for Metal-Polymer Contact Electrification. *Journal of Electrostatics* , 32, 1-29.
- Lee, L. H. (1978). A Surface Interaction Model for Triboelectrification of Toner-Carrier. *Photo. Sci. Eng.* , 22, 228.
- Lehmiche, D. J. (1949). Static in Textile Processing. *Am. Dyes., Rptr.* , 38 (24), 853.
- Lewis, A. R. (1999). *Dielectrics*.
- Lo, L. Y., Li, Y., Yeung, K. W., & Yuen, C. W. (2007). Indicating the Development Stage of Nanotechnology in the Textile and Clothing Industry. *International Journal of Nanotechnology* , 4 (6), 667-679.
- Lowell. (1984). Charge Accumulation by Repeated Contacts of Metals to Insulators. *J. Phys. D.: Appl. Phys.* , 17, 1859.
- Lowell. (1991). Mechanisms of Contact Charging and Charge Accumulation: Experiments on Soda Glass. *J. Phys. D: Appl. Phys.* , 24, 375.
- Lowell, J., & Rose-Innes, A. C. (1980). Contact Electrification. *Adv. Phys.* , 29, 947-1023.
- Lyne, G. D. (1955). Fiber friction. *Journal of Textile Institute* , 46 (1), 3-136.
- Ma, Z. Y., & Dickinson, J. T. (1991). Fracto-emission from Embedded Intergases. *J. Appl. Phys.* , 70, 4797.
- Medley, J. A. (1950). Frictional Electrification and Gaseous Discharge . *Nature* , 166, 524.
- Medley, J. A. (1954). The Discharge of Electrified Textiles. 45 (2).
- Mizes, H. A., Conwell, E. M., & Salamida, D. P. (1990). Direct Observation of Ion Transfer in Contact Charging between a Metal and a Polymer. *Appl. Phys. Lett.* , 56, 1597.
- Morton, W. E., & Hearle, J. W. (2008). *Physical Properties of Textile Fibres*. Cambridge, England: Woodhead Publishing in association with the Textile Institute .
- Nemeth, E., Albrecht, V., & Schubert, G. (2003). Polymer Tribo-electric Charging: Dependence on Thermodynamic Surface Properties and Relative Humidity. *Journal of Electrostatics* , 3 (16).

- Niels, J. (1998). *Electrostatics*. New York: International Thomson Publishing.
- Ohara, K. (1980). Relationship between Frictional Electrification and Molecular Motion of Polymers. *J. Electrostatics* , 9, 107-115.
- Ohara, K. (1980). Relationship between Frictional Electrification and Molecular Motion of Polymers. 9, pp. 107-115. *Journal of Electrostatics*.
- Ohara, K., Nakamura, I., & Kinoshita, M. (2001). Frictional Electrification between Flat Surfaces of Polymers and of Langmuir-Blodgett Layers. *Journal of Electrostatics* , 51-52, 351-358.
- Owen, M. J. (1990). *Electrostatic discharge control*. New York: McGraw-Hill Publishing Company.
- Paschen, F. (1889). Ueber die zum Funkenübergang in Luft, Wasserstoff und Kohlensäure bei verschiedenen Drucken erforderliche Potentialdifferenz. *Annalen der Physik* , 5, pp. 69-75.
- Pascoe, M. W., & Tabor, D. (1956). The Friction and Deformation of Polymers. *A235* (210).
- Patterson, J. D., & Bailey, B. C. (2007). *Solid-state physics : introduction to the theory*. Berlin : Springer.
- Pethig, R. (1983). The Physical Characteristics and Control of Air Ions for Biological Studies. *J Bioelectricity* , pp. 15-35.
- Puetz, J., & Aegerter, M. A. Chemical Nanotechnology for Transparent Conducting Coating on Thin-glass and Plastic-foil Substrates. *Journal of the Society for Information Display* , 13 (4), 321-328.
- Rigden, J. S. (1996). *Macmillan Encyclopedia of Physics*. Simon & Schuster.
- Robins, E. S., Rose-Innes, A. C., & Lowell, J. (1975). Are Adsorbed Ions Involved in the Contact Charging between Metals and Insulators? 27. *Inst. Phys. Conf. Ser.*
- Rose, S. G., & Ward, G. S. (1957). Contact Electrification Across Metal-Dielectric and Dielectric-Dielectric Interfaces. *J Appl. Phys.* , 121.
- Rose-Innes, A. C., & Homewood, K. P. (1982). An Accumulation of Contact Charge on Insulators Repeated Touched by Metals. *J. Phys. D., Appl. Phys.* , 15, 2283.
- Rose-Innes, A. C., & Lowell, J. (1980). Contact electrification. 29, 947-1023.

- Ruckdeschel, R. F., & Hunter, P. L. (1977). Thermionic return currents in contact electrification. *Journal of Applied Physics* , 48 (12), 4898-4902.
- Sawa, G., & Calderwood, J. H. (1971). Dependence of surface Conduction Current in Oxidized Polyethylene on Electric Field at Various Humidities. *J. Phys. C: Solid St. Phys.* , 4, 2313.
- Sereda, P. J., & Feldman, R. F. (1964). Electrostatic charging on fabrics at various humidities. 55 (5), T288-T298.
- Serway, R. A., & Jewett, J. W. (2007). *Physics for Scientists and Engineers*, 7 edition. Brooks Cole.
- Taylor, D. M., & Secker, P. E. (1994). *Industrial Electrostatics: Fundamentals and Measurements*. Tanton, Somerset, England: Research Studies Press; New York: J. Wiley.
- Tipler, P. A. (1987). *College Physics*. Worth.
- Welker, R. W., Nagarajan, R., & Newberg, C. E. (2006). *Contamination and ESD control in high-technology manufacturing*. New Jersey: John Wiley & Sons, Inc.
- Welker, R. W., Nagarajan, R., & Newberg, C. E. (2006). *Contamination and ESD Control in High-technoogy Manufacturing*. New Jersey: Wiley & Sons, Inc.
- Wikipedia_Humidity*. (n.d.). Retrieved from <http://en.wikipedia.org/wiki/Humidity>
- Yager, W. A. (1947). *Digest on Literature on Dielectrics* (Vol. X). Murray Hill, NJ: Bell Telephone Laboratories.
- Yu, Z. Z., & Watson, P. K. (1989). Contact Charge Accumulation and Reversal on Polystyrene and PYFE Films upon Repeated Contacts. *Journal of Physics D: Appl. Phys.* , 798.
- Zimmer, E. (1970). Electrostatic Charging of High-Polymeric Insulating Materials. 60, 465-468.
- Zimmerman, K. A., Langford, S. C., & Dickson, J. T. (1991). Electrical Transients during Interfacial Debonding and Pullout of a Metal Rod from an Epoxy Matrix. *J. Appl. Phys.* , 70, 4808.

3 OBJECTIVES

The literature review indicates that despite of plenty of research in the area of electrostatic generation and control, there has not been a universally agreed explanation regarding the mechanism of static generation and dissipation, and there are still questions, which have not been answered, such as:

- Does rubbing speed affect charge generation on polymers?
- What is the effect of contact force between two surfaces on contact and frictional electrification?
- Is charge generated on nylon higher than that generated on the other polymers, such as PP and PET?
- Does charge on polymeric surfaces decay exponentially?
- What is the difference of antistatic effect of nonionic, cationic, and anionic finishes, when they are applied on polymer surfaces?
- What is the minimum concentration of surface finish required to control static on polymer surface?

The literature review also indicates that there are discrepancies among published research, For example, nylon was generally positively charge after rubbing against stainless steel, however, it was sometimes negatively charged (London, 1966). Another example, charge was not always increased with rubbing speed (Hersh and Montgomery, 1955). Possible explanations for those disagreements are the differences in sample preparation, experimental procedures, and coupling effect with the level of accuracy of the systems used. The literature review on the measurement of electrostatic generation and dissipation (section 2.5) disclosed a number of drawbacks:

- Initial surface cleaning procedures (prior to testing) were not emphasized (or not mentioned) in their reports (Hubbard, 1967) (Robins, Rose-Innes, & Lowell, 1975) (London, 1966) . However, the sample cleaning is a critical issue because even one molecular layer of contamination could dramatically change the surface's electrification properties (ASTM 4470-97);
- Calibration for charge detecting devices was not mentioned in those reports (Medley, 1954) (Ohara K. , 1980) (Hersh & Montgomery, 1956). However, static

signal are extremely sensitive and thus the detecting devices must be calibrated regularly under the same environmental conditions as formal testing.

- The testing conditions were established by sealed chambers using different chemical solutions to vary humidity, which might be limiting (London, 1966) (Medley, 1954);
- Manual testing for contact or rubbing is susceptible to subjective error (Chubb, 2002, Sereda and Feldman, 1964);
- The accuracy of the measurement is questionable due to the manual transfer of sample to the measuring unit (Chubb, 2002, Sereda & Feldman, 1964);
- Charge generated on sample surface was predicted from charge measured on another material, which is connected with or contacted against the sample. However, this could not reflect the real charge generated on sample surface since different surfaces have different charge capacities and resistance (Robins, Rose-Innes, & Lowell, 1975).
- Last but not the least, the devices and procedures used were very complicated and this could have led to reduced accuracy and questionable repeatability of results (Ohara, 1980, Hersh and Montgomery, 1955).

Those discrepancies reported on electrification of polymers and the limitations of previous studies promoted the undertaking a more comprehensive research in this area, using advanced charge detecting devices, motion control systems, environmental control system, and consistent sample preparation and testing procedures.

The overall goal of this project is to obtain a better understanding of the mechanism of static behavior of polymeric surface, and to find the effects of different parameters, such as the rubbing speed, contact force, relative humidity, temperature, and surface finishes, on static generation and dissipation of commonly used polymers in textiles. This work is expected to provide the industry with evaluation techniques that support the development of polymeric products with enhanced processing and performance properties.

The objectives are achieved through conducting experiments using three devices, a linear tester, a rubbing tester, and a contact tester. The devices and signal analysis are

described in Chapters 4, 5, and 6. Utilizing the devices, the effects of different parameters on charge generation and dissipation were studied. Chapter 4 discusses the effect of rubbing speed on charge generated between yarn and pin. Chapter 5 discusses the effects of rubbing speed and contact force on frictional electrification between parallel polymeric surfaces. Chapter 6 investigates the effects of contact force, relative humidity, and temperature on contact electrification between polymeric surfaces. In addition, Chapter 7 discusses both the contact and frictional electrification of polymeric surfaces after they are treated by three types of antistatic finishes.

4 FRICTIONAL ELECTRIFICATION OF YARN AND PIN

This chapter is modified from a manuscript entitled “Effect of relative rubbing speed on the tribo-electrification of continuous filament yarn by stainless steel pin”, by L. Liu, W. Oxenham, A. M. Seyam, and T. Theyson, which has been accepted by the *Journal of Textile Institute*.

4.1 Introduction

In the textile industry, a considerable amount of static may be generated whenever fibres, yarns, or fabrics rub over another solid. It creates hazards, affects the quality of products and the efficiency of manufacturing processes. To minimize the impact of static electrification, it is necessary to obtain a better understanding of mechanisms involved in charge generation and dissipation. A particular issue of importance to the current study is the question whether rubbing speed plays an important role in the tribo-electrification of yarns.

While a full review of previous work is given in Chapter 2, it was believed useful, to briefly include those of direct relevance to the present study. The mechanism of electrostatics was first developed by Harper (1957) and confirmed experimentally by Lowell and his colleagues (1980) who established the theory of simple contact charging between two metals. Attempts at better understanding of the contact charging of insulators was much more difficult, especially in the case of polymeric surfaces, which are irregular, not 100% crystalline, and usually contain “impurities”. Furthermore, it was found that charge could flow back from the insulator to the metal after charge generation, which caused the discrepancy between most theoretical and experimental results (Castle 1997).

Another difficulty for understanding the electrostatic phenomenon is that the tribology theory is complex, which in turn means that frictional charging is more complicated than simple contact charging. It is known that when two surfaces contact, real contact only occurs at the tips of their asperities. When sliding occurs, the real contact junctions will be sheared. The real contact area is related to the surfaces’ roughness and the asperities’ deformation properties (Howell, Mieszkis, & Tabor 1959, and Gupta, 2009). As to the complex effect of speed on friction, it was found for example, that for lubricated yarns, the coefficient of friction increased when the rubbing speed increased. This is a practical example of the added complication introduced by additives (essentially deliberately applied “impurities”) which mean that some consideration must also be given to the influence of hydrodynamic factors (Lyne, 1955). Additionally, it is also interesting to note that friction could be reduced by modulating

vibration (Armstrong-Hélouvry, 1991), which is a factor that is of significance in a moving thread line. For those approaches applied to reduce friction, their ultimate goal is usually to control the electrostatic charging and reduce wear or surface attrition of the various component surfaces. While there is much work on friction and on static electrification, the correlation between these is still not well understood.

Previous researchers have investigated the effect of rubbing speed on tribo-electrification of polymers by rubbing yarns against metals or by rubbing yarns against each other (Hersh and Montgomery, 1955, London, 1966, Ohara, 1980, Komatsu, 2004). It is evident that their reported observations were not consistent and in some cases conflict with each other. Possible explanations for this disparity are the differences in experimental procedures (equipment and measuring techniques) coupled with the accuracy of the systems used. First, initial surface cleaning and conditioning procedures (prior to testing) were not emphasized (or not mentioned) in their reports. This is a critical issue because even one molecular layer of contamination could dramatically change the surface's electrification properties (Ohara, 2001). Secondly, calibration for charge detecting devices was not mentioned in those papers, however, static signal are extremely sensitive and thus the detecting devices must be calibrated regularly under the same environmental conditions as formal testing. Thirdly, the testing conditions were established by sealed chambers using different chemical solutions to vary humidity, which might be limiting. Last but not the least, the devices and procedures used were very complicated and this could have led to reduced accuracy and questionable repeatability of results.

The discrepancy reported on tribo-electrification of polymers and the limitations of the devices used in previous studies prompted a series of projects to undertake some more comprehensive research in this area. The overall goal of this research is to obtain a better understanding of the mechanism of static electrification on polymeric surfaces based on experiments, and to relate these findings to the static charge issues in textile processing. In a previous publication (Seyam, Cai, & Oxenham, 2009), a “Linear Tester” was introduced for measuring the static charge generation and dissipation of continuous moving yarn when rubbing against a “charging pin”. In another publication (Suh et al.,

2010), the developed linear tester was used to investigate the influence of ambient conditions and processing parameters on the static generation and dissipation on polyester multifilament yarn when rubbed against a stainless steel pin.

In the present work, the charge pin on the “Linear Tester” has been modified so that it can now rotate at prerequisite speeds. This allows the study of tribo-electrification at different levels of relative rubbing speed, together with the role of absolute moving speed of the yarn and the pin. The study includes the influence of the relative rubbing speed on the tribo-electrification of different filament yarns when rubbed against different size stainless steel pins. The multifilament yarns included in the study were nylon treated with lubricant; finish free nylon; finish free polyester; and finish free polypropylene.

4.2 Experimental

4.2.1 Equipment and test protocol

The “Linear Tester” was modified and used in this work to generate and measure electrostatic charge on a moving yarn (Figure 4.1). The apparatus consists of a Constant Tension Transport (CTT) system, a rotating pin (referred to as the charge pin), two potential probes, a tensiometer, a vibration sensor, and a computer. The CTT unit (Lawson-Hemphill[®]) was calibrated and used for transporting yarn at the desired speed and input tension. The yarn output tension was monitored continuously by an onboard tensiometer. A stainless steel rotational pin was installed on the CTT, so that it created a 60° yarn/pin contact angle with the moving yarn (Figure 4.2). The pin’s rotational speed could be set at different levels and for each test and the speed was checked with a tachometer. Two potential probes (Model 1017, Monroe Electronics[®]) were used to measure the yarn surface potential. For each run, the probe-to-yarn spacing was adjusted precisely by the aid of micrometer to 3 mm when the yarn and pin were running and on the backside of the yarn; grounding metal plates were placed parallel to yarn with a 57 mm spacing. The plates acted as a background of zero potential, shielding the sensor from any stray electrical fields.

The chopped signal inside the probe is proportional to the potential difference between the yarn surface and the sensor assembly. In the setup described above, an area of 8 mm diameter in front of the probe was detected at 99% resolution (Monroe Electronics, Inc., 1991). One of the potential probes was set 3 cm away from the yarn/pin separation point, which was called probe-I, and the potential it measured was called potential-I. The other probe was 40 cm away from the yarn/pin separation point, which was named as probe-II and the potential measured was potential-II. Each probe was connected to a voltmeter (Model 244A, Monroe Electronics[®]), which can measure potential in the range ± 3 kV for 3 mm probe-to-surface spacing and this can be increased to ± 30 kV using a gradient adaptor. The probes and voltmeters were all calibrated before testing. When the adaptor was used, its position was adjusted based on the manual. The output of two voltmeters and the tensiometer were input into a computer. In addition to the charge potential and yarn tension measurement, a piezoelectric sensor (model 303A03, PCB Piezotronics[®]) was bonded to the pin/motor supporting panel and was used to monitor any possible vibration in the rotating pin. This precautionary step was taken since it was considered that unwanted vibrations could result in variations in contact and thus possible variations in tribocharging. Signals detected were recorded by a computer and analyzed automatically by SpectraPLUS[®] software. All equipment was housed inside an environmental room that can provide temperature and relative humidity control of $\pm 0.1^\circ\text{C}$ and $\pm 1.0\%$ RH.

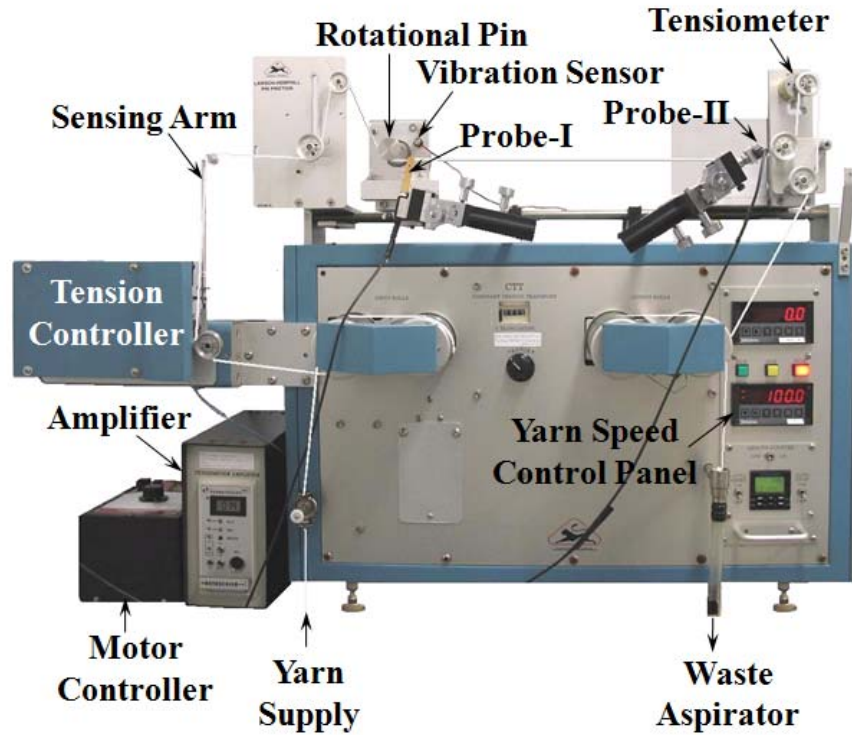


Figure 4.1 Linear Tester

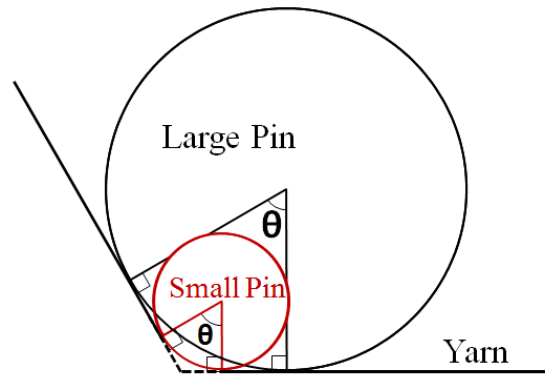


Figure 4.2 Yarn/pin contact angle (same contact angle for pins of two sizes), $\theta=60^\circ$

4.2.2 Materials and experimental designs

Two experimental designs were used for studying the effect of relative rubbing speed, V_y-V_p , on tribo-electrification of yarns against stainless steel charge pin, where V_y and V_p represent yarn speed and surface speed of charging pin, respectively. Experimental

design-I was used to investigate the behaviour of nylon with 1.2% anionic commercial lubricant, when rubbed against two different diameter pins, D_{pin} (6.35 and 25.4 mm in diameter), and three levels of yarn transporting speed. This set up facilitated a range of relative speed (V_y-V_p), since the pin could be rotated either in the same direction as the moving yarn or in the counter direction to the yarn. Experimental design-II was used to study finish free yarns of three different polymeric materials, when using a constant pin size and yarn transporting speed. Table 4.1 and 4.2 list the parameters used in each experiment.

The yarn used in experiment design-I was 420/72 nylon (420 denier comprised of 72 filaments) and the yarns used in experimental design-II were 200/60 (200 denier /60 filaments). Yarns were pre-tensioned at 0.12 cN/denier (50 cN for experimental design-I and 24 cN for experimental design-II) and all tests were conducted at a relative humidity of 43% and temperature of 21°C (suggested by AATCC Test Method 84), with all yarn samples being conditioned for one week prior to testing. The friction pin, rollers and guides on the CTT machine were all cleaned with ethanol and de-ionizing gas before running each type of yarn. All tests were conducted in a random sequence. The measurement responses are potential-I (volt), potential-II (volt), output tension (cN or gf), and vibration amplitude (dB). The data collection rate for each response was 100 points/second, and sampling time was 20 seconds for each run. Three replications were carried out for each condition. The calculated responses are contact force (cN), friction force (cN), coefficient of friction, and vibration force (cN).

Table 4.1 Experimental design-I

Parameters	Levels
Pin Diameter (mm)	6.35, 25.4
V_y (m/min)	50, 100, 150
V_y-V_p ¹ (m/min)	-150, -100, -50, -25, 0; 25, 50, 100, 150

¹: when the smaller pin was used, six speed levels were not achievable because the motor's maximum rotational speed (9140 rev/min) determined the V_p maximum to be 182 m/min.

Table 4.2 Experimental design-II (D_{pin} : 25.4 mm, V_y : 100 m/min)

Parameters	Levels
Materials	Nylon, PP, PET
V_y - V_p (m/min)	-100, -50, -25, 0, 25, 50, 100

4.3 Calculated responses

The contact force, friction force, and coefficient of friction on the yarn section in contact with pin were calculated from the yarn input and output tensions. The yarn input tension was set by the CTT machine. Its variation was within $\pm 3\%$ regardless of the speed of the yarn or the pin. This was verified by a tensiometer mounted 10 cm before the pin. The yarn moving speed was also set by CTT and the variation in speed was $\pm 1\%$, when a tachometer was used to track the machine speed. The output tension, monitored by the tensiometer, changed as the relative speed (yarn to pin) changed. The contact force and friction force on each point of contact are different; however, the total force on the yarn section in contact with pin can be calculated by equation [2-1] and [2-2] respectively.

$$N = (T_2 + T_1) \times \sin (\theta/2) \quad [2-1]$$

$$F = (T_2 + T_1) \times \cos (\theta/2) \quad [2-2]$$

where, T_1 is the absolute value of yarn tension on the looser side (cN or gf); T_2 is the absolute value of yarn tension on the tighter side (cN or gf), θ is the angle of contact (Figure 2), which is $\pi/3$ in this work; N (cN or gf) is the absolute value of contact force on the yarn section being contacted; and F (cN or gf) is the absolute value of friction force on the yarn section being contacted. The force diagrams are shown in Figure 4.3.

When the yarn/pin relative rubbing speed was negative ($V_y < V_p$), it was found that yarn output tension (T_1 in Figure 4.3 left) was smaller than the input tension. The friction force promotes the movement of the yarn, which had the same direction as the yarn output tension. When the yarn/pin relative speed was positive ($V_y > V_p$), the yarn output tension (T_2 in Figure 4.3 right) was higher than the input tension (T_1 in Figure 4.3 right). The friction force hindered the movement of the yarn so its direction was the same as the input tension on the yarn.

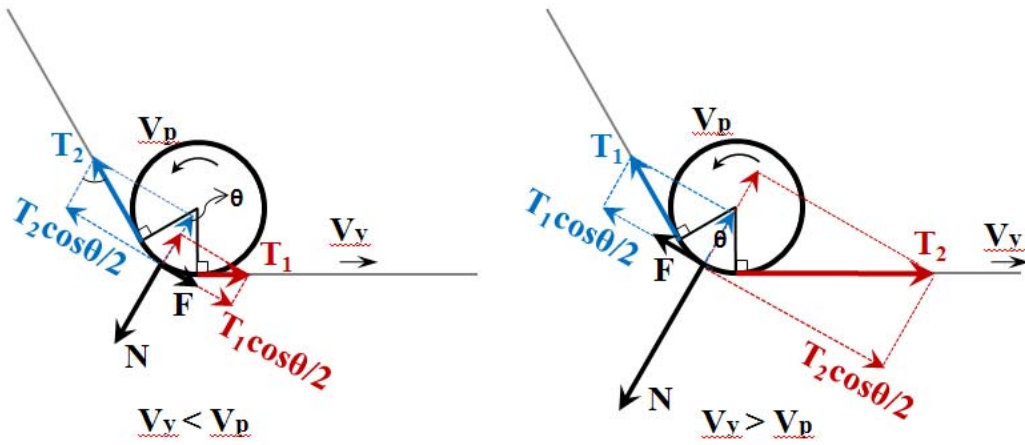


Figure 4.3 Force diagram analysis on the yarn section contacted with pin when V_y was smaller than V_p (left) and when V_y was larger than V_p (right)

The coefficient of friction was calculated from the input and output tension by the Simple Capstan Equation as shown in equation [2-3].

$$e^{\mu\theta} = T_2/T_1 \quad [2-3]$$

where, μ is the coefficient of friction (dimensionless), θ is the angle of contact (rad), which is $\pi/3$ in this work, T_1 is absolute value of yarn tension on the looser side (cN or gf), and T_2 is absolute value of yarn tension on the tighter side (cN or gf).

Additionally, the electrical signal generated by the piezoelectric sensor, was recorded by the computer. The vibration force (cN) was calculated based on the piezoelectric sensor's sensitivity, which is 1cN/10mV.

4.4 Results and analysis

4.4.1 Experimental design-I

When 25.4 mm diameter pin was used, the measurement responses (potential-I, potential-II, yarn output tension, and pin vibration amplitude) and the calculated responses (contact force, frictional force, coefficient of friction, and vibration force) are shown in Figure 4.4 to 2-13. Each data point represents the average of 6000 readings (three replications for each condition and 2000 readings in each replica). The error bars with standard deviations of 6000 readings are also shown in the charts.

Figure 4.4 shows that the yarn surface potential detected by the first probe (potential-I) is minimal when the yarn/pin relative speed approaches zero. This indicates that the charge is minimal when the friction between two surfaces is the smallest. The data in Figure 4.4 is also drawn corresponding to V_y as shown in Figure 4.5 and corresponding to V_p as shown in Figure 4.6, both of which show that charge was minimal when V_y was close to V_p . The effect of yarn/pin relative rubbing speed on charge potential is also confirmed from the data obtained from the second probe (potential-II) as shown in Figure 4.7. Thus, friction plays a more complicated role in static charging, and it should not be simply considered as charging by contact and separation (zero yarn/pin relative rubbing speed).

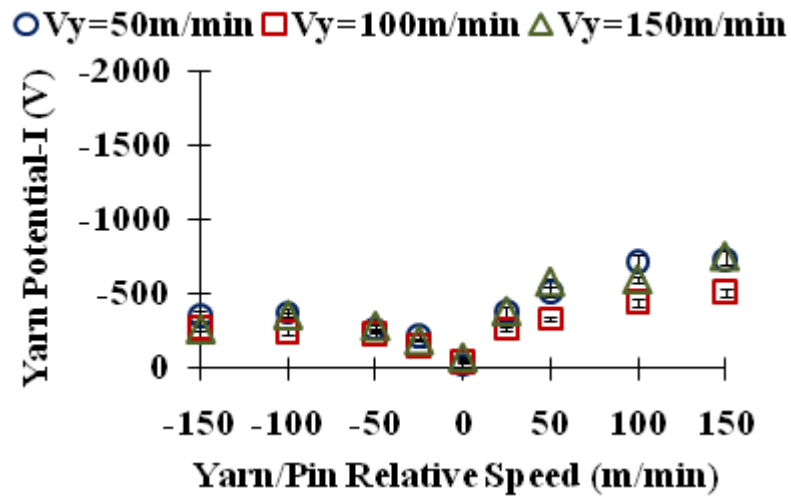


Figure 4.4 Effect of yarn/pin relative rubbing speed on yarn surface potential measured by the probe-I (pin: stainless steel cylinder of 25.4 mm diameter, yarn: 420/72 nylon multifilament with anionic lubricant)

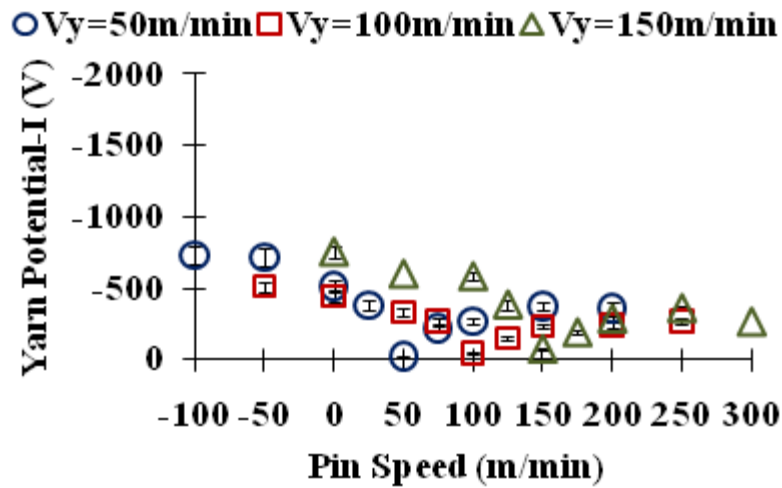


Figure 4.5 Data of figure 4.4 corresponding to the speed of charge pin

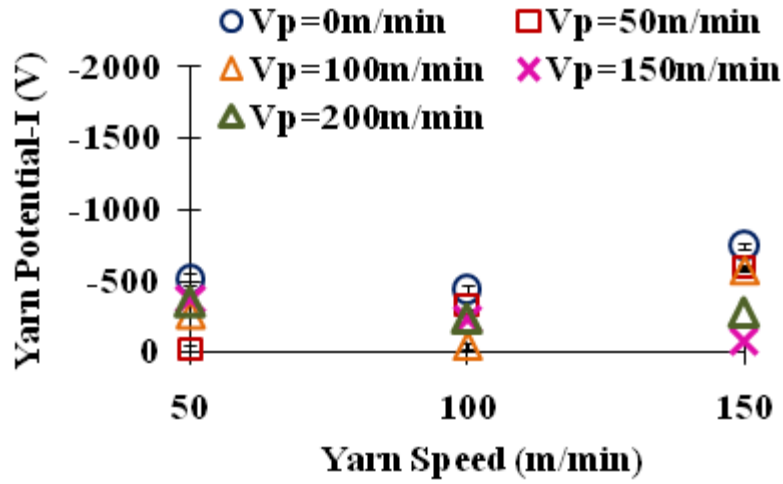


Figure 4.6 Data of figure 4.4 corresponding to the speed of yarn

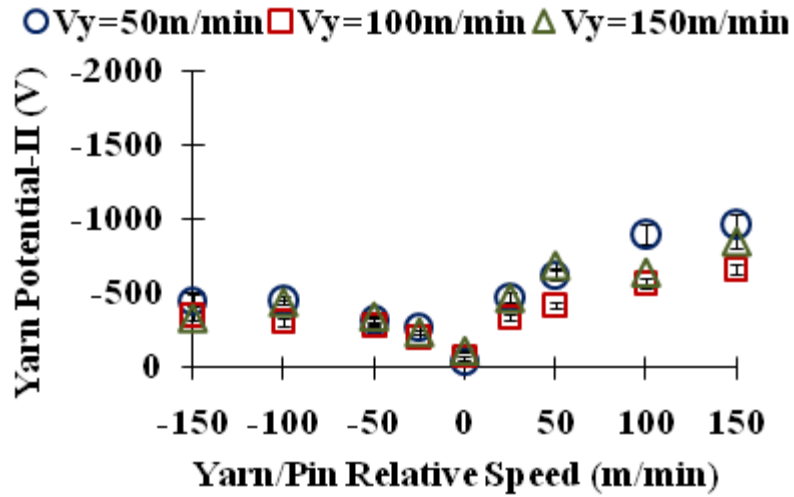


Figure 4.7 Effect of yarn/pin relative rubbing speed on yarn surface potential measured by the probe-II (pin: stainless steel cylinder of 25.4 mm diameter, yarn: 420/72 nylon multifilament with anionic lubricant)

Figure 4.8 shows the measured yarn output tension, which is higher than the input tension (constant as 50 cN) when the yarn/pin relative speed is positive ($V_y > V_p$) and is lower than the input tension when the relative speed is negative ($V_y < V_p$). The calculated

contact force is shown in Figure 4.9, which is also higher than 50 cN when yarn/pin relative speed is positive and is lower than 50 cN when yarn/pin relative speed is negative. These can be explained by the force analysis of yarn/pin contact section as mentioned above (Figure 4.2).

Figure 4.10 and 4.11 show the calculated friction force and the coefficient of friction, respectively. Both of them perform similar tendency as that of yarn potentials corresponding to the yarn/pin relative rubbing speed. When the friction force was minimal (the coefficient of friction was also minimal), the charge generation was the smallest. Figure 4.12 shows the correlation between friction force and potential-I. It is clear from the chart that the potential increased as the friction force increased.

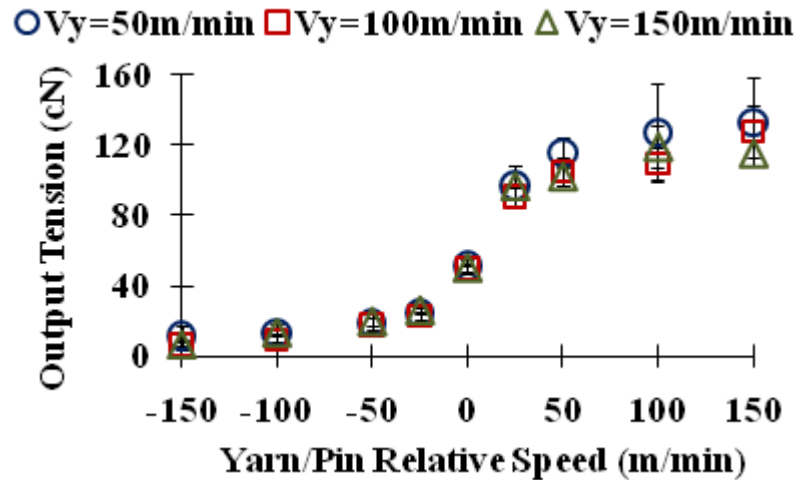


Figure 4.8 Effect of yarn/pin relative rubbing speed on yarn output tension (pin: stainless steel cylinder of 25.4 mm diameter, yarn: 420/72 nylon multifilament with anionic lubricant)

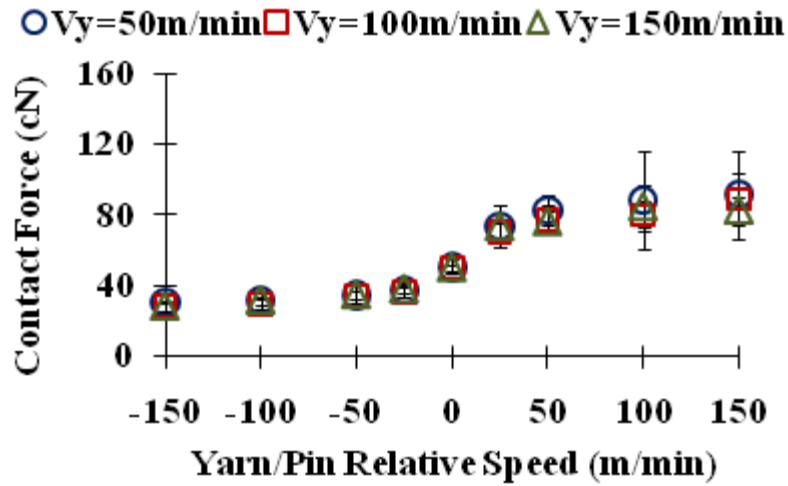


Figure 4.9 Effect of yarn/pin relative rubbing speed on contact force on yarn (pin: stainless steel cylinder of 25.4 mm diameter, yarn: 420/72 nylon multifilament with anionic lubricant)

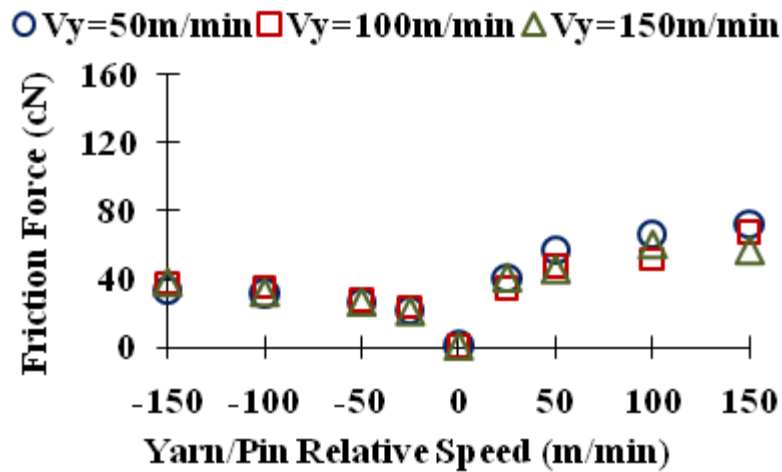


Figure 4.10 Effect of yarn/pin relative rubbing speed on friction force on yarn (pin: stainless steel cylinder of 25.4 mm diameter, yarn: 420/72 nylon multifilament with anionic lubricant)

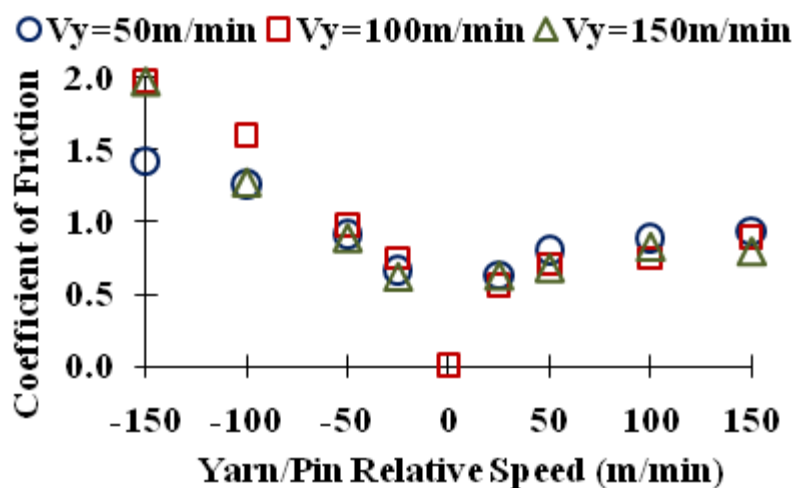


Figure 4.11 Effect of yarn/pin relative rubbing speed on yarn/pin coefficient of friction (pin: stainless steel cylinder of 25.4 mm diameter, yarn: 420/72 nylon multifilament with anionic lubricant)

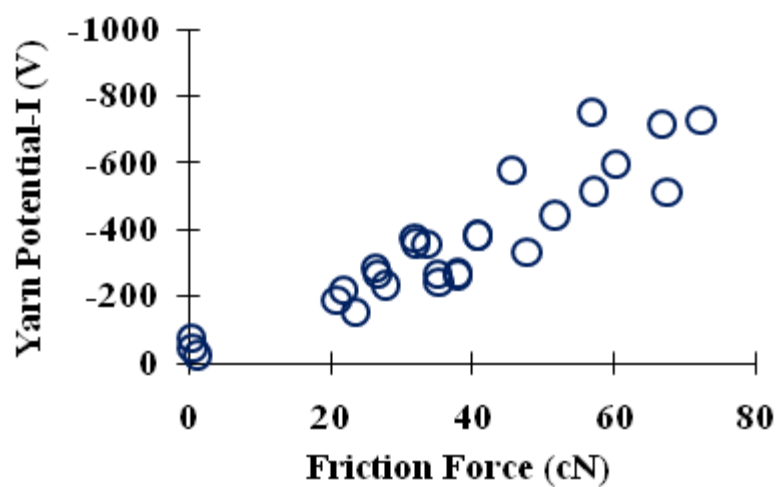


Figure 4.12 Correlation between yarn potential-I and yarn/pin friction force (pin: stainless steel cylinder of 25.4 mm diameter, yarn: 420/72 nylon multifilament with anionic lubricant)

Additionally, the pin's vibration (Figure 4.13) at different levels of rotating frequency was also investigated to estimate its effect on friction and tribo-electrification. The vibration force is calculated as shown in Figure 4.14, which is much smaller (less than 0.3 cN) comparing to the contact force on yarn (30 to 90 cN). Therefore, the effect of vibration on friction and electrification will be disregarded in subsequent discussions in this work.

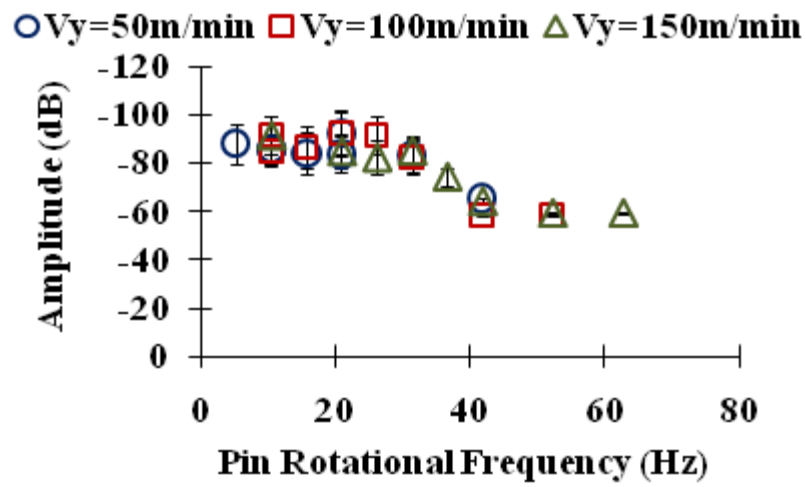


Figure 4.13 Pin vibration amplitude measured at different rotating frequency (pin: stainless steel cylinder of 25.4 mm diameter, yarn: 420/72 nylon multifilament with anionic lubricant)

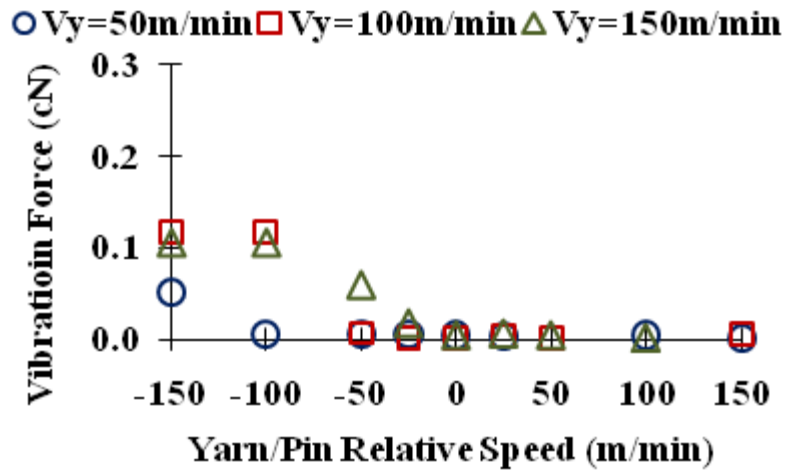


Figure 4.14 Vibration force calculated at different yarn/pin speeds (pin: stainless steel cylinder of 25.4 mm diameter, yarn: 420/72 nylon multifilament with anionic lubricant)

When the 6.35 mm diameter pin was used to rub against the nylon filament, it was found that more charge was generated than that by rubbing against the 25.4 mm diameter pin. The values of potential-I and potential-II are shown in Figure 4.15 and 4.16, respectively. In similar behaviour to that observed when rubbing against the 25.4 mm diameter pin, the charge is minimal when the relative rubbing speed approaches zero.

It is interesting to note that the absolute value of potential-II was always higher than that of potential-I when observed in the same run. This was unexpected considering that the probe-II was farther away from the yarn/pin separation point, where charge should have begun to decay, and thus potential-II should be lower than potential-I. The same tendency was observed when the probes and voltmeters were switched to determine whether a possible error might have been introduced by differences in the sensors. It was thought that the difference might be associated with differences in the surrounding electric field, because there was the stainless steel charge pin close to probe-I, while there was no similar pin placed close to probe-II. A simple trial was carried out by also putting a stainless steel pin close to probe-II, to mirror the set-up at probe-I. Under this set-up the absolute value of potential-II decreased and became consistently smaller than potential-I.

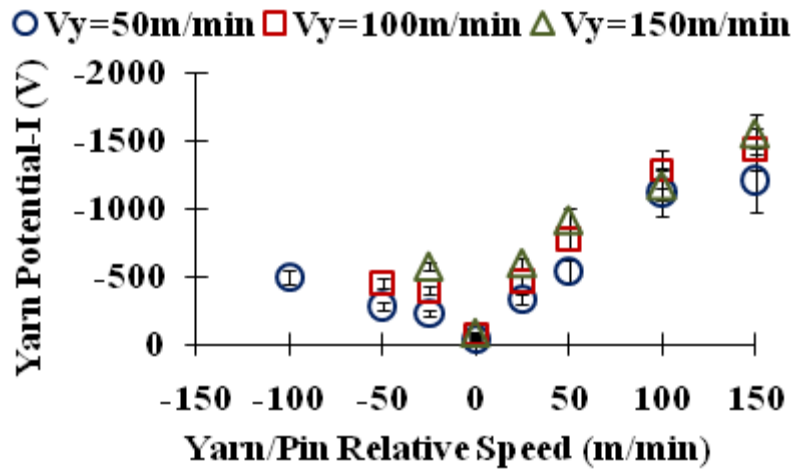


Figure 4.15 Effect of yarn/pin relative rubbing speed on yarn surface potential measured by the probe-I (pin: stainless steel cylinder of 6.35 mm diameter, yarn: 420/72 nylon multifilament with anionic lubricant)

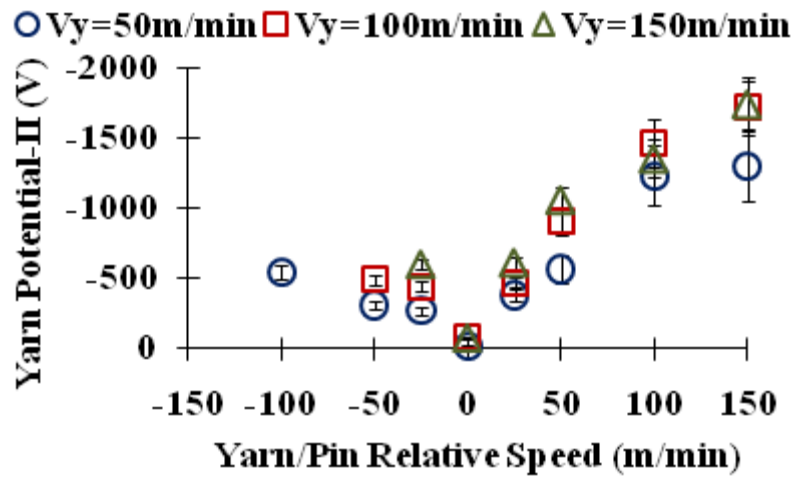


Figure 4.16 Effect of yarn/pin relative rubbing speed on yarn surface potential measured by the probe-II (pin: stainless steel cylinder of 6.35 mm diameter, yarn: 420/72 nylon multifilament with anionic lubricant)

This explanation (that the pin was influencing the values from Probe-I, was further supported by a specifically designed test. The probe-I was placed at different distance from the charge pin while the probe-II was fixed at the same position. Figure 4.17 shows the yarn potential detected by the two probes. It is clear that potential-II was around the same level in the different runs, however, the absolute value of potential-I decreased as probe-I got closer to the stainless steel pin.

In this work, since the spacing from the sensitive aperture of probe-I to the yarn/pin separation point was 3 cm, thus, the probe-I registered less charge than probe-II. However since the positions of probe-I and probe-II were kept constant during all the tests, the values measured by the probe-I can be compared with other data obtained from probe-I in different runs. Similarly, the values measured by the probe-II can be compared with each other, however, potential-I was not compared with potential-II in subsequent trials.

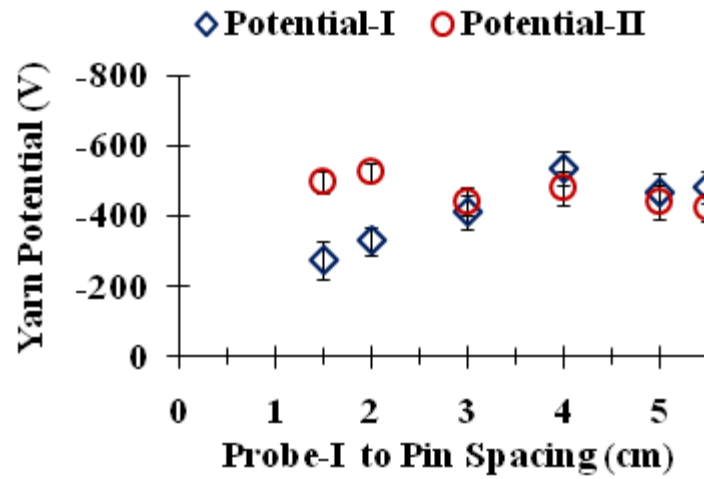


Figure 4.17 Effect of probe-I to pin spacing (the spacing from the aperture of probe-I to the yarn/pin separation point) on measured yarn potential (the position of probe-II was fixed) (yarn: nylon with lubricant, pin: stainless steel cylinder of 25.4 mm diameter; $V_y = 100$ m/min, $V_p = 0$, input tension=50 cN)

When the 6.35 mm diameter pin was used, the measured yarn output tension corresponding to the yarn/pin relative rubbing speed is shown in Figure 4.18. The trend is similar to that observed when rubbing the 25.4 mm diameter pin. When the yarn/pin relative speed is positive, the output tension increased as the relative speed increased. When the yarn/pin relative speed is negative, the output tension decreased as the absolute value of relative speed increased. The contact force, friction force, and coefficient of friction were calculated from the value of input and output tension, and the results are shown in Figures 4.19, 4.20 and 4.21, respectively. The trends were also similar to what was observed by rubbing the 25.4 mm diameter pin.

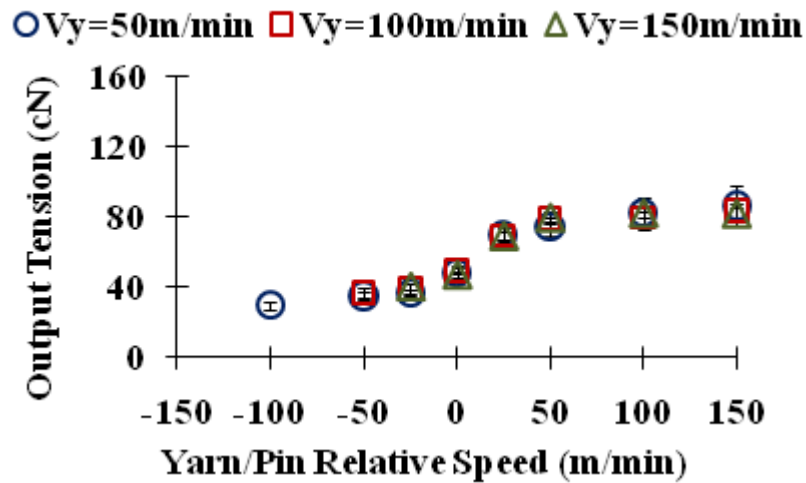


Figure 4.18 Effect of yarn/pin relative rubbing speed on yarn output tension (pin: stainless steel cylinder of 6.35 mm diameter, yarn: 420/72 nylon multifilament with anionic lubricant)

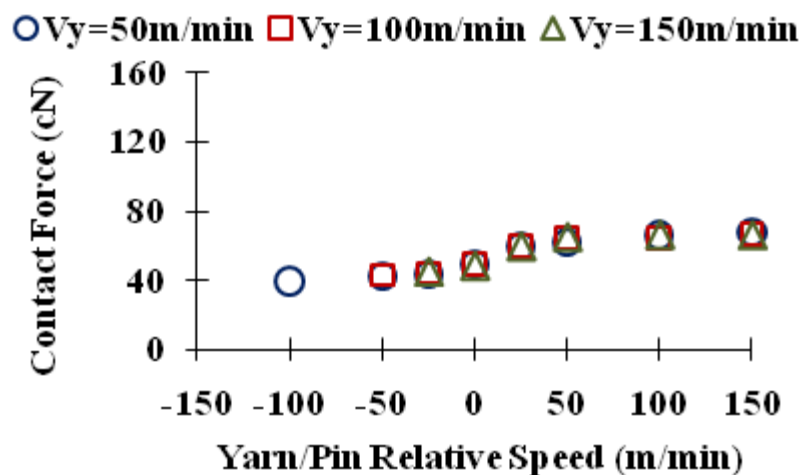


Figure 4.19. Effect of yarn/pin relative rubbing speed on yarn/pin contact force (pin: stainless steel cylinder of 6.35 mm diameter, yarn: 420/72 nylon multifilament with anionic lubricant)

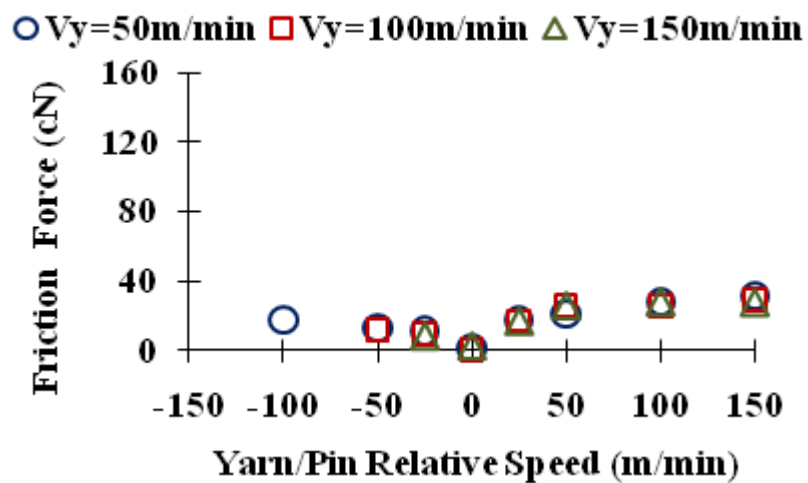


Figure 4.20 Effect of yarn/pin relative rubbing speed on yarn/pin friction force (pin: stainless steel cylinder of 6.35 mm diameter, yarn: 420/72 nylon multifilament with anionic lubricant)

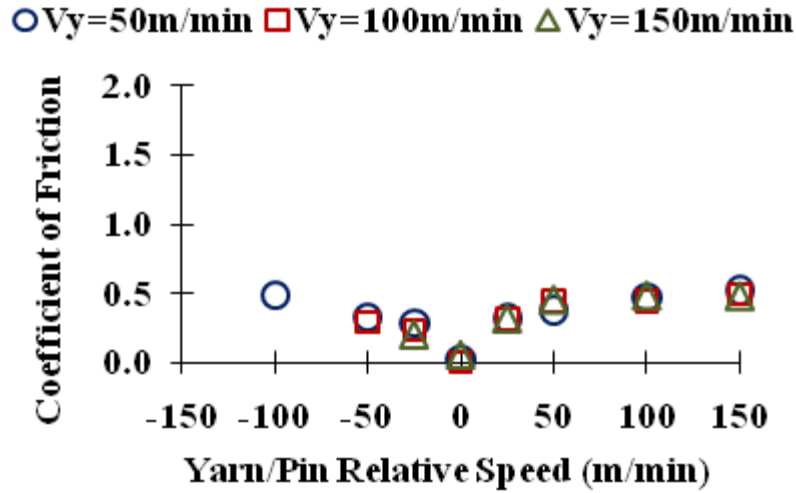


Figure 4.21 Effect of yarn/pin relative rubbing speed on yarn/pin coefficient of friction (pin: stainless steel cylinder of 6.35 mm diameter, yarn: 420/72 nylon multifilament with anionic lubricant)

4.4.2 Experimental design-II

Selected parameters were used in experimental design-II to investigate the effect of relative rubbing speed on the electrification of three different finish free yarns made from nylon, PET and PP. The stainless steel pin of 25.4 mm diameter was used and the yarn transport speed was kept as 100 m/min.

Experiments found that nylon yarn was always positively charged while PET and PP yarns were always negatively charged by rubbing against stainless steel. These agree with other researchers' tribo-electric series (Diaz and Felix, 2004). However, only the absolute charge potential values are shown in Figure 4.22 (potential-I) and Figure 4.23 (potential-II) for the convenience of comparison.

Figures 4.22 and 4.23 indicate that the relative rubbing speed has a significant effect on the amount of charge generated on nylon, while relative speed has only a minor influence on the amount of charge generated on the other two yarns. For nylon, the yarn surface potential increases almost linearly with the increase of yarn/pin speed difference. When the speed difference between the yarn and the pin approached 100m/min, the voltage measured by the first probe approached 10,000 volts. For PET, the mean value of

absolute charge increases as the speed difference increased; however, this effect is not significant once the variation is taken into consideration. For PP, the effect of relative rubbing speed is significant on the charge generation; however, the slope of charge against speed is much smaller than that of nylon. In the present study it was found that when the relative speed was not zero, the charge on nylon was much higher than polyester; however at zero relative speed the polyester had a slightly higher charge.

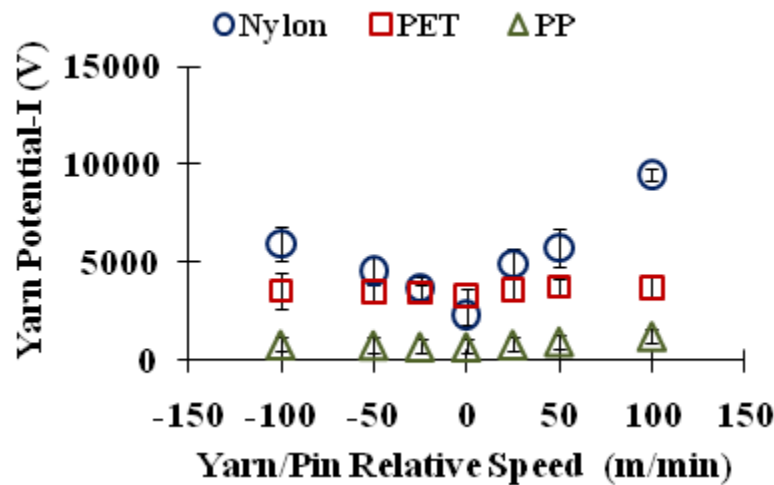


Figure 4.22 Effect of yarn/pin relative rubbing speed on finish free yarns' surface charge potential measured by the first probe (pin: stainless steel cylinder of 25.4mm diameter)

The trends of the effects of relative rubbing speed on the output tension, friction force, contact force and coefficient of friction were similar for nylon, PET, and PP as shown in Figures 4.24, 4.25, 4.26 and 4.27, respectively. At the same level of relative speed, the friction of PP was significantly higher than both PET and nylon, but as indicated above this was not reflected in the charge generated. Figure 4.28 shows the charge potential-I of three different yarns corresponding to their yarn/pin friction force. It reveals that charge on finish free nylon increases dramatically as the friction force increases; however, the influence of friction on potential for the finish free PET and PP was only marginal. It is thus clear that when restricting studies to a particular fibre type frictional force may play a role in the potential generated. However when several types of

fibre are studied the effects of friction cannot be generalized and the polymer type dominates any trends.

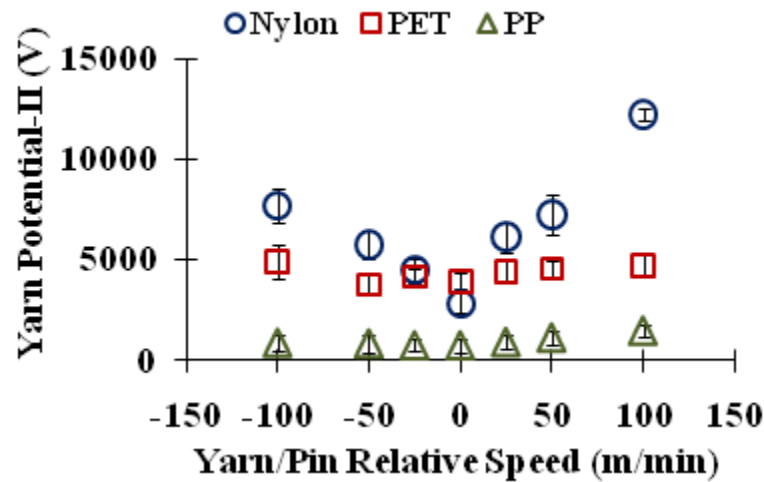


Figure 4.23 Effect of yarn/pin relative rubbing speed on finish free yarns' surface charge potential measured by the second probe (pin: stainless steel cylinder of 25.4mm diameter)

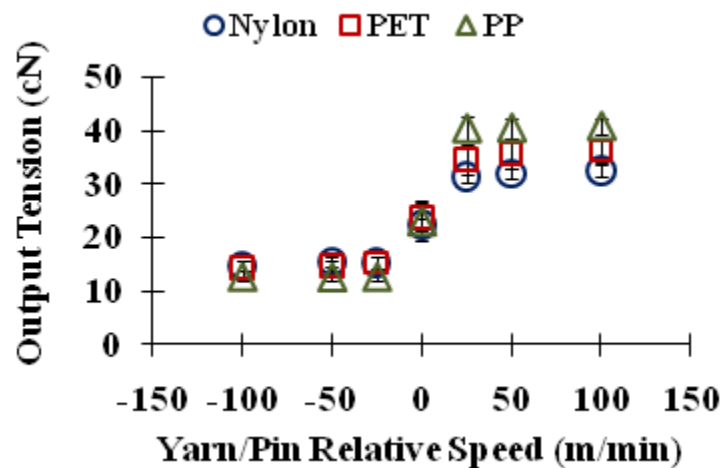


Figure 4.24 Effect of yarn/pin relative rubbing speed on yarn output tension (pin: stainless steel cylinder of 25.4mm diameter)

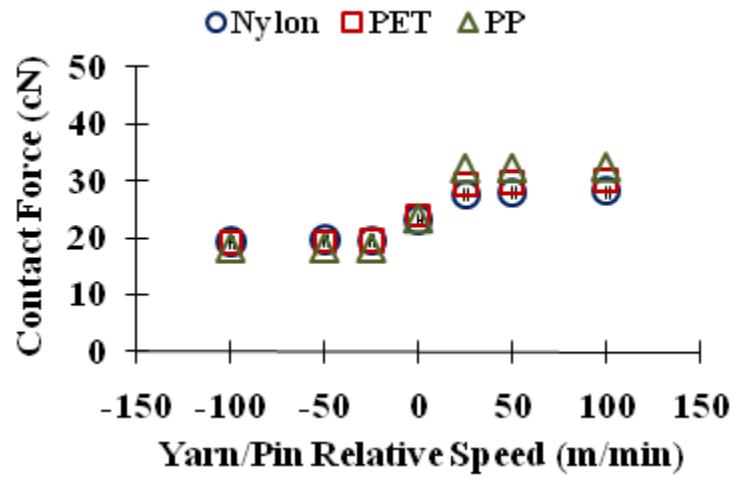


Figure 4.25 Effect of yarn/pin relative rubbing speed on yarn/pin contact force (pin: stainless steel cylinder of 25.4mm diameter)

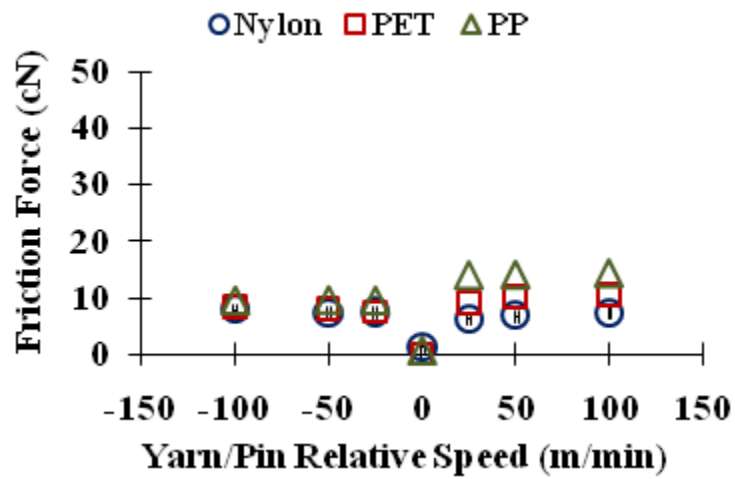


Figure 4.26 Effect of yarn/pin relative rubbing speed on yarn/pin friction force (pin: stainless steel cylinder of 25.4mm diameter)

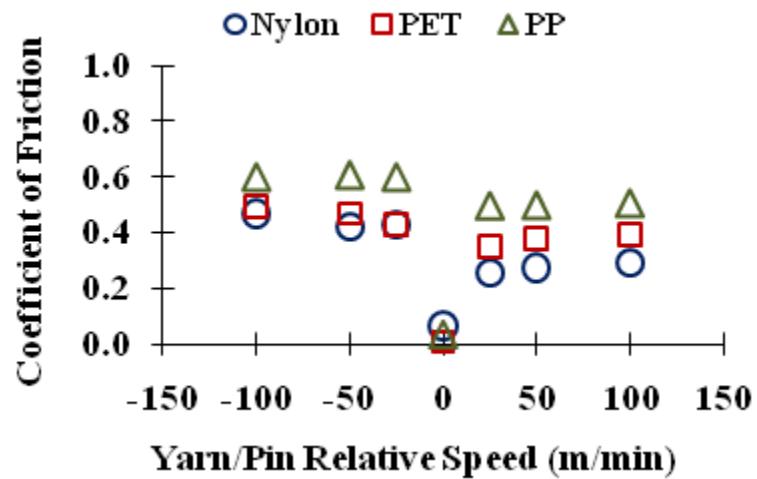


Figure 4.27 Effect of yarn/pin relative rubbing speed on yarn/pin coefficient of friction (pin: stainless steel cylinder of 25.4mm diameter)

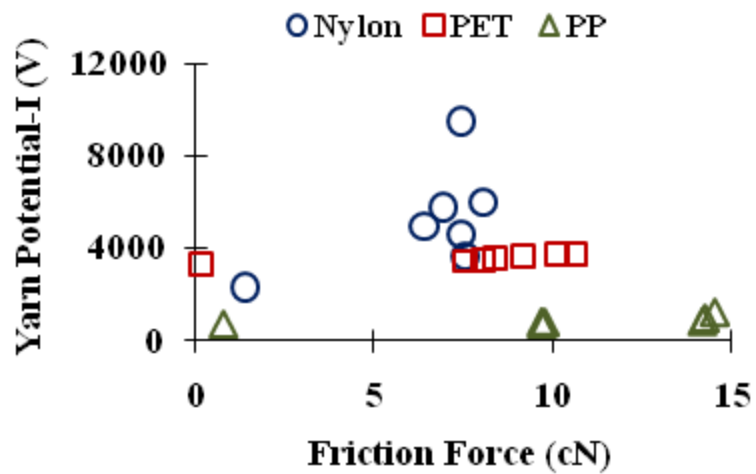


Figure 4.28 . Charge potential-I on finish free yarns corresponding to the yarn/pin friction force

4.5 Conclusion

The developed equipment enabled a more accurate investigation of tribo-electrification of continuous filament yarns against a rotating surface at different levels of relative rubbing speed. It was found that charge generated on a nylon multifilament yarn with 1.2% anionic lubricant, after rubbing against a stainless steel pin, was minimal as the relative rubbing speed approached zero. This was found to be true regardless of the absolute moving speeds of yarn and pin. The calculated friction force and coefficient of friction also yield the smallest values when the relative speed approaches zero. It can be concluded that more static was generated by friction than that generated merely by contact and separation without relative rubbing, and the tribo-electrification increased as the relative rubbing speed increased. The results also showed that less charge was generated when larger pin was used when the relative rubbing speed was at the same level. Based on these findings, the electrostatic could be effectively controlled in industry by reducing the relative rubbing speed between surfaces such as using rotating rollers rather than fixed guides.

From the investigation on different types of finish free yarns after rubbing against stainless steel charge pin, it was found that the nylon yarn was positively charged when rubbed against stainless steel while the PET and PP yarns were always charged negatively. The surface potential of nylon increased almost linearly with the increase of relative rubbing speed, while the surface potential of PET and PP increased slightly and levelled off as the relative speed increased.

The study indicated that the fibre type (polymer type) was the dominant factor for the tribo-electrification, and it was further influenced by the relative rubbing speed.

References

Armstrong-Hélouvry, B. (1991). *Control of machines with friction*. Boston: Kluwer Academic Publishers.

- Castle, P.G. (1997). Contact charging between insulators. *Journal of Electrostatics*, 40(1), p. 13-20.
- Diaz, A.F. and Felix-Navarro, R.M. (2004). A semi-quantitative tribo-electric series for polymeric materials: the influence of chemical structure and properties. *Journal of Electrostatics*. 62(4), p. 277-290.
- Gupta, B. S. (2007). *Friction in Textile Materials*. London: Woodhead.
- Harper, W.R. (1957). The generation of static charge. *Advances in Physics*, 6(24), p. 365-417.
- Hersh, S.P. and Montgomery, D.J. (1955). Static electrification of filaments. *Textile Research Journal*, 25(4), p. 279-295.
- Howell, H.G., Mieszkis, K.W., & Tabor, D. (1959). *Friction in textiles*. New York: Textile book publishers in association with the Textile Institute.
- Komatsu, T.S. (2004). Static electrification by asymmetric rubbing. *Applied Surface Science*, 235(1-2), p. 60-64.
- London, J.J. (1966). *Effects of pretension and yarn speed on electrostatic charge generation on continuous filament yarns* (Master Thesis). North Carolina State University.
- Lowell, J. and Rose-Innes, A.C. (1980). Contact electrification. *Advances in Physics*, 29(6), p. 947-1023.
- Lyne, D.G. (1955). Fibre friction. *Journal of Textile Institute*, 46(1), p. 3-136.
- Monroe Electronics, Inc. (1991). Instruction Manual. Lyndonville, New York.
- Ohara, K. (1980). Relationship between frictional electrification and molecular motion of polymers. *Journal of Electrostatics*, 9(2), p. 107-115.
- Ohara, K., Nakamura, I., and Kinoshita, M. (2001). Frictional electrification between flat surfaces of polymers and of Langmuri-Blodgett layers. *Journal of Electronics*, 51-51(1-4), p. 351-358.
- Seyam, A. M., Cai, Y., and Oxenham, W. (2009). Devices for measuring electrostatic generation and dissipation on the surfaces of polymeric materials. *Journal of Textile Institute*. 100(4), p. 338-349.

Suh, M., Seyam, A.M., Oxenham, W. and Theyson, T. (2010). Static generation and dissipation of polyester continuous filament yarn. *Journal of Textile Institute*. 101(3), p. 261-269.

5 FRICTIONAL ELECTRIFICATION OF POLYMERIC PLATES

This chapter is modified from a manuscript entitled “Frictional electrification on polymeric flat surfaces”, by L. Liu, A.M. Seyam, and W. Oxenham, which is submitted to *Journal of Engineered Fibers and Fabrics*.

5.1 Introduction

Electrostatic charge is generated by contact and separating two different surfaces. Based on a “Surface State Model”, which is an idealized electron-transfer model, the generated charge polarity and magnitude can be predicted (Harper, 1957). When two different surfaces are contacted, electrons attempt to transfer from the surface of higher Fermi level to the surface of lower Fermi level. The charge transferred to the surface is proportional to the difference of their Fermi Levels. After separation, the transferred electrons are trapped on the surface and the surface is negatively charged (Taylor and Secker, 1994). However, experimental results generally do not agree with the predicted results, especially when polymeric surfaces were examined (Castle 1997). Since polymeric surfaces are irregular, not 100% crystalline, and usually contain “impurities”, it is difficult to determine their Fermi Levels. Furthermore, the phenomenon becomes more complicated in frictional charging than that in contact charging. When friction (sliding/rubbing) occurs, the real contact junctions between two surfaces are sheared, which is related to the surfaces’ roughness and deformation properties (Howell, Mieszkis, & Tabor 1959; Gupta, 2009). The correlation between friction and electrification is still unclear answers for many questions such as will more charge be generated by friction than by repeated contacts and separations, and does charge increase as rubbing speed increase?

In textiles, most of the materials are polymers, and their frictional electrification has been investigated by rubbing fiber against fiber (Hersh and Montgomery, 1955), fiber against cylinder (Medley, 1954), yarn against cylinder (Suh. et al., 2010; London, 1966; Ballou, 1954), film against cylinder (Ohara, 1980), fabric against cylinder/roller (Sereda and Feldman, 1964; Ballou, 1954), and plastic disk against disk (Komatsu, 2004). It is evident that their reported observations were not consistent and in some cases conflicted with each other. For example, nylon was generally positively charge after rubbing against metal, however, it was sometimes negatively charged (London, 1966). For another example, charge was not always increased with rubbing speed (Hersh and Montgomery, 1955). Possible explanations for these disparities are the differences in sample preparation (surface contamination and texture) experimental procedures (equipment and

measuring techniques) coupled with the level of accuracy of the systems used. In another research of Ohara (2001), a high-precision friction apparatus was constructed to investigate the frictional electrification between two flat surfaces. The study revealed that:

- (a) Charge increases as the number of friction cycles increases
- (b) More charge was generated on nylon than on other polymers (polyester, polycarbonate, polypropylene, polystyrene, etc.)
- (c) Charge increases as the surface roughness decreases

However, these conclusions were all based on experiments of only five or six cycles of rubbing. The answers to the following questions were not addressed: When the charge will get saturated? What is the difference of saturation levels for different polymers? And, what are the impacts of rubbing speed and contact force on the saturation levels?

The discrepancy reported on tribo-electrification of polymers and the limitations of the experiments in previous studies prompted us to conduct comprehensive research in the area of electrostatic generation/dissipation of polymeric materials. The overall goal of this work is to gain a better understanding of the mechanism of static generation and dissipation on polymeric surfaces and to relate these findings to the static charge issues in textile processing. In this study, finish free nylon, PP, and PTFE surfaces were prepared to be rubbed against stainless steel flat surface for 50 cycles (which was found to be the maximum number of cycles required to reach charge saturation for the materials studied) at different levels of rubbing speed and contact force to find their effects on charge generation and dissipation. In addition, surfaces (nylon, PP, PTFE, stainless steel) were rubbed against each other to find out their tribo-electric series. A rubbing device (Seyam, Cai, & Oxenham, 2009) was modified, which can provide forward-and-backward rubbing motion between two surfaces (movable rubbing head or rubber and fixed sample in form of plate) at different levels of speed, contact force, and stroke length. The rubbing head can also provide up-and-down movement to realize repeated contacts and separations.

The surface charge potential of the rubbing plate (sample) was detected continuously by a potential probe, which was fixed with the rubbing head.

5.2 Experimental

5.2.1 Charge generation/dissipation measurement device

Figure 5.1 shows the device developed for measuring the surface charge potential of a fixed rubbing plate rubbing against a movable rubbing head. The rubbing plate is mounted on a metal grounded fixture and the rubbing head is attached to a metal shaft by double sided adhesive tape. The contact force between the rubbing plate and the rubbing head can be adjusted by adding different loads (weight blocks) on top of the shaft. The shaft is held by a bush so that the shaft can move up/down inside the bush freely. A potential probe (Model 1017, Monroe Electronics[®]) is mounted on one side of the bush. The bush is connected to a stepper motor that move the assembly of bush, rubbing head, load, shaft, and the potential probe in reciprocating motion. The rubbing movement can be precisely controlled and pre-programmed through user interface.

During measurement of charge, the potential probe is moved forward-and-backward. When the rubbing head moves forward, the probe is trailing the rubbing head and detects the charge newly generated on the surface of rubbing plate. When the rubbing head moves backward, the probe is leading the rubbing head and monitors the charge retained on the surface. The distance from the detecting aperture of the probe (facing rubbing plate) to the left edge of the rubbing head is fixed as 20 mm and the probe is kept above the rubbing plate with 3 mm spacing. By this setup, charge in the area of 8 mm diameter on the rubbing plate surface can be detected at 99% resolution (Monroe Electronics, Inc., 1991).

The device is housed inside a walk-in environmental room where temperature and humidity are precisely controlled.

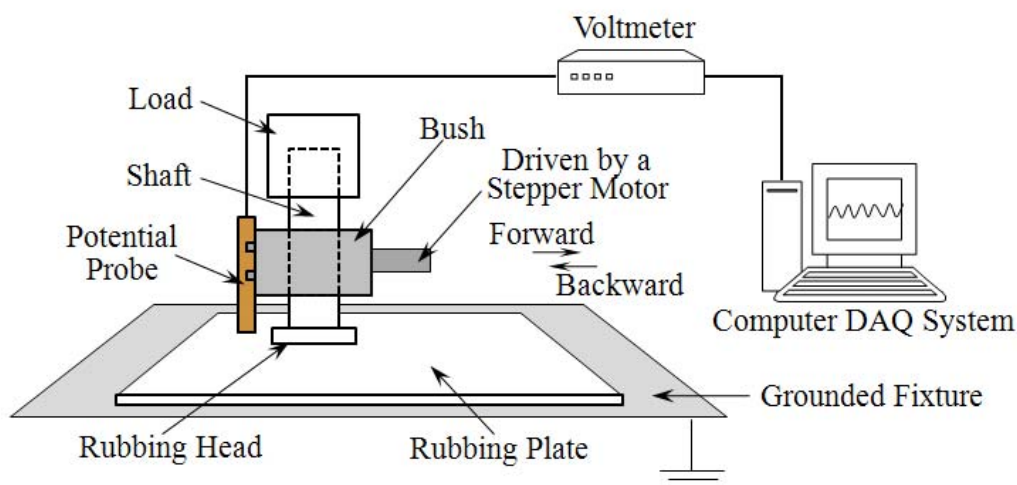


Figure 5.1 Rubbing tester

5.2.2 Materials and experimental designs

Finish free nylon 6,6, polypropylene (PP), stainless steel (SS), and polytetrafluoroethylene (PTFE) were prepared as rubbing heads of dimensions $10 \text{ mm} \times 20 \text{ mm} \times 3 \text{ mm}$ and as rubbing plates of dimensions of $300 \text{ mm} \times 90 \text{ mm} \times 3 \text{ mm}$. The edges of rubbing heads were polished to avoid any scratching in rubbing against rubbing plates. Each sample was cleaned and de-ionized using ethanol, ionized water, and ionized gas respectively to remove contaminations and initial charge that may have accumulated from handling. The initial surface charge of each sample was checked by the potential probe before each test and if it was not zero, the cleaning and de-ionizing procedure was repeated until no charge was detected on the test sample. All samples were conditioned inside the environmental room at the temperature of 21°C and relative humidity (R.H.) of 43% for at least 24 hours before testing.

Three sets of experiments were conducted to evaluate the charge behavior of nylon, PP, and PTFE. Tables 5.1 to 5.3 depict the parameters and their levels. The first experiment was used to find the effect of the force between the two surfaces on the static generation and dissipation of nylon, PP, and PTFE plates in rubbing against stainless steel. Four levels of contact force were used and three replications were conducted for

each run. The fixed parameters were rubbing speed of 47 mm/second, rubbing stroke length of 52 mm, and number of rubbing cycles (forward and backward stroke/cycle) was 50. In the 50th cycle, the rubbing head was stopped after the forward stroke and was not moved backward (49 ½ cycles or 99 strokes were conducted). At this moment the probe is monitoring the potential of the sample at the middle of the rubbed area (see section 5.3.1 for details). The charge decay on the plate was recorded at this position for 30 seconds.

The second experiment was carried out to evaluate the effect of rubbing speed on charge generation and dissipation of nylon, PP, and PTFE after rubbing against stainless steel. Four levels of rubbing speeds, including zero speed, which was repeated contacts and separations, were used. Again three replications were conducted for each run. The constant parameters were contact force of 1 N, rubbing stroke length of 52 mm, and 50 cycles of rubbing. The repeated contacts/separations were realized by raising and releasing the shaft for 99 times at the same location without forward/backward movement. After the 99th contact/separation, the probe was moved (at 47 mm/second) to the charged area to measure the surface potential.

The third experiment was designed to find the tribo-electric series of nylon, stainless steel, PP, and PTFE by rubbing against each other. Three replications were conducted for each run. The constant parameters were rubbing speed of 47 mm/s, contact force of 1 N, rubbing stroke length of 52 mm, and the number of rubbing cycles was 50.

The acceleration/deceleration of rubbing movement was constant as 400 mm/s² for the three experiments, which was selected after carrying out trials using accelerations/decelerations in the range of 150-4000 mm/s². At 400 mm/s² acceleration/deceleration, the movement took 0.12 second to accelerate from 0 to 47 mm/s (constant rubbing speed used in experimental design I) and it took 0.12 second to decelerate from 47 mm/s to 0, without jerky motion (happened when the acceleration/deceleration was too high). The rubbing speeds were selected after conducting trials at speeds in the range of 20-100 mm/s. The speed of 47 mm/s used in experimental design I was around the middle of the range. The other two levels of speed used in experimental design II, 27 mm/s and 95 mm/s, were selected to represent low and

high levels of speed. All the three speeds provided smooth rubbing motion. The selected contact forces (0.4, 1, 1.5, and 2 N) provided good contact between two surfaces a matter that led to measurable charge potential, and they did not cause severe friction between the two surfaces, which would block the movement.

All the experiments were conducted at temperature of 21°C and relative humidity of 43%. The temperature of 21°C is recommended by standard testing methods related to electrostatics (AATCC 76, AATCC 84, AATCC 134, and NFPA 56). The standards, however, did not specify relative humidity and suggested that the test be done under relative humidity of choice depending on the investigated materials. The 43% R.H. was selected in this investigation since static is more of an issue at lower levels of humidity and this was the lowest R.H. available at 21°C for the environmental room used. The number of contact, 50 cycles, was also decided after preliminary trails. It was indicated that charge usually leveled off before 50 cycles of rubbing for samples used in this work, thus, additional rubbing did not provide more information. Additionally, for all the tests, the data collection rate was 100 points/second, which was enough to provide reasonable data points per cycle (120) without loss of any details of signal.

The responses for each experiment were charge potential on the rubbing plate after first cycle of rubbing and 50 cycles of rubbing (V_{50}), potential retained (V) and normalized potential retained ($V/V_{50} \times 100, \%$) after 30 seconds.

In industrial application and consumer products, polymer surfaces are subjected to simple rubbing or multiple rubbing cycles. This is the reason behind characterizing the charge generation after one cycle and 50 cycles of rubbing. As stated earlier, 50 cycle of rubbing causes the charge to reach its maximum. Characterizing the maximum charge is a significant issue to determine the problem that that the charge may cause. The charge decay parameters provide significant information on whether a surface treatment is needed to expedite the charge decay.

Table 5.1 Experimental design I used to study the effect of contact force on static generation/dissipation of polymers after rubbing against stainless steel

Parameters	Levels
Material of Rubbing Plate	Nylon, PP, PTFE
Contact Force (N)	0.4, 1, 1.5, 2
Total Runs ¹	3×4= 12

¹Each run was replicated 3 times and a total of 36 observations were obtained for each response (3×4×3 replications = 36)

Table 5.2 Experimental design II for studying the effect of rubbing speed on static behavior of polymers after rubbing against stainless steel

Parameters	Levels
Material of Rubbing Plate	Nylon, PP, PTFE
Rubbing Speed (mm/sec)	0, 27, 47, 95
Total Runs ¹	3×4 = 12

¹Each run was replicated 3 times and a total of 36 observations were obtained for each response (3×4×3 replications = 36)

Table 5.3 Experimental design III for investigating static properties of polymers after rubbing against each other

Parameters	Levels
Material of Rubbing Plate	Nylon, PP, PTFE
Material of Rubbing Head	Stainless Steel, Nylon, PP, PTFE
Total Runs ¹	3×4 = 12

¹Each run was replicated 3 times and a total of 36 observations were obtained for each response (3×4×3 replications = 36)

5.3 Signal analysis

5.3.1 Charge generation

Figure 5.2 shows the charge potential on nylon in terms of time. The charge potential signal is also corresponding to the rubbing movement at each point of time. The location of potential probe, rubbing head, and rubbing area (the area rubbed by the rubbing head) at starting point ($t = 0$) and at reversing point ($t = 1.2 \text{ second} = 46.48 \text{ mm} / 47 \text{ mm/sec} + 0.12 \text{ sec acceleration time} + 0.12 \text{ sec deceleration time}$) are shown above the potential-time curve. At point A_1 , the rubbing head and the probe started moving forward. The rubbing head rubbed against the rubbing plate. The probe was trailing the rubbing head and detected the surface potential of the rubbing plate, which was zero outside the rubbing area. At point B_1 , the probe moved into the rubbing area, thus the sample charge is detected. At point C_1 , the probe was reached the most forward point (end of forward stroke) at almost the middle of the rubbing area and the motion was reversed. At point D_1 , the probe left the rubbing area (same position as that of point B_1) and surface potential decreased to zero. The period T_1 represents the time during which the rubbing head and probe moved forward while the period of T_2 is the time during which the rubbing head and probe moved backward. Points A_2 , B_2 , C_2 , and D_2 are the same as above for the second cycle of rubbing. Figure 5.2 shows that the charge potential in the second cycle of rubbing (represented by potential at point C_2) is higher than the potential generated in the first cycle of rubbing (represented by C_1).

It is shown in Figure 5.2 that the potential curves of forward and backward strokes were not symmetric. The charge potential detected in the forward stroke was higher than that detected in the backward stroke when it passed by the same position. This is because in the forward stroke, the probe is trailing the rubbing head and detected the charge been newly generated. However, in the backward stroke, the probe is leading the rubbing head and detected the charge, which was generated in the previous forward stroke, retained on the rubbing plate. The latter charge is less due to decay. The charge decay depends on polymer type. For some polymers such as polyester and polypropylene, the charge decay is very slow and did not show difference in the forward and backward stroke.

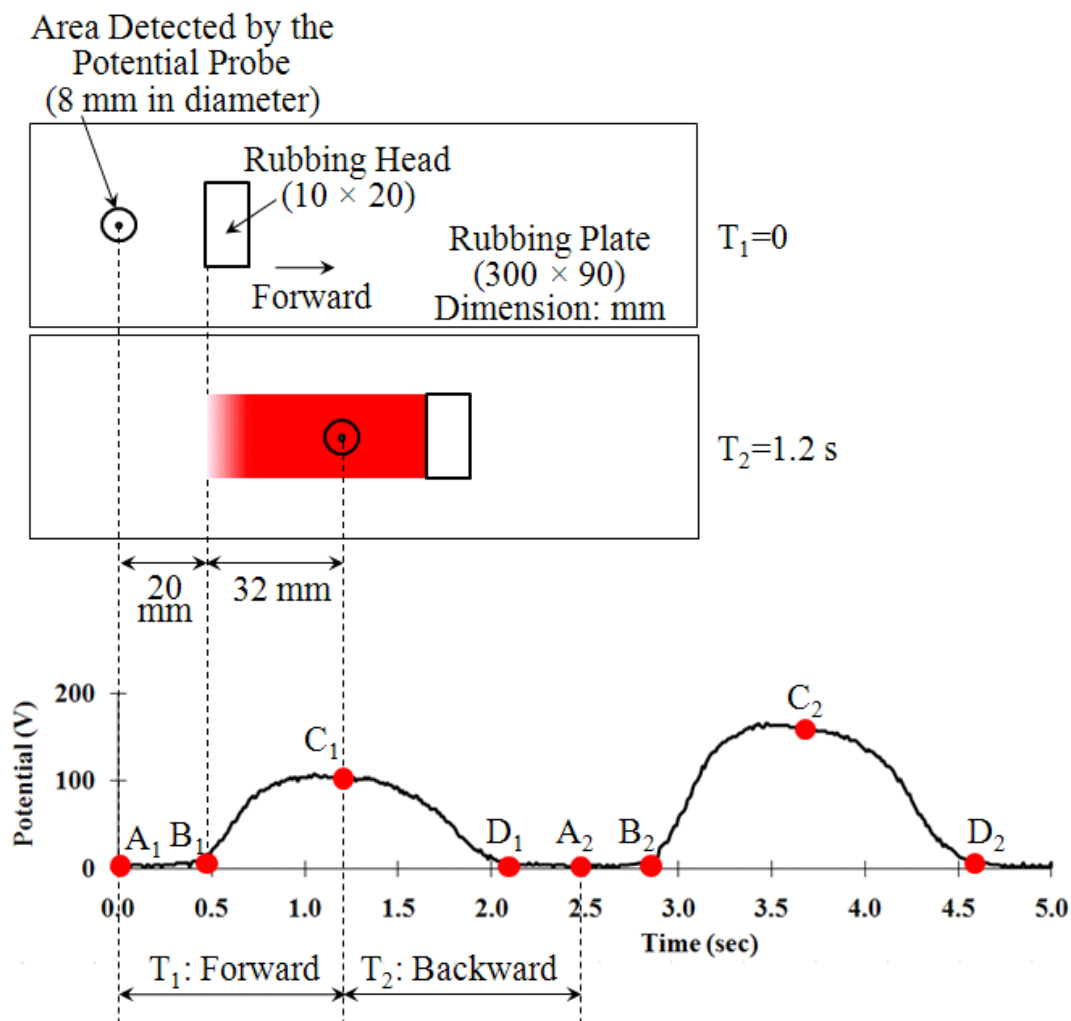


Figure 5.2 Charge potential on nylon in terms of time and locations of potential probe, rubbing head, and rubbing area at starting point ($t = 0$) and at reversing point ($t = 1.2$ second) in the first cycle

5.3.2 Charge accumulation

The detected signal shows that charge accumulated on polymeric surfaces by repeated rubbing. The saturation level and the time when the saturation was reached varied from polymer to another. Figure 5.3 shows the charge potential on nylon surface due to rubbing against stainless steel. The charge increased and leveled off at about 240 V as the number of rubbing cycle increased. This could be explained by several reasons:

- The increase of potential with number of rubbing may be caused by the increase of real contact area between two surfaces, which is related to the deformation of polymers (Lowell and Rose-Innes, 1980).
- The repeated contacts may be expected to increase the charge if the insulator is slightly conducting, because the charge tends to spread (under its own Coulomb repulsion) into the bulk, making room from more charge to be deposited during the next contact (Harper, 1967).
- As the number of rubbing cycle increase, the electrons or ions on nylon surface available for transfer decreases, thus the charge generation get difficult (Lowell and Rose-Innes, 1980).
- Charge decays on nylon plate during the time interval between each cycle (2.4 seconds). The charge saturation is reached when the charge dissipation and generation were in balance.

Figure 5.4 indicates that the charge on PTFE surface as a result of rubbing against stainless steel reached the saturation level at about -600 V after just two or three cycles of rubbing and kept almost constant with more rubbing cycles. Figure 5.5 shows the charge on PP surface also reached the saturation at about -83 V after two or three rubbing cycles.

Figures 5.3, 5.4, and 5.5 also show the charge decay on nylon, PTFE, and PP for 30 seconds after the 50 cycles. The analysis of charge decay will be addressed in section 5.4.1.

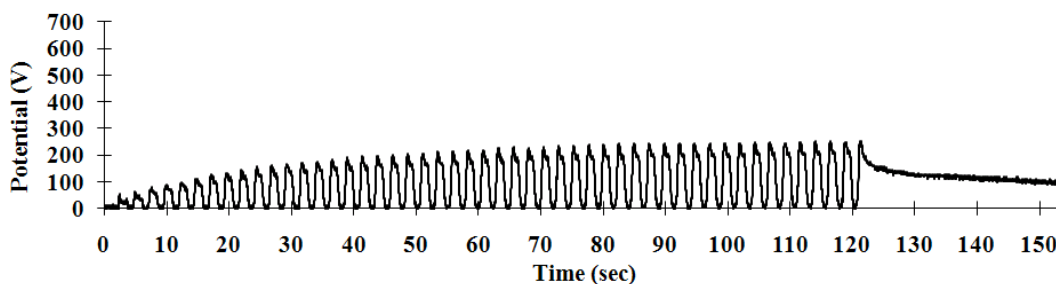


Figure 5.3 Charge accumulations in 50 cycles and charge decay on nylon surface

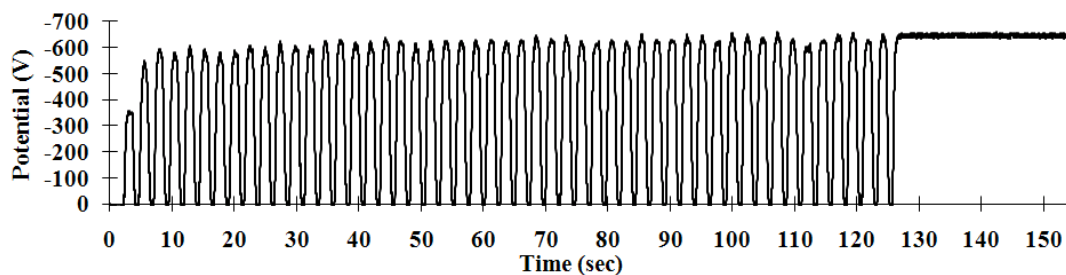


Figure 5.4 Charge accumulations in 50 cycles and charge decay on PTFE surface

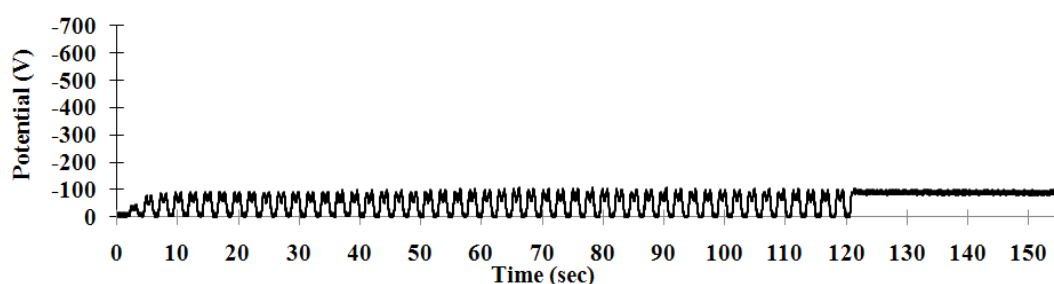


Figure 5.5 Charge accumulations in 50 cycles and charge decay on PP surface

5.4 Results and discussion

5.4.1 Experimental design I

Experiments showed that nylon was always positively charged (e.g. Figure 5.3), while PP and PTFE were always negatively charged (e.g. Figures 5.4 and 5.5) by rubbing against stainless steel. In order to compare the magnitude of charge generated under different conditions, only the absolute value (without polarity) of surface charge potential were compared. Figure 5.6 shows the absolute charge generated on polymers after the first cycle of rubbing and Figure 5.7 shows the absolute charge generated on polymers after 50 cycles of rubbing at different levels of contact force. Comparing the charge potential values in Figure 5.6 and Figure 5.7, it is shown that charge after 50 cycles of rubbing is much higher than charge after the first rubbing, for reasons discussed in section 5.3.2.

Figure 5.6 and 5.7 revealed that for PP, the charge increased almost linearly as the contact force increased from 0.4 N to 2 N. For nylon, charge was not significantly affected by the contact force. For PTFE, charge increased as the contact force increased from 0.4 N to 1.5 N, and then leveled off when the contact force increased from 1.5 N to 2 N. The difference might be caused by the difference of deformation properties of those surfaces. Howell, et al. (1959) found that when two surfaces contact the real contact area increased as the applied contact force increased. For polymeric surfaces, the elastic deformation is more significant for surface with lower Young's modulus. The modulus for materials used in this work was 1,655 mega Pascal (or 240,000 psi) for the PTFE and the PP, and 2,827 mega Pascal (or 410,000 psi) for the nylon (Manufacture data sheet, Industrial Plastic Supply, Inc.). Therefore, the real contact area of the PTFE and the PP could be increased, during the rubbing test, as the contact force increased, while, there was little deformation for the nylon. Since more real contact area would provide more particles to participate in the charge generation, it is expected that the charge potential increased significantly on PTFE and PP as the contact force increased, while there will be no significant charge increase on nylon. Furthermore, Rose and Ward (1957) showed that chemical bonds on polymers surfaces might be broken under the contact force. The broken chemical segments can provide electrons or ions to promote the charge generation. Therefore, charge generation increased as the contact force increased.

Both Figure 5.6 and Figure 5.7 show that the absolute charge generated on the PTFE was more than that on nylon and PP exhibited the lowest charge. This might be due to the difference in their surface chemical compositions and structures. Generally, polymer surface is composed of irregular crystalline and amorphous regions. The molecular segments existing in the amorphous region are more than that in the crystalline region. Polymer with a lower crystallinity might have more molecular segments on its surface, which can provide more free particles (electrons or ions), and promote the charge generation. Since, the crystallinity is about 40% for nylon, 43-48% for PTFE, and 80% for PP (Morton, 1975, Rae and Dattelbaum, 2004), charge generated on PP was found to be lower than that on nylon and PTFE. Nylon contains amine groups on its surface (-CO-NH-), which are highly polarized and could promote the charge generation. However, the

real contact area of nylon might be much lower than that of PTFE as discussed in previous paragraph (the modulus of nylon is higher than that of PTFE), thus, charge observed on nylon was still lower than that of PTFE.

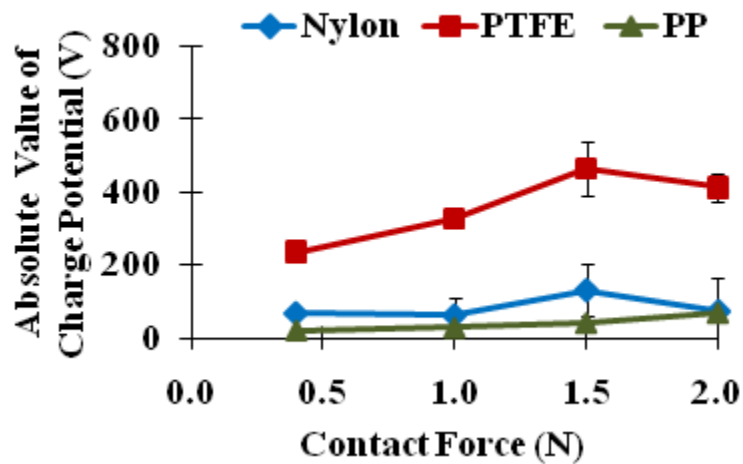


Figure 5.6 Effect of contact force on charge generated on polymer surfaces after the first cycle of rubbing against stainless steel (rubbing speed: 27 mm/sec)

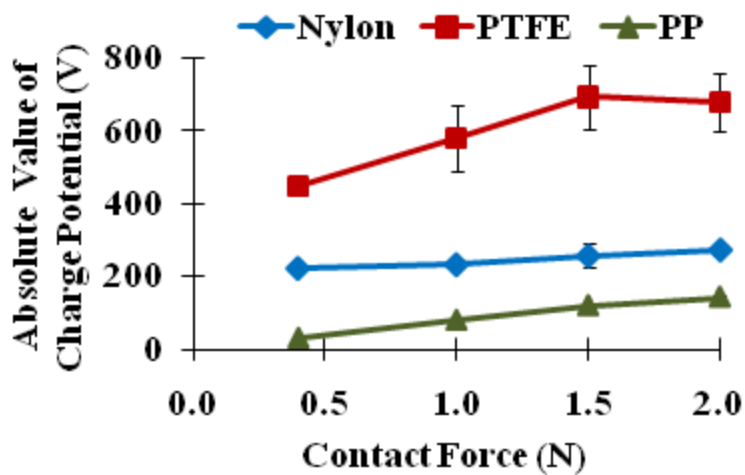


Figure 5.7 Effect of contact force on charge accumulated on polymer surfaces after 50 cycles of rubbing/contact against stainless steel (rubbing speed: 27 mm/sec)

The charge retained on three polymers after 30 seconds, which is a measure of charge decay, is shown in Figure 5.8 and the normalized charge retained is shown in Figure 5.9. It is shown that, after 30 seconds, charge retained on the nylon decreased to 60% or lower of the initial potential, while charge retained on the PTFE and the PP were the same as the initial potential indicating no charge decay within the time of measurement. The absolute charge retained on the PTFE was still the highest among the three polymers.

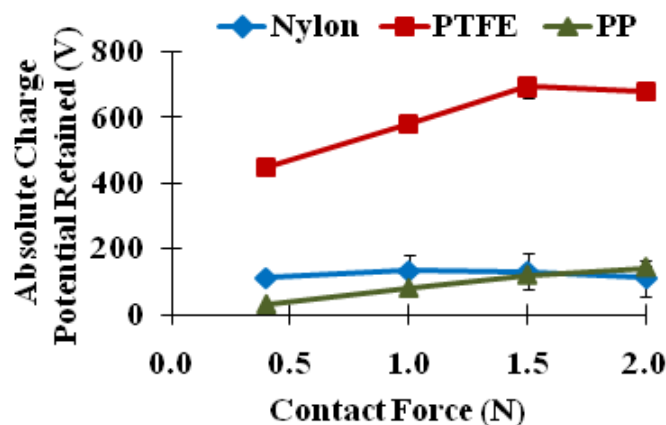


Figure 5.8 Effect of contact force on charge retained on polymer surfaces after 30 seconds of decay time

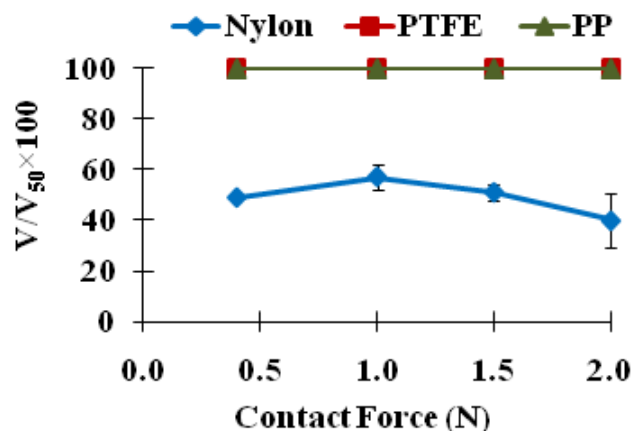


Figure 5.9 Effect of contact force on normalized charge retained on polymer surfaces after 30 seconds of decay time

Figure 5.10 shows the charge signals of the first two cycles of rubbing the three polymers. It can be seen that the curves for PTFE and PP within each cycle are symmetrical, while the curve for nylon is not. This reflects that there was no charge decay on PTFE and PP surfaces, while charge had decayed obviously in the backward stroke on nylon surface within a cycle (short time).

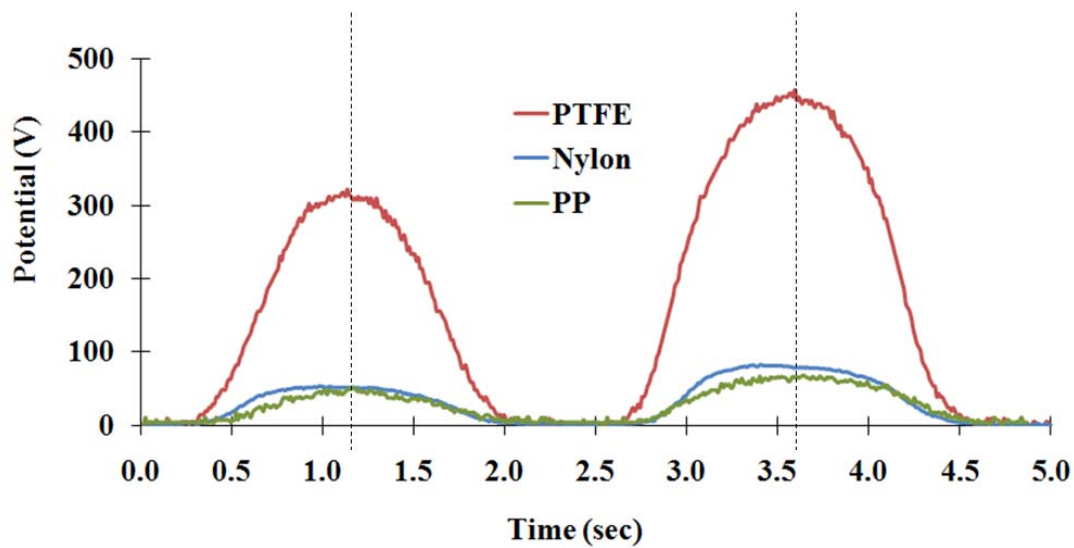


Figure 5.10 Charge potential of the first and second cycles of rubbing (contact force: 1N, rubbing speed: 47 mm/sec)

The results of the charge decay on nylon, PTFE, and PP in 30 seconds after the 50 cycles are shown in Figure 5.3, 5.4, and 5.5. For nylon, the charge decayed exponentially with time, and charge decayed to less than half of the initial charge within 30 seconds. For PTFE or PP surfaces, no charge decay was observed within 30 seconds. The typical curve of charge decay on nylon is regressed as shown in Figure 5.11, which was found to fit the following equation with R^2 value of 0.968.

$$V = 98e^{-0.5774t} + 135e^{-0.009293t}$$

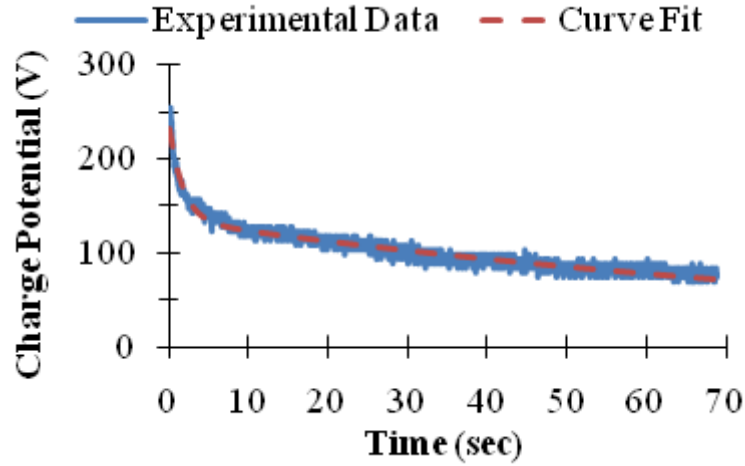


Figure 5.11 Exponential behavior of charge decay of nylon

In the rubbing device setup (Figure 5.1), a grounded plane was placed under the charged rubbing plate and there were grounded metal parts surrounding the charged surface. These are the bush, the shaft, the load, and the driving rod. Considering this device setup, a description of charge decay on the rubbing plate is shown in Figure 5.12, which is developed based on the decay mechanism for insulators (Jonassen, 1998). The decay of the charge occurs partly due to that the electrical flux (field lines) from the surface extended through the air toward the surrounding metal parts on the top, and part of the flux extended through the polymer bulk towards the substrate of the grounded plane.

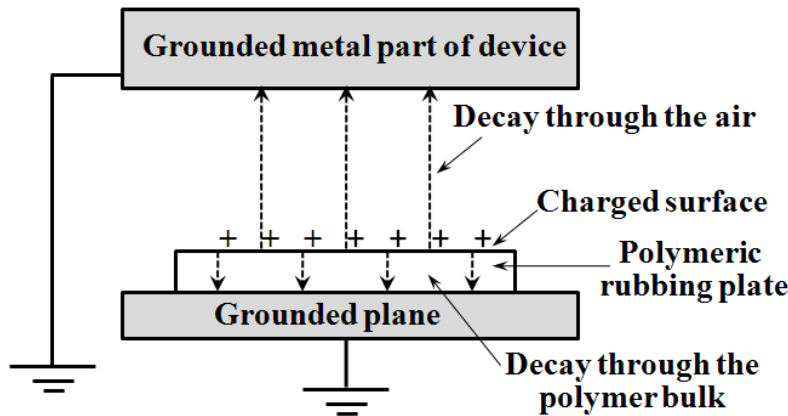


Figure 5.12 Charge decay model of a charged polymeric rubbing plate

Additionally, since the rubbing plate (300×90 mm) is larger than the rubbing area (52×20 mm; red rectangle in Figure 5.2), charge might move along the surface from the rubbing area to the surrounding areas on the plate (spread), which contributed to the decrease of the monitored charge potential. Literature (Ottewill, 1975) showed that charge could move along a polymeric surface when the humidity is high or the polymer has hydrophilic properties. In this work, only nylon is hydrophilic polymer (2% moisture content at 21°C and 43% R.H.) and PP and PTFE are hydrophobic, therefore, charge on nylon moved along its surface, while charge on PP and PTFE did not move during the 30 seconds of measurements.

Figures 5.3 to 5.5, and 5.11 depict different charge decay for different polymer. The rate of charge decay is determined by the properties of the medium, which could be the surrounding air, the nature of the surface and the bulk of rubbing plate. Thus the differences between the three polymers decay behavior can be explained as follows:

- Although the environmental condition was kept constant, however, the moisture absorbed/adsorbed on different polymeric rubbing plate is different, which affect the ability of charge moving (spreading) along the surface. Since the moisture content under temperature of 21°C and 43% R.H. was about 2% for nylon and

about 0% for PTFE and PP (Morton, 1975), thus, the charge moving on the nylon surface was faster than that the other two materials.

- The electrical properties (resistivity and dielectric constant) of polymers varied, which could affect the decay through the polymer to the substrate grounded plane. The dielectric constants were 3.6 for the nylon, 2.1 for the PTFE and 2.3 for the PP. The bulk resistivity is about 10^{15} ohm for the nylon, 10^{22} - 10^{24} ohm for the PTFE and 10^{20} ohm for the PP (Manufacture data sheet, Industrial Plastic Supply, Inc.), thus the charge might decay faster through the nylon than the other two polymers.

5.4.2 Experimental design II

Four levels of rubbing speed, including zero speed, which is equivalent to repeated contacts/separations, were used in experimental design II to find whether more charge was generated by rubbing than by contacts/separations, and whether the frictional charge is affected by the rubbing speed. The charge observed after the first cycle of rubbing is shown in Figure 5.13 and the charge after 50 cycles of rubbing is shown in Figure 5.14. It is shown that, for PTFE and nylon, the charge generated by friction was higher than that generated by repeated contacts/separations. For PP, however, the charges generated by contact and rubbing are close. During the rubbing, the real contact junctions between two surfaces are sheared, then the real contact area is increased, and molecular segments are broken and appease on the surface, which promotes the charge generation. However, this effect of rubbing might be not significant on PP, because of its higher crystalline structure; therefore not many molecular segments appear on the surface, even under the friction, to contribute to charge generation.

Figures 5.13 and 5.14 also indicate that, when the rubbing speed was not zero, the charge was not affected by the rubbing speed. It is worth mentioning that, in Chapter 4, on the frictional electrification between yarn and cylinder, it was found that charge increased significantly as the relative rubbing speed increased from 400 mm/sec to 1600 mm/sec. Therefore, it can only be concluded that frictional electrification is not affected

by rubbing speed at low speed levels, used in this research. Our device is limited in speed and it is recommended to conduct research to examine the phenomenon at higher speed than that used here.

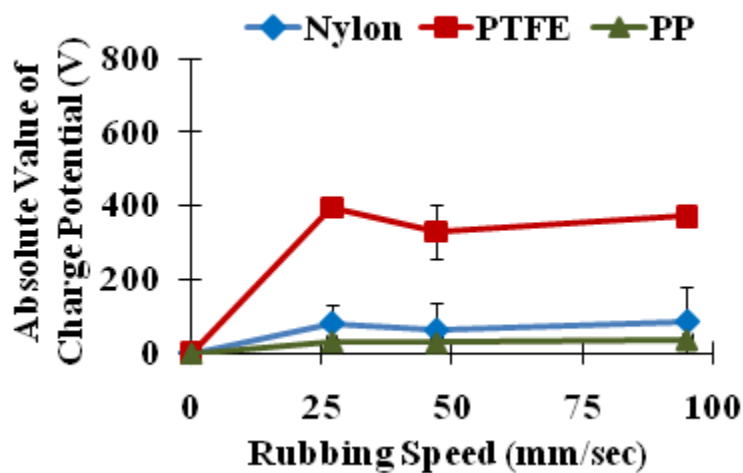


Figure 5.13 Effect of rubbing speed on charge generated on polymeric surface after the first cycle of rubbing or the first contact/separation against stainless steel

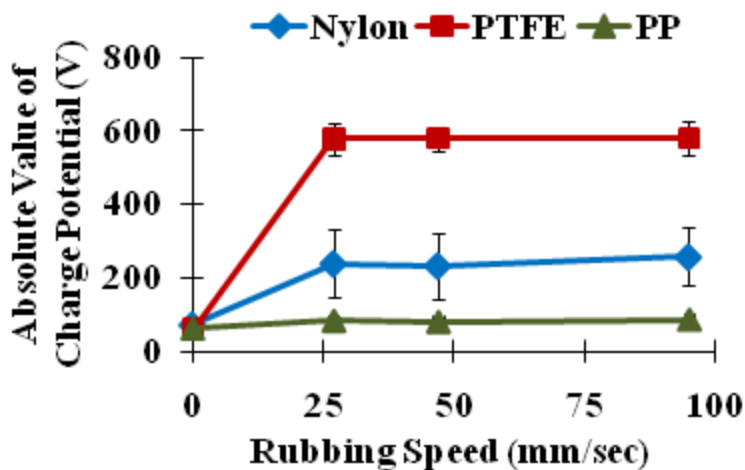


Figure 5.14 Effect of rubbing speed on charge generated on polymeric surface after 50 cycles of rubbing (99 strokes) or 99 contacts/separations against stainless steel

The charge retained on polymer surfaces after 30 seconds of decay time is shown in Figure 5.15 and the normalized charge retained as the percentage of the initial potential is shown in Figure 5.16. Again, the charge on the nylon surface decayed to 60% or lower compared to the initial potential, while the PTFE and PP did not show any decay.

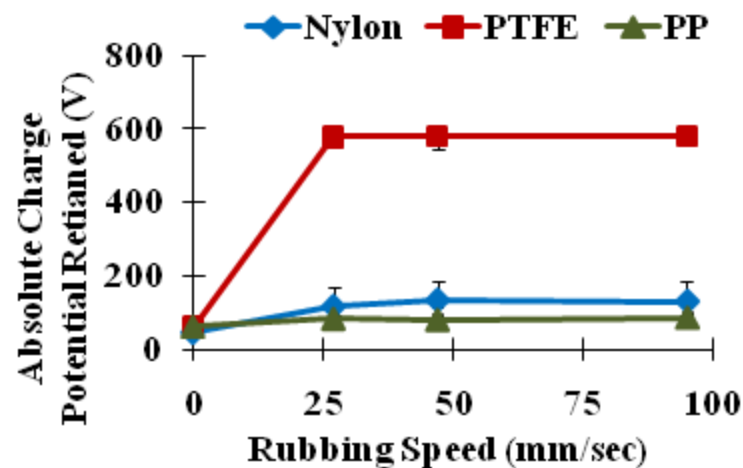


Figure 5.15 Effect of rubbing speed on charge retained on polymeric surfaces after 30 seconds of decay

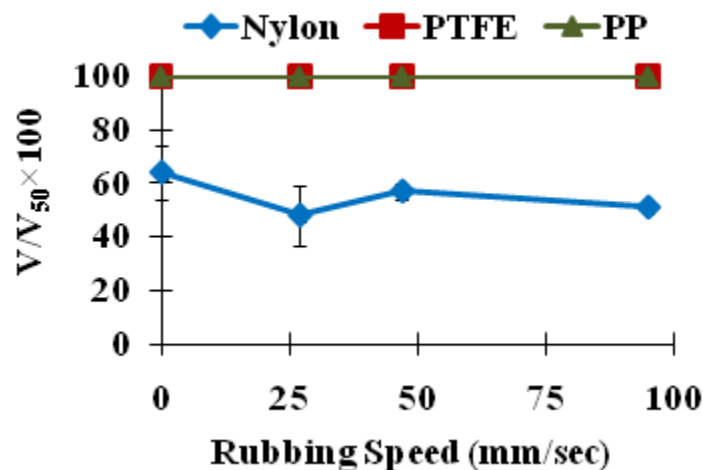


Figure 5.16 Effect of rubbing speed on normalized charge retained on polymeric surfaces after 30 seconds of decay

5.4.3 Experimental design III

Frictional electrification between the nylon, PP, PTFE, and stainless steel flat surfaces was investigated at constant contact force and rubbing speed to find their tribo-electric series. The surface charge potential (both the charge polarity and magnitude) are shown in Figure 5.18 and Figure 5.19. It is shown that the PTFE was always negatively charged after rubbing against the other three surfaces, nylon was always positively charged, and the PP was negatively charged except rubbing against the PTFE, thus, the tribo-electric series of these four materials is as follows:

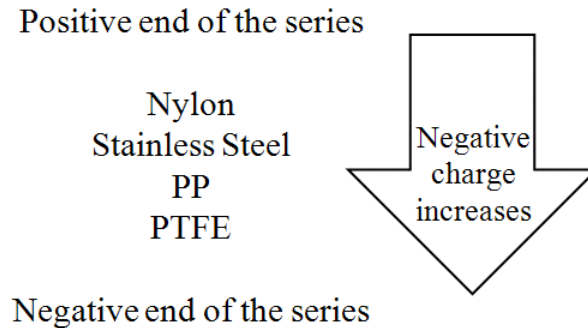


Figure 5.17 Triboelectric series of nylon, stainless steel, PP, and PTFE

Previous research indicated that the tribo-electric series was only concluded as the sequence of charge polarity by rubbing two materials against each other. However, it was also stated that the charge magnitude decreased as the position in the tribo-electric series between two materials getting closer (Ballou, 1954, Welker, 2006). Our experimental results do not support this statement. Figures 5.16 and 5.17 show that the charge magnitude on PTFE decreased as the other material (rubbing head) changed from stainless steel to nylon, and then to PP, which did not agree with the tribo-electric series resulted from the charge polarity (Figure 5.17). This could be explained by that the magnitude of charge is affected by the stiffness of surfaces, in other words; the contact

area dominated the amount of charge generated here and does not correlate to the position of a material in the tribo-electric series.

Furthermore, it is evident from these results that the charge measured on the rubbing plate cannot be used to infer the charge on the rubbing head. Indeed when the polymers used for rubbing plate and rubbing head are interchanged, very different results can be found. For example, when nylon rubbing against PTFE, the magnitude of charge observed on nylon (58 V) is not equal to that observed on PTFE (212 V). This could be attributed to the difference in decay behavior discussed earlier since the measurement is monitored with lag time between the charge and measurement by the probe.

The results of the absolute charge retained on the surface and normalized charge retained (not shown) indicated that charge on nylon decreased to about 60% or less amount of the initial charge, while the other two materials did not show any charge decay in 30 seconds. This supports the findings of experimental design I discussed in section 5.4.1.

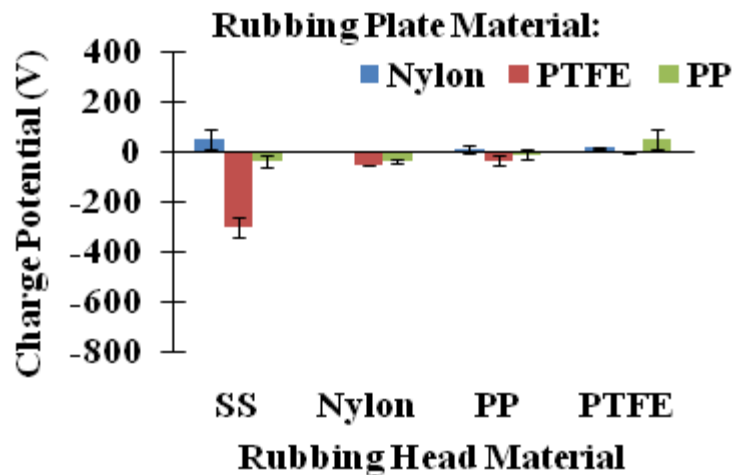


Figure 5.18 Charge potential on rubbing plate after the first cycle of rubbing against the rubbing head (rubbing speed: 47 mm/sec, contact force: 1N)

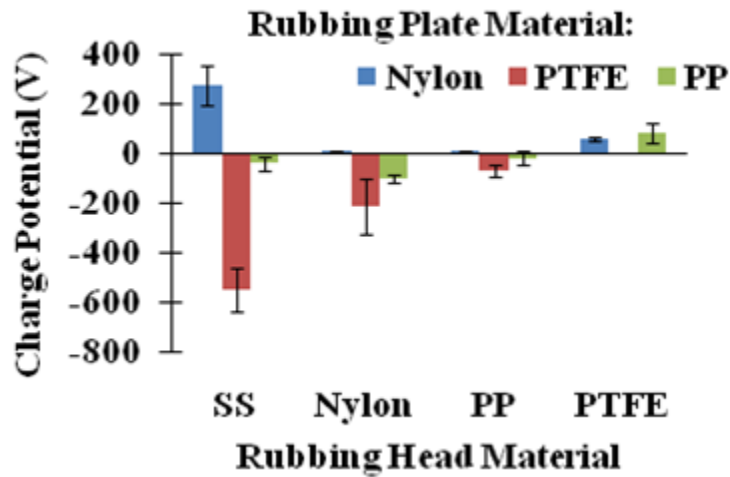


Figure 5.19 Charge potential on rubbing plate after 50 cycles of rubbing against the rubbing head (rubbing speed: 47 mm/sec, contact force: 1N)

5.5 Conclusion

Our automated rubbing device enabled an investigation of tribo-electrification between two parallel surfaces at any desired number of cycles of rubbing under different levels of contact force and rubbing speed. It was found that charge accumulated on nylon surface in repeated rubbing and leveled off after about 40-50 cycles, while charge on PTFE and PP reached the charge saturation after only 2 or 3 cycles. Charge on nylon decreased to 60% or less of the initial charge (charge accumulated after 50 cycles of rubbing), while charge on PTFE and PP did not decay within 30 seconds.

When the three examined polymers were rubbed against stainless steel surface, it was found that charge on PTFE and PP increased as the contact force increased, however, the effect was not seen on nylon. The study also showed that charge generated on nylon and PTFE due to rubbing was higher than due to repeated contacts/separations. However, this effect was not observed on PP. Rubbing speed in the range 27-95 mm/sec did not show significant difference on charge generation on the three polymers studied.

The tribo-electric series of four materials were established by rubbing against each other under the same contact force and rubbing speed, which indicated that the series was nylon (+), stainless steel, PP, and PTFE (-) from positive to negative. The charge observed on one surface did not reflect the charge generated on the other been rubbed against it due to difference in decay behavior.

Our findings could be used to characterize polymers electrostatic behavior and identify whether a polymer requires antistatic finish treatment to reduce/eliminate the problems of such material during processing or while use by consumers.

References

Ballou, J.W., "Static Electricity in Textiles" (1954), *Textile Research Journal*, 24(2), p.146-155.

Castle, P.G., "Contact charging between insulators" (1997), *Journal of Electrostatics*, 40 (1), p. 13-20.

Gupta, B.S., "Friction in Textile Materials" (2007), London: Woodhead.

Harper, W.R., "The generation of static charge" (1957), *Advances in Physics*, 6(24), p. 365-417.

Hersh, S.P. and Montgomery, D.J., "Static electrification of filaments" (1955), *Textile Research Journal*, 25(4), p. 279-295.

Howell, H.G., Mieszkis, K.W., & Tabor, D., "Friction in textiles" (1959), New York: Textile book publishers in association with the Textile Institute.

Jonassen, N., "Electrostatics" (1998), New York: Chapman and Hall.

Komatsu, T.S., "Static electrification by asymmetric rubbing" (2004), *Applied Surface Science*, 235(1-2), p. 60-64.

London, J.J., "Effects of pretension and yarn speed on electrostatic charge generation on continuous filament yarns" (Master Thesis) (1966), North Carolina State University.

Medley, J.A., "Discharge of electrified textiles" (1954), *Journal of Textile Institute*, 45(2), p. 123-141.

Morton, W.E. and Hearle, J.W., “*Physical Properties of Textile Fibers*” (1975), London: Heinemann, p. 171.

Ohara, K., “Relationship between friction electrification and molecular motion of polymers” (1980), *Journal of Electrostatics*, 9(2), p. 107-115.

Ohara, K., Nakamura, I., and Kinoshita, M., “Frictional electrification between flat surfaces of polymers and of Langmuri-Blodgett layers” (2001), *Journal of Electronics*, 51-51(1-4), p. 351-358.

Ottewill, R.H., “Static Electrification” (1975), *IPPS Conference*, London: Institute of Physics. 27, p. 56

Rae, P.J. and Dattelbaum, D.M., “The properties of poly(tetrafluoroethylene) (PTFE) in compression” (2004), *Polymer*, 45(22), p. 7615-7625.

Suh, M., Seyam, A.M., Oxenham, W., and Theyson, T., “Static generation and dissipation of polyester continuous filament yarn” (2010), *Journal of Textile Institute*, 101(3), p. 261-269.

Seyam, A.M., Cai, Y., and Oxenham, W., “Devices for measuring electrostatic generation and dissipation on the surfaces of polymeric materials” (2009), *Journal of Textile Institute*, 100(4), p. 338-349.

Taylor, D.M. and Secker, P.E., “*Industrial Electrostatics: Fundamentals and Measurement*” (1994), New Jersey: John Wiley & Sons, Inc.

6 CONTACT ELECTRIFICATION OF POLYMERIC PLATES

This chapter is modified from a manuscript entitled “Contact electrification of polymeric surfaces”, by L. Liu, W. Oxenham and A.M. Seyam, which is submitted to *Indian Journal of Fiber and Textile Research*.

6.1 INTRODUCTION

Synthetic polymers are widely used because they offer excellent properties and relatively low price. However, most of the synthetic polymers have a common drawback, which is that electrostatic charge is easy to generate but hard to dissipate, which causes problems in industry. For example, in textiles, charge can be generated on synthetic fibers/filaments when they are transported across rollers and guides. The generated charge may cause the films/fibers/filaments to cling on parts of the machine and therefore cause the production line to stop, which results in the irregularity of products and low manufacturing efficiency. More severely, the charge may be sufficient to cause sparks and lead to fires and explosions in the plants. Therefore, it is extremely important to understand the mechanisms of static behavior of synthetic polymers, so that efforts can be made to minimize its negative impact.

The static generation can be classified into contact electrification (charging by contact and separation of two different surfaces) and frictional electrification (charging by dynamic rubbing of two surfaces). Compared to the frictional electrification, the contact electrification is simpler for analysis since there is no concern about the rubbing speed and its interactions with other factors (e.g. temperature and contact area) on the static generation. There have been several studies on the contact electrification of polymeric plates (Lowell and Rose-Innes, 1980, Castle, 1997, Homewood and Rose-Innes, 1982). It was revealed that charge increased as the number of contacts increased, and the rate of increase of charge decreased as the number of contacts increased and a saturation value appeared after many cycles of contacts. However, there is no universally agreed explanation on the issue that why the charge increases with number of contacts. One of the important factors influencing the charge generation is the contact area between two contacted surfaces. The researches of Coste and Pechery (1981) and Ohara et al. (2001) indicated that charge would increase as the surface roughness decreased. The reason lies in that the increase of the real contact area would provide more electrons or ions to participate in the charge transfer. In addition to the effect of contact area, researchers have attempted to understand the influence of environmental conditions on contact electrification (Medley, 1954, Sawa and Calderwood, 1971, Awakuni and

Calderwood, 1972, Sereda and Feldman, 1964, and Greason, 2000). However, it is evident that in some cases the reported observations were in conflict with each other. For example, Sereda and Feldman (1964) and Medley (1954) pointed out that charge would increase as the relative humidity (R.H.) increased. After the charge reached a maximum value, the charge decreased rapidly as the R.H. kept increasing. Ohara (1980) found that charge could reach a maximum value and then decreased as the temperature increased. However, Greason (2000) found that charge kept decreasing as the R.H. and the temperature increased. Possible reasons for this disparity could be attributed to the differences in experimental procedures coupled with the accuracy of systems used.

In order to gain a better understanding of the static behavior of polymers, this work examines the contact electrification of flat polymeric surfaces that are commonly used in industry. PTFE, nylon 6,6 and PP were tested for static charging under different levels of contact force, relative humidity, and temperature.

6.2 EXPERIMENTAL

6.2.1 Contact device

The device used to measure the amount of electrostatic charge generated on a sample after contacting a polymeric surface is shown in Figures 6.1 and 6.2. The device is housed inside a walk-in environmental room where temperature and humidity are precisely controlled. The Faraday tube is used for determining the charge amount. For each contact, the stepper motor drives the contact head with controlled speed and force to establish contact of the sample with the polymeric flat surface, and then the contact head is withdrawn into the Faraday tube, thus static charge amount can be detected after each contact and separation (cycle). The procedure is repeated in order to measure the charge accumulation after certain number of cycles that enable the evaluation of saturation charge (maximum charge that the surface can accumulate). The charge amount is measured by a Keithley® 6514 electrometer. The contact force is monitored by a Transducer Techniques® compression load cell. The desired test parameters (contact force, number of contacts, rate of data collection, and contacts/minute) can be precisely

controlled and pre-programmed through user interface. The static generation/dissipation data are automatically captured using computer data acquisition (DAQ) system.

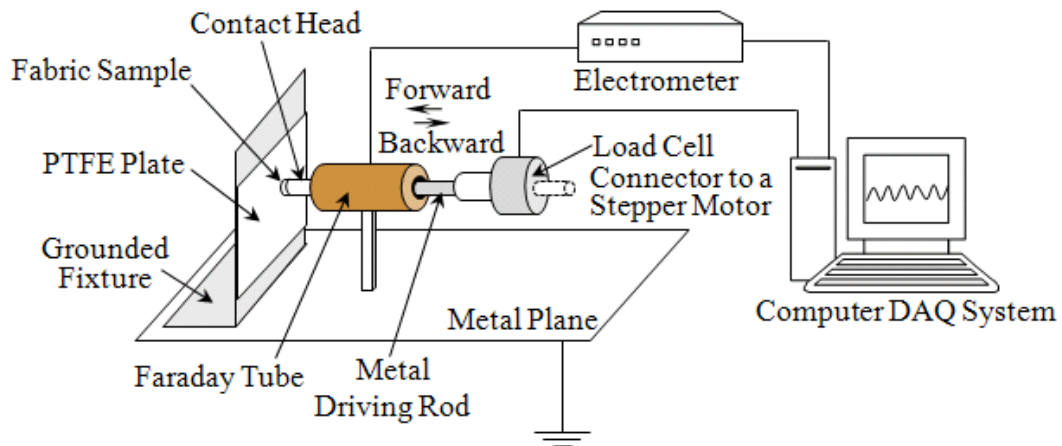


Figure 6.1 A Diagram of the contact charge generation/dissipation measurement device

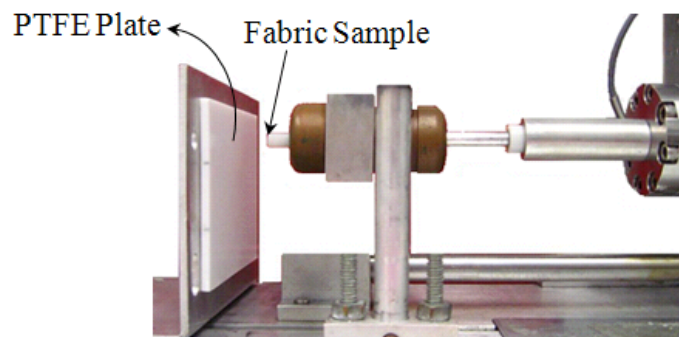


Figure 6.2 Image of the contact device

6.2.2 Signal analysis

6.2.2.1 Charge generation

Figure 6.3 shows a typical static charge (expressed in Pico Coulomb, pC) data of repeated contact test. At the start of the test (time zero), the charge is zero with the contact head inside the Faraday tube. The test starts by moving the contact head forward (toward the metal or polymeric surface, PTFE in this case). At point A_1 , the first contact between the two surfaces was established and then the contact head movement was reversed backward (away from the PTFE surface). At point B_1 , the charged sample began to enter the Faraday Tube and at point C_1 the sample was moved entirely inside the Faraday tube. At point D_1 the sample was at the middle of the Faraday tube and contact head motion was reversed. At point E_1 the sample began to leave the Faraday tube until it was completely outside the tube at point F_1 . Points A_2 , B_2 , C_2 , D_2 , E_2 , and F_2 are the same as above for the second contact and separation cycle. The period T_1 represents the time during which the contact head moved forward while the period T_2 is the time during which the contact head moved backward. Figure 6.3 shows that the charge after the second contact (represented by charge at point C_2 , D_2 , or E_2) is higher than the charge generated after the first contact (represented by charge of point C_1 , D_1 , or E_1).

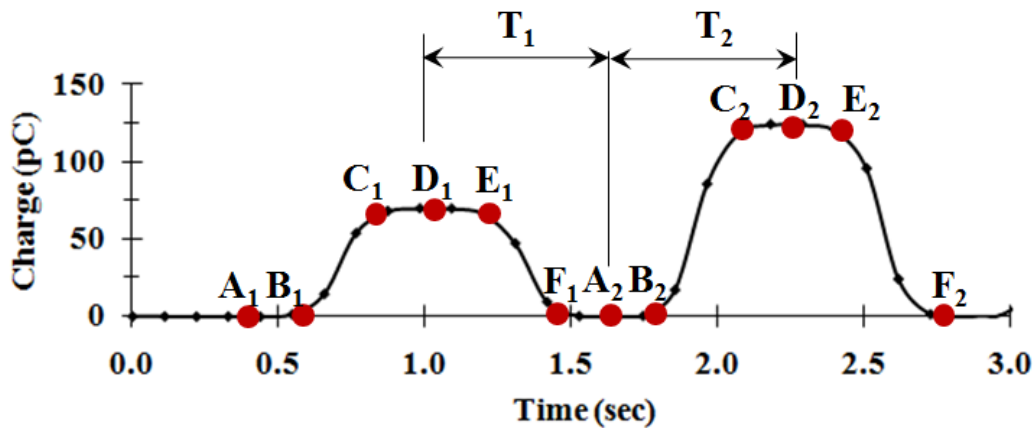


Figure 6.3 Typical static charge data of repeated contact test

6.2.2.2 Determination of charge saturation

We established procedure to determine the charge saturation (maximum charge that the material can hold under certain experimental conditions) of a material. The first step is to run repeated contact test for large number of cycles as shown in Figure 6.4. Then use the charge after each contact along with the corresponding cycle number to derive an exponential regression equation that fits the data. Figure 6.5 shows the experimental data (dots) of Figure 6.6 and the derived exponential regression relationship (continuous line) of charge generated in terms of cycle number. The general form of regression equation that fits the data is

$$Q = a + b \times e^{-cn} \quad [6-1]$$

Where a, b, and c are constants, Q is charge in Pico Coulomb, and n is a positive integer representing the number of contacts (1, 2, 3...).

Equation 6-2 shows the derived equation that fits the data of Figure 6.5 with R₂ value of 0.9953.

$$Q = 207 - 210 \times e^{-0.08961n} \quad [6-2]$$

The charge after first contact (Q₁) can be obtained when substituting n=1 into equation [6-2] as follows:

$$Q = a + b \times e^{-0.08961n} = 207 - 210 \times 0.9143 = 15 \text{ pC}$$

The charge saturation (Q_s) can be obtained when substituting n= ∞ into equation [6-2] as follows:

$$Q = a + b \times 0 = 207 \text{ pC}$$

The equation allows the determination of charge generated after any desired number of cycles.

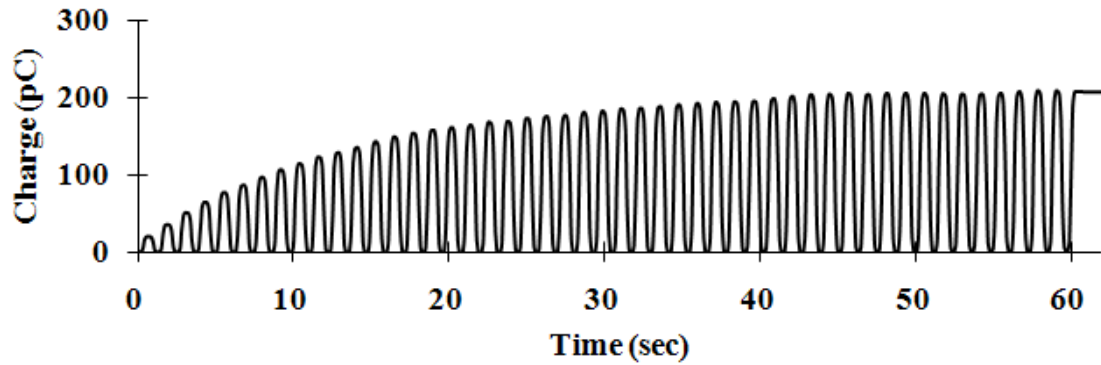


Figure 6.4 Electrostatic charges of 50 cycles of contact

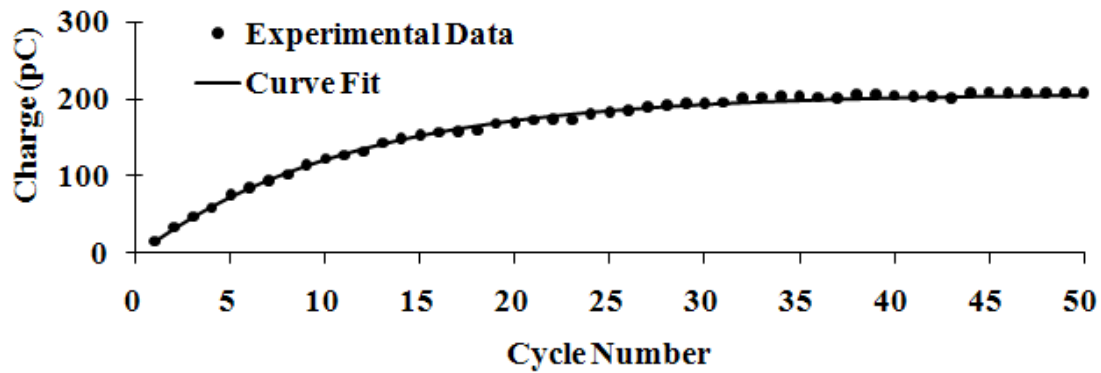


Figure 6.5 Experimental data of Figure 6.4 and derived exponential regression relationship of charge generated in terms of cycle number

From a range of experimental runs, it was found that the charge saturation in most runs was reached after 50 contacts. This fact was supported by calculating the charge saturation at different number of cycles as well as infinite number of contacts. Additionally, the rank of the cycle number-charge relationship in terms of parameters studied is the same for 50, 100, or infinite contacts. This is the reason why the charge generation after 50 contacts was selected as response for the experimental design.

Previous literature (Lowell and Rose-Innes, 1980) indicated that the charge increased as the number of contact increased. The rate of increase of the charge decreased as contacts were repeated, and after many contacts, the charge appeared to saturate. The reason why this happens is not, however, understood. Several explanations have been put forward, but each of them is applicable to only a certain kind of material:

- 1) The increase of charge with number of contacts may be a result of the fact that the charge transferred depends on the total time of contact (Lowell and Rose-Innes, 1980).
- 2) The increase of charge with number of contacts may be caused by the increase of real contact area, which is related to the viscoelastic deformation of polymeric surfaces, produced by repeated contacts (Lowell and Rose-Innes, 1980).
- 3) The repeating contacts may be expected to increase the charge if the polymeric surface is slightly conducting, because the charge tends to spread (under its own Coulomb repulsion) into the bulk, making room for more charge to be deposited during the next contact (Harper, 1967).

6.2.3 Sample preparation

The device (Figure 6.2) used to measure the amount of electrostatic charge generated on a contact head after contacting a fixed contact plate (polymeric or metal). In this work, finish free nylon, PP, PTFE, and stainless steel rods were machined to the required shape of contact head, which is cylinder of 6.35 mm diameter (Figure 6.7). One end of the contact was drilled for mounting onto a driving rod. The other end of the contact head was flat surface, which would contact and separate with the fixed contact plate. After the initial machining, each contact head was smoothed by sand paper (grit size: 2000) and water to reduce their surface roughness. Additionally, nylon, PP, PTFE and stainless steel plates were cut as 10×10 cm to be used as the fixed contact plate. All the contact heads and contact plates were cleaned by ethanol, deionizing water, and deionizing gas, and then kept inside an environmental room under required condition for at least 24 hours. Before each test, the initial charge on the contact head and the contact plate was measured and if it was not zero, the cleaning procedure was repeated again.

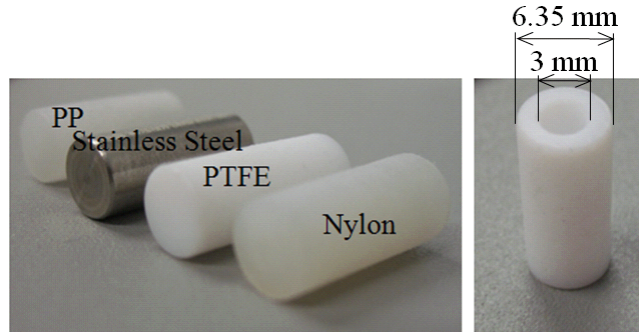


Figure 6.6 Images and dimensions of contact heads

6.2.4 Experimental design

Two sets of experiments were conducted. The first dealt with evaluation of static generation on PTFE contact head after contacting against nylon contact plate (Table 6.1). The second addressed static generation on nylon, PTFE, stainless steel and PP surfaces when contact against each other (Table 6.2). Tables 6.1 and 6.2 depict the parameters and their levels.

Table 6.1 Experimental design I

Parameters	Levels
Relative Humidity (%)	43, 55, 65
Temperature (°C)	21, 25, 30
Contact Force (N)	11, 14, 17
Total Runs ¹	$3 \times 3 \times 3 = 27$

¹Each run was replicated 3 times and a total of 81 observations were obtained for each response ($3 \times 3 \times 3 \times 3 = 81$)

The fixed parameters for the first experiment were: PTFE contact head; nylon contact plate; 72 cycles/min contact frequency; 17 points/sec data collection rate. The responses considered for this experiment were charge generated on the PTFE contact head after the first contact, 50 contacts, 100 contacts, and 120 contacts.

Table 6.2 Experimental design II used to investigate the static generation of nylon, PP, stainless steel, and PTFE by contact against each other

Parameters	Levels
Relative Humidity (%)	43, 65
Temperature (°C)	21, 30
Contact Head Material	Nylon, PP, Stainless Steel, PTFE
Contact Plate Material	Nylon, PP, Stainless Steel, PTFE
Total Runs ¹	$2 \times 2 \times 4 \times 4 = 64$

¹Each run was replicated 3 times and a total of 192 observations were obtained for each response ($2 \times 2 \times 4 \times 4 \times 3 = 192$)

The following parameters were fixed for the second experiment: 14 N contact force; 72 cycles/min contact frequency; 17 points/sec data collection rate. The response considered for this experiment was charge generated on the contact head after 50 contacts.

6.2.5 Statistical analysis

The data of the measured parameters were processed using Analysis of Variance (ANOVA) to reveal the influence of the main parameters and their interactions on the responses listed above.

6.3 RESULTS

6.3.1 Experimental design I

The ANOVA indicated that the effect of contact force on charge generation is significant for charge generated after the first, 50, 100, and 120 cycles of contact. The p-value is 0.0094 for the response of charge generated after the first contact, 0.0008 for charge after 50 contacts, 0.0003 for charge after 100 contacts, and 0.0004 for charge after 120 contacts (if the p-value < 0.05, it indicates that the effect is significant at 95% confident level). Figures 6.8, 6.9, 6.10, and 6.11 show the charge generated on PTFE after the first

contact, 50 contacts, 100 contacts, and 120 contacts against nylon. Each value in the figures represents the mean of 3 replications. Although there are a few exceptions (charge generated under 25°C and 43% R.H. and under 25°C and 65% R.H.), the absolute charge generally increases as the contact force increases from 11 N to 17 N. This can be explained by the fact that with higher force the contact area between the nylon and PTFE surfaces increases (Pascoe and Tabor, 1956). The increase of contact area allows greater transfer of electrons from the nylon to the PTFE, which causes more negative charge generated on the PTFE.

Figure 6.12 shows typical curves of charge generated in repeating contacts under the three levels of contact force. It is found that charge saturation in most runs was reached after 50-100 contacts. Additionally, the rank of the cycle number-charge relationship in terms of parameters studies is the same for 50, 100, or 120 contacts.

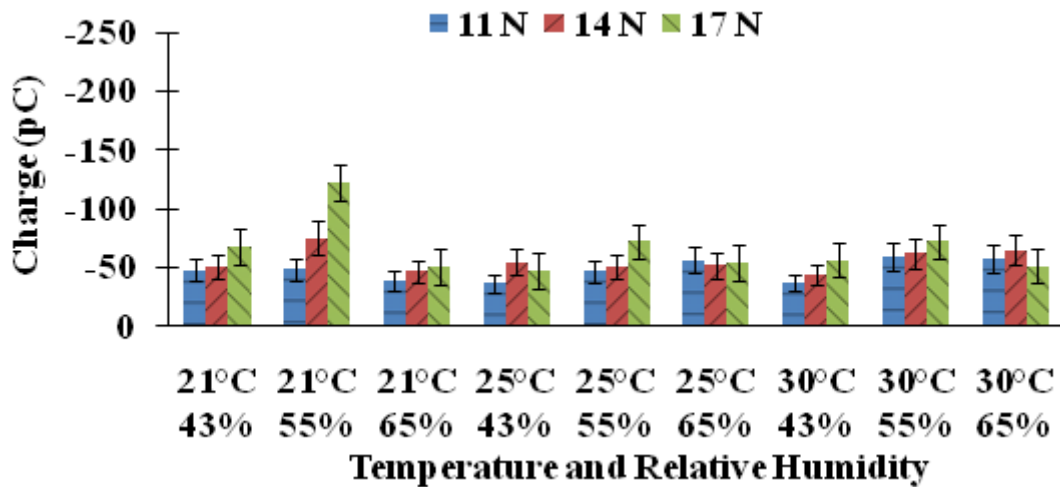


Figure 6.7 Charge generated on PTFE after the first contact against nylon

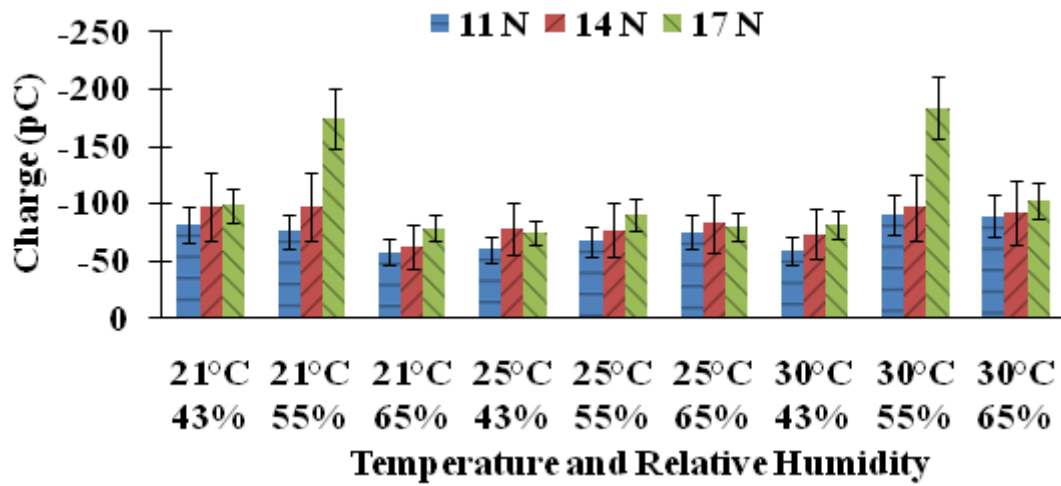


Figure 6.8 Charge generated on PTFE after 50 cycles of contacts against nylon

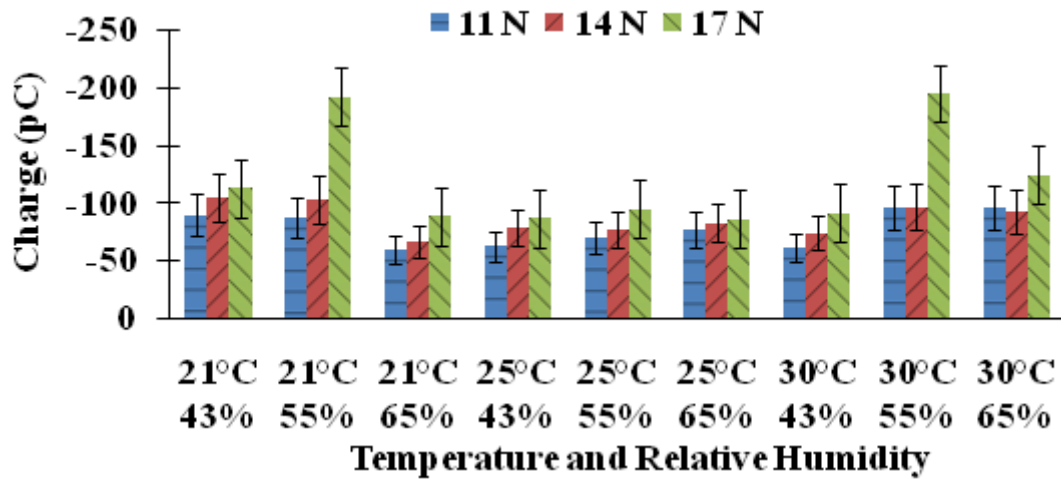


Figure 6.9 Charge generated on PTFE after 100 cycles of contacts against nylon

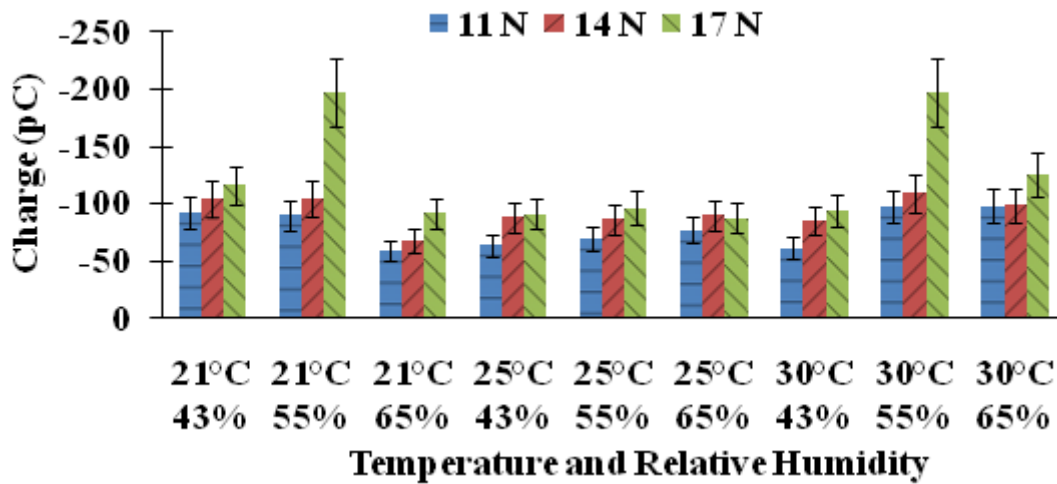


Figure 6.10 Charge generated on PTFE after 120 cycles of contacts against nylon

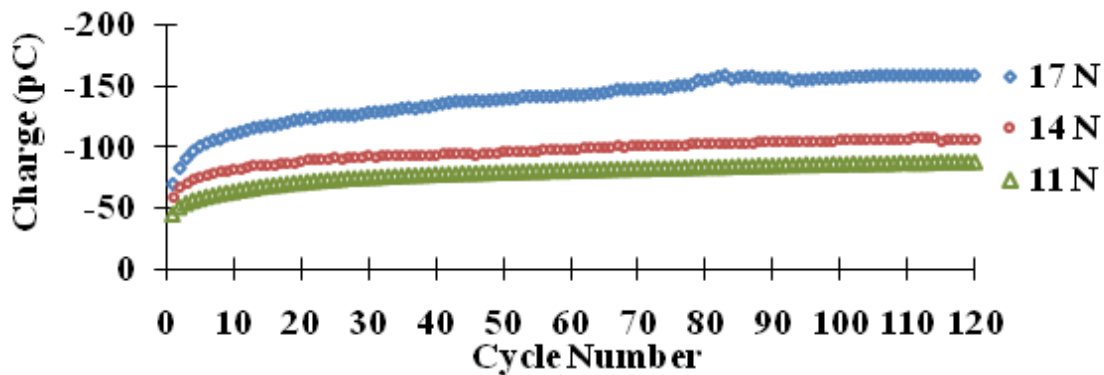


Figure 6.11 Charge generated on PTFE by repeated contacts/separations against nylon, at different contact force (temperature of 30°C and R. H. of 30%)

The ANOVA indicated that when the data was collectively analyzed the effect of R.H., temperature, and their interaction on charge generation is significant irrespective of the number of contacts (p-values are smaller than 0.05). The values of charge generated after 50 contacts (data shown in Figure 6.9) are sorted by relative humidity as shown in Figure 6.13 and by temperature in Figure 6.14. Figure 6.13 shows no general trends and only in two cases were immediately observable difference present (at the temperature of

21° and 25°C, R.H. of 55%, and the contact force of 17 N). Similarly, no general trends were observed for the difference of temperature with only the two data points mentioned above showing any major difference. The statistically significant differences seem to be very influenced by the two highest values.

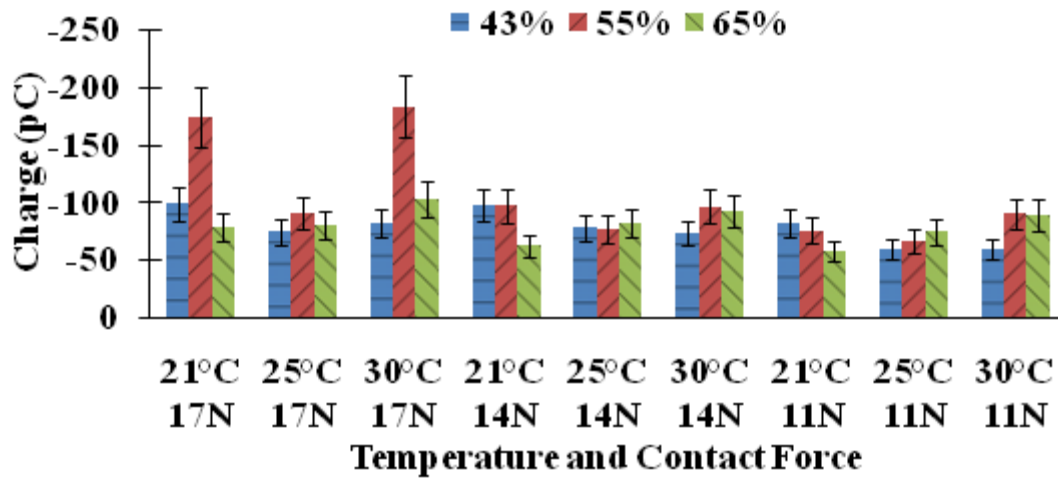


Figure 6.12 Data of Figure 6.9 sorted by the relative humidity

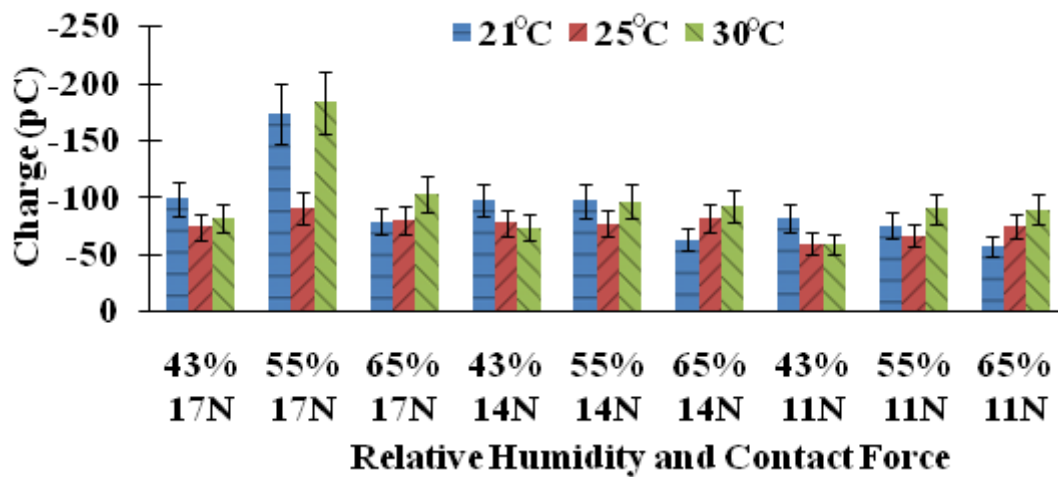


Figure 6.13 Data of Figure 6.9 sorted by the temperature

6.3.2 Experimental design II

In experimental design II, the nylon, PP, stainless steel and PTFE surfaces were contacted against each other. It was found that the PTFE was always negatively charged and the nylon was always positively charged after contacting (and separating from) the other three materials. The PP was negatively charged against nylon and stainless steel, and it was positively charged against the PTFE. According to these observations, the triboelectric series for these four materials can be summarized in the order of nylon (+), stainless steel, PP, and PTFE (-). The material close to the positive end of the series is positively charged when contact against materials close to the negative end of the series. This agrees with other researchers' tribo-electric series (Diaz and Felix, 2004).

Figure 6.15 shows the charge generated on PP after 50 contacts against other materials. It is shown that the amount of charge on PP after contacting nylon is larger than that after contacting PTFE, and the charge on PP after contacting stainless steel is lowest. There is no general trends exhibited for the effect of R.H. on charge generated. Figure 6.15 also shows that the higher charge is generated at the higher temperature irrespective of humidity. This could be the combine results of different effects:

- At a given relative humidity, the water content in the air at high temperature is more than that at low temperature. At the R.H. of 43%, there was about 12 g of water per kilogram of air when the temperature was 21°C, while 20 g of water per kilogram of air when the temperature was 30°C (Perry and Green, 2007). The water in the air can be adsorbed on synthetic polymeric surface, though the surface is hydrophobic. The water molecules on polymeric surface may perform in two ways: 1) Charging - water performs like media for charge transfer, and thus potentially increase charging; 2) Dissipation - water acts as conductor, which may help the charge moving along the surface or into the bulk (Sereda and Feldman, 1964).
- The mobility of molecules increase as temperature increases. Based on this law, the mobility of molecules on polymeric surface increases as the temperature increases, which can promote the charge transfer (Ohara, 1980). Meanwhile, the mobility of molecules in the air increases as the temperature increases, which may promote the charge dissipation through the air (Jonassen, 1998).

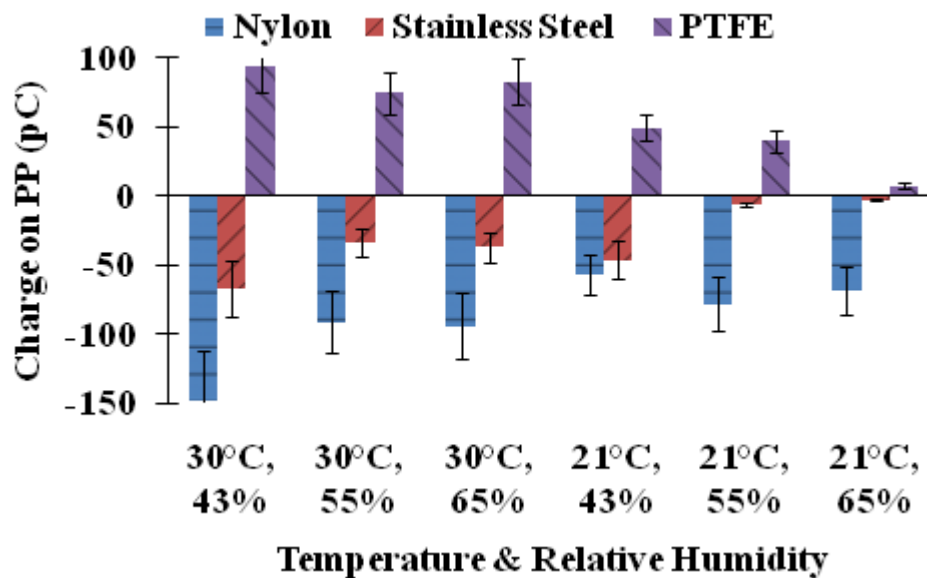


Figure 6.14 Charge generated on PP after 50 cycles of contacts against nylon, stainless steel, and PTFE

Figure 6.16 shows the charge generated on PTFE after 50 cycles of contacts against other materials. The charge on PTFE after contacting nylon is highest, while the charge generated on PTFE after contacting PP is variable with temperature and humidity; however no clear trend is evident. It is interesting to note that the charge generated on PTFE after contacting nylon is higher than contacting other materials, however, the charge observed on nylon after contacting other materials is always very low (< 15 pC).

Additionally, no charge was observed on the stainless steel contact head, which is expected from a good conductor.

It is evident from these results that the charge measured on the contact head cannot be used to infer the charge on the contact plate. Indeed when the polymer used for contact plate and contact head are interchanged very different results can be found. For example, PP generates a significant charge when contacted against the PTFE plate, but PTFE only generates a small charge when contacted against the PP plate.

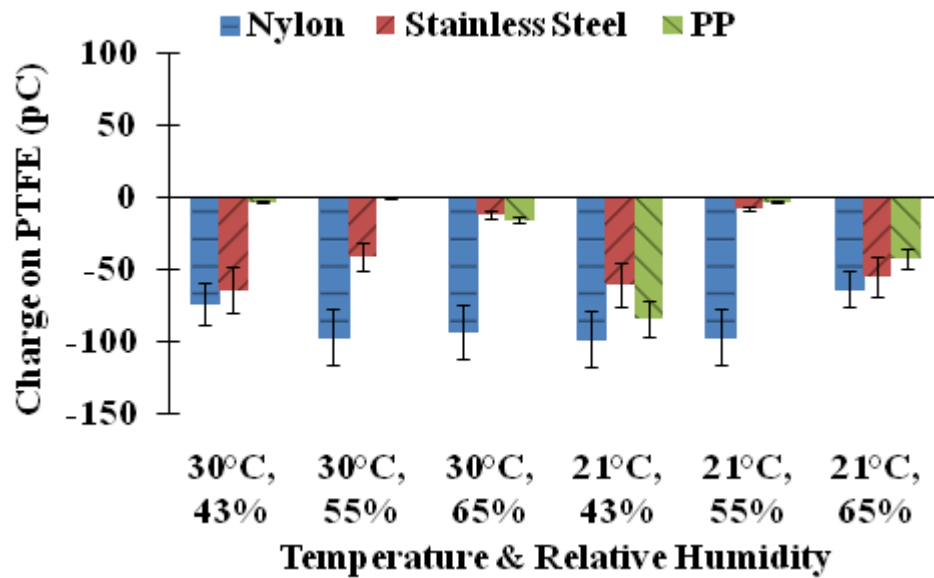


Figure 6.15 Charge generated on PTFE after 50 cycles of contacts against nylon, stainless steel, and PP

6.4 Conclusions

The contact electrification tests between finish free PTFE and nylon surfaces revealed that charge increases as contact force increases. The triboelectric series of four different materials was investigated by contacting against each other. It was found that their triboelectric series was nylon (+), stainless steel, PP, and PTFE (-). The absolute charge generated on nylon was much lower than that generated on PP or PTFE. Additionally, it is found that charge generated on one surface can not represent the charge on the other surface by which it is contacted.

Reference

- Awakuni, Y. and Calderwood, J.H. (1972). Water vapour adsorption and surface conductivity in solids. *Journal of Physics D-Applied Physics*, 5(5), p.1038-1045.
- Castle, G.S.P. (1997). Contact charging between insulators. *Journal of Electrostatics*, 40&41, p.13-20.
- Coste, J. and Pechery, P. (1981). Influence of surface profile in polymer-metal contact charging. *Journal of Electrostatics*, 10(5), p.129-136.
- Diaz, A.F. and Felix-Navarro, R.M. (2004). A semi-quantitative tribo-electric series for polymeric materials: the influence of chemical structure and properties. *Journal of Electrostatics*. 62(4), p. 277-290.
- Greason, W.D. (2000). Investigation of a test methodology for triboelectrification. *Journal of Electrostatics*, 49(3-4), p.245-256.
- Homewood, K.P. and Rose-Innes, A.C. (1982). Investigation of contact-charge accumulation on insulators repeatedly touched by metals. *Journal of Physics D-Applied Physics*, 15(11), p.2283-2296.
- Jonassen, N. (1998). *Electrostatics*. New York: Chapman and Hall.
- Lowell, J. and Rose-Innes (1980). Contact electrification. *Advances in Physics*, 29(6), p.947-1023.
- Medley, J.A. (1954). The discharge of electrified textiles. *Journal of Textile Institute*, 45(2), p.123-141.
- Ohara, K. (1980). Relationship between frictional electrification and molecular motion of polymers. *Journal of Electrostatics*, 9(2), p.107-115.
- Ohara, K. (2001). Frictional Electrification between Flat Surfaces of Polymers and of Langmuir-Blodgett Layers. *Journal of Electronics*, 51, p.351-358.
- Perry, R.H. and Green, D.W (2007), Perry's Chemical Engineers' Handbook (8th Edition). New York: McGraw-Hill.
- Sawa, G, Calderwood, J. H. (1971) Dependence of surface conduction current in oxidized polyethylene on electric field at various humidities. *Journal of Physics C-Solid State Physics*, 4(15), p.2313.

Sereda, P.J. and Feldman, R.F. (1964). Electrostatic charging on fabrics at various humidities. *Journal of Textile Institute*, 55(5), p.288-298.

Seyam, A. M., Cai, Y., and Oxenham, W. (2009). Devices for measuring electrostatic generation and dissipation on the surfaces of polymeric materials. *Journal of Textile Institute*. 100(4), p. 338-349.

7 ELECTRIFICATION OF POLYMERIC SURFACES TREATED BY ANTISTATIC FINISHES

This chapter is modified from a manuscript entitled “Electrification of antistatic treated polymeric surface”, by L. Liu, T. Theyson, W. Oxenham, and A.M. Seyam, which has been submitted to *Journal of Textile Institute*.

7.1 INTRODUCTION

Static charge generation and control are still major issues in the full range of textile processes. While, there have been considerable discussion on innovative concepts relating to static charge control, the major commercial technology for controlling static charge during polymer processing remains the combination of topically applied antistatic agents (additives that accelerate the static dissipation process) together with humidity control and/or ionized air in the processing environment. Most antistatic agents are surfactants (composed of hydrophilic and hydrophobic sub-structures) that interact with the surface of the textile polymer and assist in absorbing/holding moisture to the surface, which further enhances the static dissipation process. By their own ionic character and water that is attracted to the surface, these materials can provide a low resistance pathway for the conduction of static charge to ground. To be effective on polymer surfaces, such agents must have a basic affinity for the surface, but not be so strongly attached that it interferes with the mobility of the molecule that provides the basis for improved surface conductivity (Holme, 1998).

When the performance objective is to control static charge during both the processing stage and in the final textile product, other, more “durable” or “permanent” methods of static control have been used or suggested. These include:

- Improving the conductivity of the fibrous assembly by incorporating a conductive fiber into the yarn (Holme, 1998)
- Increasing the conductivity of the base polymer through the addition of conductive additives such as carbon or carbon nanotubes (Lo, et al., 2007)
- Chemically modifying the surface through chemical grafting or high energy process (plasma, etc.) to increase the polarity and surface conductivity of the polymer (Kan and Yuen, 2008)

Several reviews are available that cover the use of these types of approaches to generate static control apparel for use in a variety of environments (Holme, 1998; Kowalski and Wroblewska, 2006)

The purpose of this work is to provide a better understanding of the charge generating process (contact charging and frictional charging) on traditional fiber forming

polymers (polypropylene and nylon) and the impact of applying traditional nonionic and ionic antistatic agents to these processes. While it is widely recognized that traditional antistatic finishes can assist in controlling static charge through providing accelerated dissipation once the charge is generated, there is little work on the effect of these materials on the actual static generation process. In this work, three types of static control finishes (nonionic, cationic, and anionic) are applied to polypropylene (PP) and nylon 6, 6 surfaces at four different solution concentration levels. Contact and frictional electrifications between the polymeric surfaces and stainless steel were conducted by automatically controlled contact and rubbing devices (section 5.2.1 and 6.2.1). The charge generated on the polymeric surfaces is monitored in order to determine the effectiveness of finish and the influence of increasing surface finish concentration on the processes. This work concludes by offering insights into the processes of static charge generation and control that could provide the basis for the development of new, more efficient methods for the controlling static charge in textiles, under both manufacturing and end-use conditions.

7.2 EXPERIMENTAL

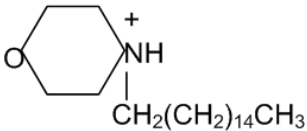
7.2.1 Sample preparation

Heavy films of polypropylene (PP) and nylon 6, 6 were shaped to required size for the contact or rubbing electrification tests (Chapter 5 and 6). The shaped surfaces were cleaned by ethanol, deionizer water, and deionizer gas to remove surface contaminants and residual static charge that might have accumulated from handling. The stainless steel contact/rubbing surfaces used in this study were also cleaned by ethanol, deionizer water and deionizer gas. Before each test, the initial charge on the investigated sample surface was measured and if this was not zero, the cleaning procedure was repeated until no charge was detected on the test sample.

Three model surface finishes, using typical fibre processing components, were prepared and used to treat the polymeric surfaces. The components and chemical

structures of the model surface finishes are given in Table 7.1. Each finish was mixed with deionizer water to make solutions of different concentrations (weight percentage of agent to solution). The solutions were sprayed on the polymeric surfaces (Figure 7-1) using an airbrush (air pressure of 206.8 kilopascal or 30 psi) following consistent procedures. The density of solution on the polymeric surface was approximately 7.2 g/m². After the treatment, the sample was moved into an environmental room for conditioning under temperature of 21°C and relative humidity of 43%. It is assumed that the bulk of the water applied to the surface evaporated in 24 hours conditioning and only the model finish and an equilibrated level of water was left on the polymeric surface. The level of active finish applied to the surface is proportional to the solution concentration used. Finish free polymeric surfaces (blank samples) were prepared following the same procedure, but using only deionizer water (solution concentration = 0). In this way, all samples in the experimental set experienced the same preparative procedure.

Table 7.1 Components of model surface finishes

Agent	Components	Structure
Base	20% POE(6) tridecyl alcohol, 40% 50HB260 (butyl initiated random EO/PO from Dow), 40% 50HB660(butyl initiated random EO/PO from Dow)	$\text{CH}_3(\text{CH}_2)_{12}(\text{OCH}_2\text{CH}_2)_6\text{OH}$ $\text{C}_4\text{H}_9(\text{CH}_2\text{CH}_2\text{O})_{17}(\text{CH}_2\text{CH}(\text{CH}_3)\text{O})_{13}\text{H}$
Nonionic Agent	10% water, 90% base	
Cationic Agent	10% water, 85% base, 5% cetyl morpholinium ethyl sulfate quaternary anti-static agent	

Anionic Agent	10% water, 85% base, 5%	$\text{CH}_3(\text{CH}_2)_4\text{CH}_2\text{CH}_2\text{O}(\text{CH}_2\text{CH}_2\text{O})_2\text{CH}_2\text{CH}_2\text{O}-\text{P}(=\text{O})(\text{OH})\text{O}^-$
	POE(2)2-ethyl hexyl phosphate (mix of mono and diester)	Or: $\text{CH}_3(\text{CH}_2)_4\text{CH}_2\text{CH}_2\text{O}(\text{CH}_2\text{CH}_2\text{O})_2\text{CH}_2\text{CH}_2\text{O}-\text{P}(=\text{O})(\text{O}^-)_2$

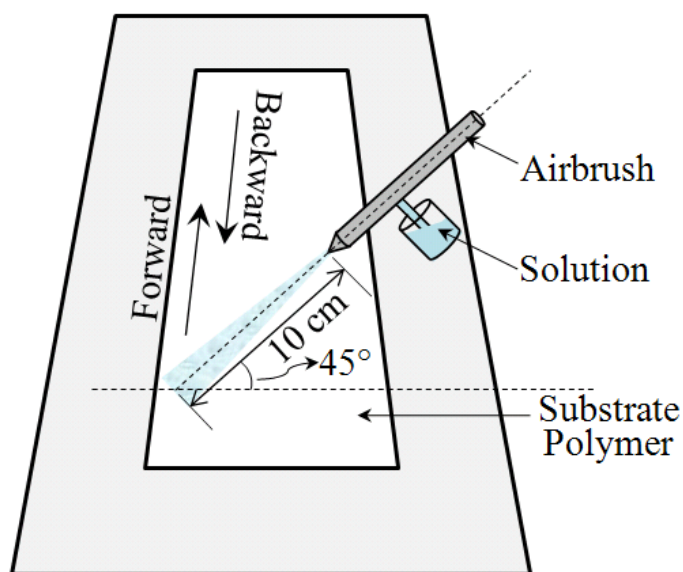


Figure 7.1 Schematic of surface treatment by an air brush

7.2.2 Experimental design

The effects of surface finishes on the electrification of polymeric surfaces were first evaluated by contact tests (experimental design I). Experimental trials were conducted on both PP and nylon surfaces. Since no charging was observed for nylon by contact, rubbing tests (experimental design II) were carried out, which is viewed as a more severe mode of electrification. In the contact tests, repeating contacts/separations were

conducted between a polymeric sample and a flat stainless steel surface. The charge generated on the polymeric surface was quantified at the end of each contact/separation using a Faraday tube. Table 7.2 shows the parameters and levels for the contact tests. The following contact test conditions were kept unchanged: 10 N contact force, 50 cycles/min contact frequency, 50 contacts, and 550 points/min data collection rate. The responses are charge generated on polymeric sample surface after the first contact and charge accumulated after 50 contacts.

In the rubbing tests, a sample was fixed on a grounded plane and was rubbed by a flat stainless steel surface automatically. The surface potential of the sample was continuously monitored by a potential probe. The parameters of rubbing tests are shown in Table 7.3. The following conditions were kept constant for the rubbing tests: nylon substrate polymer, 2 N contact force, 25 cycles/min rubbing frequency, 47 mm/sec rubbing speed, 400 mm/s² acceleration/deceleration, 52 mm rubbing stroke length (46.48 mm at constant speed + 2.76 mm acceleration + 2.76 mm deceleration), 50 cycles of rubbing, and 100 points/sec data collection rate. The responses are charge potential of polymeric sample surface after the first cycle of rubbing, after 50 cycles of rubbing, and charge decay for 1 minute after the 50th cycle of rubbing. All the experiments were conducted under temperature of 21°C and relative humidity of 43%.

Table 7.2 Experimental design I

Parameters	Levels
Substrate polymeric material	PP, nylon 6, 6
Finish Type	Nonionic, Anionic, Cationic
Solution Concentration ¹ (%)	0, 0.025, 0.05, 0.075, 0.1
Total Runs	2×3×5×3 replications=90

¹ the surface concentration of active finish applied on the polymeric surface was about 0, 1.8, 3.6, 5.4, and 7.2 mg/m², respectively.

Table 7.3 Experimental design I

Parameters	Levels
Finish Type	Nonionic, Anionic, Cationic
Solution Concentration ¹ (%)	0, 0.025, 0.05, 0.075, 0.1
Total Runs	3×5×3 replications=45

¹ the surface concentration of active finish applied on the polymeric surface was about 0, 1.8, 3.6, 5.4, and 7.2 mg/m², respectively.

7.3 RESULTS AND DISCUSSION

7.3.1 Plate/plate contact electrification

The effects of finish type and solution concentration on the charge generation are shown in Figures 7.2 and 7.3. It is shown that charge generated on PP treated by finishes is lower than that on PP blank (solution concentration = 0).

Figure 7.2 shows the charge generated on PP after the first contact against stainless steel. The effects of finish type and solution concentration on the charge generated after the first contact are not significant, which is characterized by its low value (absolute charge < 50 pC).

Figure 7.3 shows that, for PP treated by the cationic finish, charge are almost eliminated when solution concentration is 0.025% (solution composed of 0.025% active finish and 99.975% water). For PP treated by the nonionic and anionic finishes, the charge decreased as the solution concentration increased to 0.1% (solution composed of 0.1% active finish and 99.9% water) and the charge generated on PP treated by the anionic finish was lower than that from PP treated by the nonionic finish. It can be summarized that charge decreased as the solutions' concentration increased, and the cationic finish performed better than the anionic finish, and both of them worked better than the nonionic finish does.

Experiments on nylon were also conducted by repeating contacts/separations against stainless steel, however, little charge (< 15 pC in all cases including the blank) was observed on nylon.

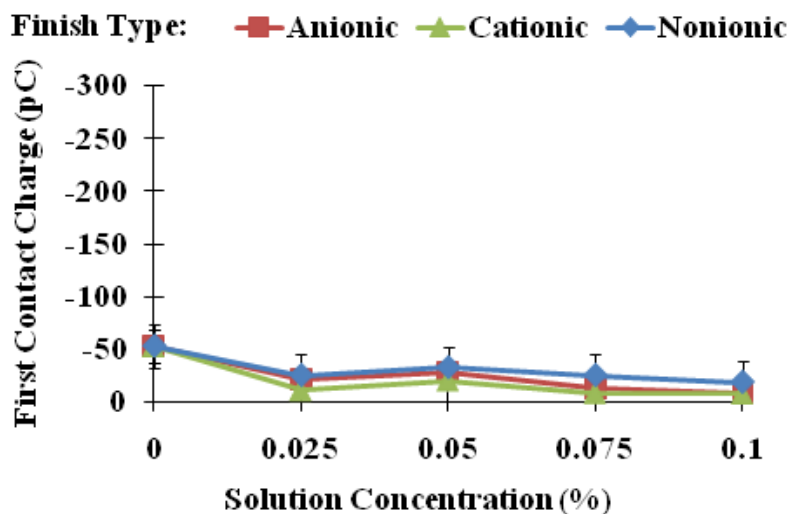


Figure 7.2 Charge generated on PP after the first contact against stainless steel

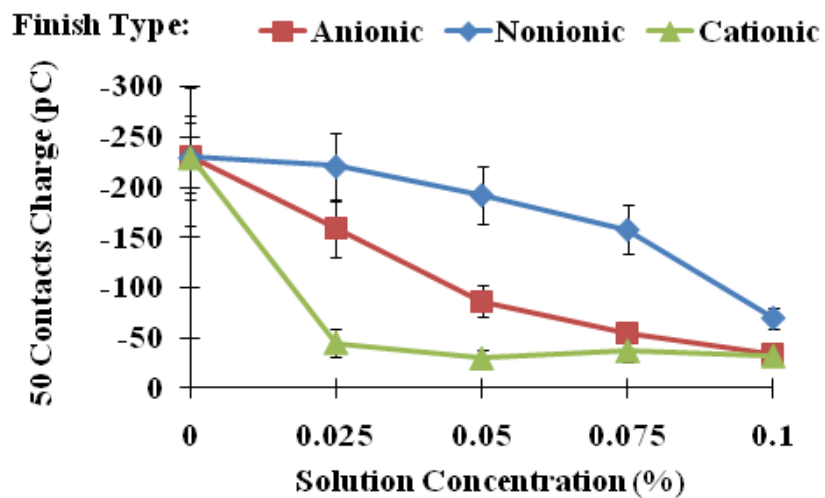


Figure 7.3 Charge generated on PP after 50 contacts/separations against stainless steel

7.3.2 Plate/plate rubbing electrification

The nylon surfaces were charged by rubbing against stainless steel flat surface. It was observed that the nylon surfaces were always positively charged and the charge potential on a nylon blank surface was about 430 V after 50 cycles of rubbing. However, after surface treatment by the nonionic finish, the nylon surface potential decreased significantly as shown in Figure 7.4. It is shown that, both of the charge generated after the first cycle of rubbing and the charge accumulated after 50 cycles of rubbing decreased as the solution concentration increased. No charge was observed when the solution concentration reached 0.1%.

Rubbing experiments were also conducted for nylon treated by the cationic and anionic finishes, where no charge was observed at any level of treatment application. Therefore, the cationic and anionic finishes controlled static generation better than the nonionic finish.

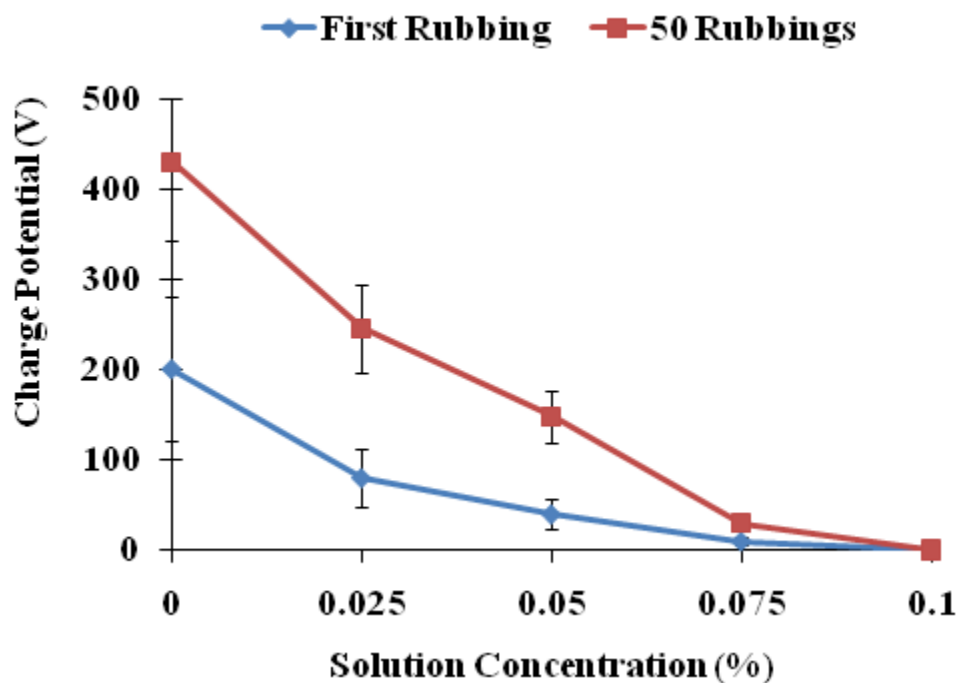


Figure 7.4 Surface charge potential of nylon after the first cycle and 50 cycles of rubbing against stainless steel

The charge dissipation on nylon treated by nonionic solution was also investigated after the 50 cycles of rubbing as shown in Figure 7.5. The charge on blank nylon decayed faster than that on the treated surface. The phenomenon of the rate of decay increase with increasing initial charge was observed and addressed by Ieda, et al. (1967). In each case, the charge decay seems to involve two components: an initial exponential decay and a second, nearly linear decay. The experimental data were regressed and found to fit equation [7-1], [7-2], and [7-3] with R^2 value of 0.9923, 0.9791, and 0.8739, respectively:

$$V_{Blank} = 161 \times e^{-0.2064t} + 230 \times e^{-0.01085t} \quad [7-1]$$

$$V_{0.025\%} = 82 \times e^{-0.1938t} + 157 \times e^{-0.009304t} \quad [7-2]$$

$$V_{0.05\%} = 36 \times e^{-0.2736t} + 104 \times e^{-0.0045t} \quad [7-3]$$

Each of the equation is the sum of two exponential components. The curves of the exponential components and their combined regression line are shown in Figure 7.6, 7.7, and 7.8, respectively. The figures show that one of the components represents the rate of initial decay and the other represents the level of residual charge.

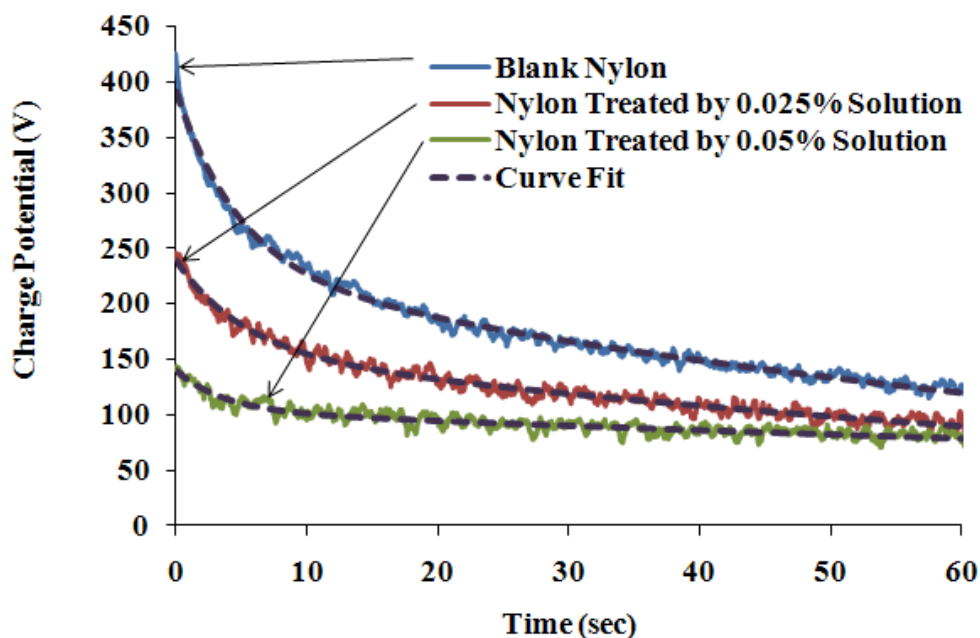


Figure 7.5 Experimental data of charge decay of blank nylon and nylon treated by nonionic finish after 50 cycles of rubbing against stainless steel and regression curves

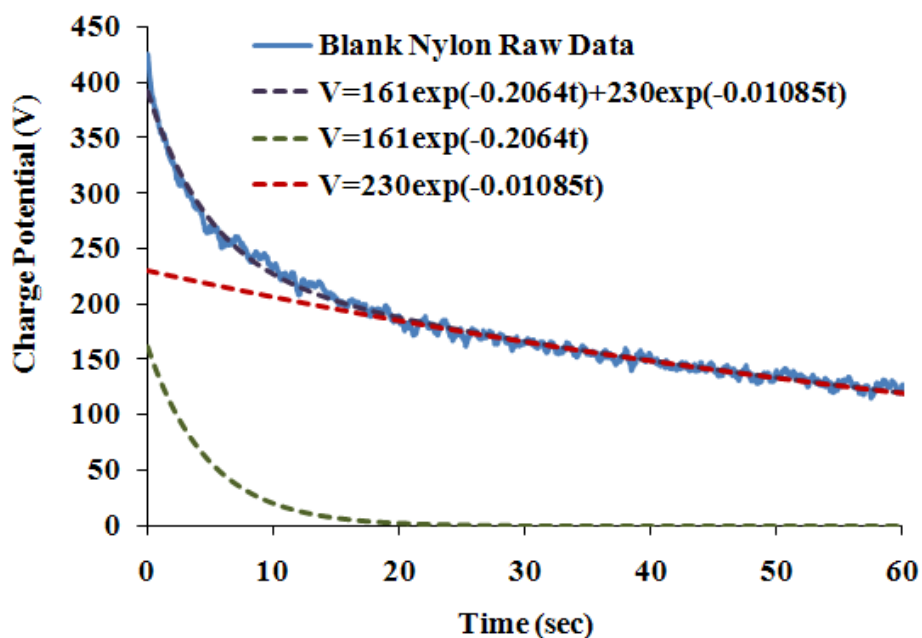


Figure 7.6 Experimental data of charge decay on blank nylon and the regression curves

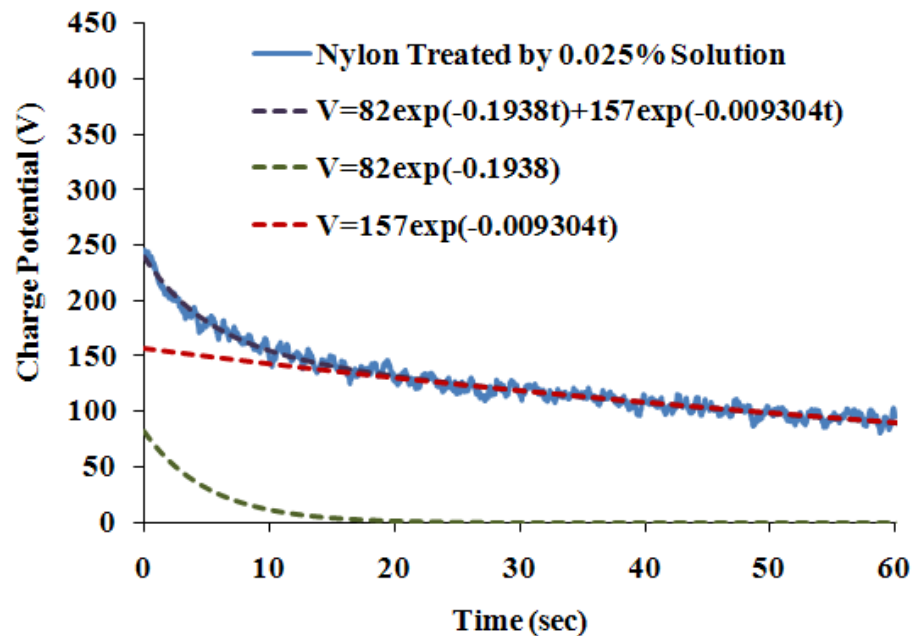


Figure 7.7 Experimental data of charge decay on nylon treated by 0.025% nonionic solution and the regression curves

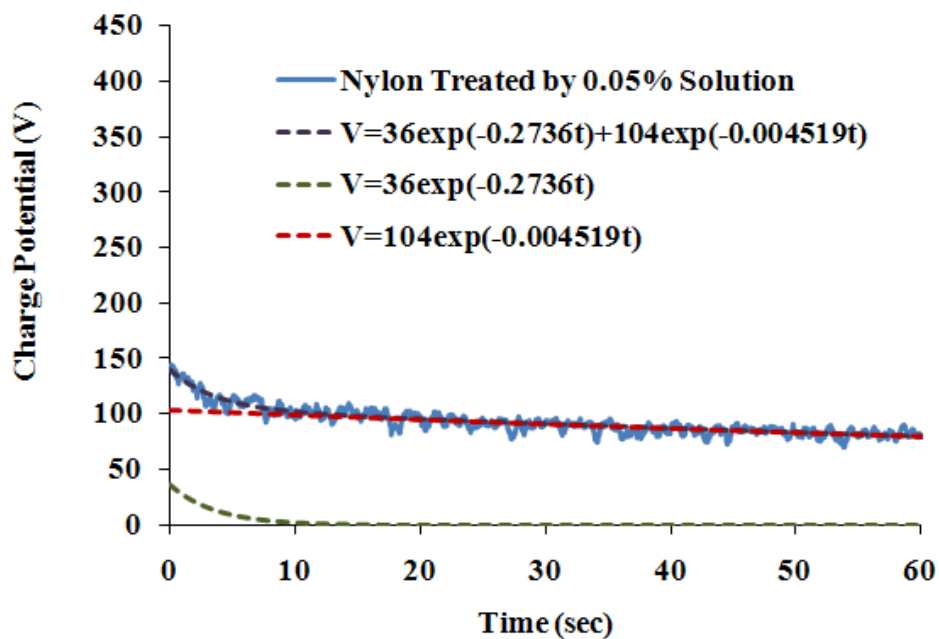


Figure 7.8 Experimental data of charge decay on nylon treated by 0.05% nonionic solution and the regression curves

Based on these curves, we have several interesting observations:

- For the “high rate decay” charge form, the size of the charge generated is highly dependent on the finish level.
- For the “low rate decay” charge form, the size of the charge goes down with the finish level, but the rate of dissipation also decreases with finish level.

The two types of decay observed here strongly suggest that there are two types of charge on the surface, each with a different decay mechanism. This possibility will be the subject of future research in this area.

7.3.3 Comparison with results of industrial yarn/pin rubbing electrification

Besides PP and nylon heavy films, nylon yarns were also treated by these three finishes. Experiments were conducted by the industry collaborator; Goulston Technologies, Inc. Charge was generated on a continuous nylon filament yarn when it was transported across a chrome pin. The nylon filament yarns were treated with 0.5% of weight percentage of active finish, which lead to about 7 mg/m² of the surface concentration. It was found that the yarn surface potential was reduced dramatically after the treatment. The charge generated on yarn treated by the anionic and cationic solutions were even lower than that treated by the nonionic solution. Figure 7.9 shows the mean values of yarn surface charge potential.

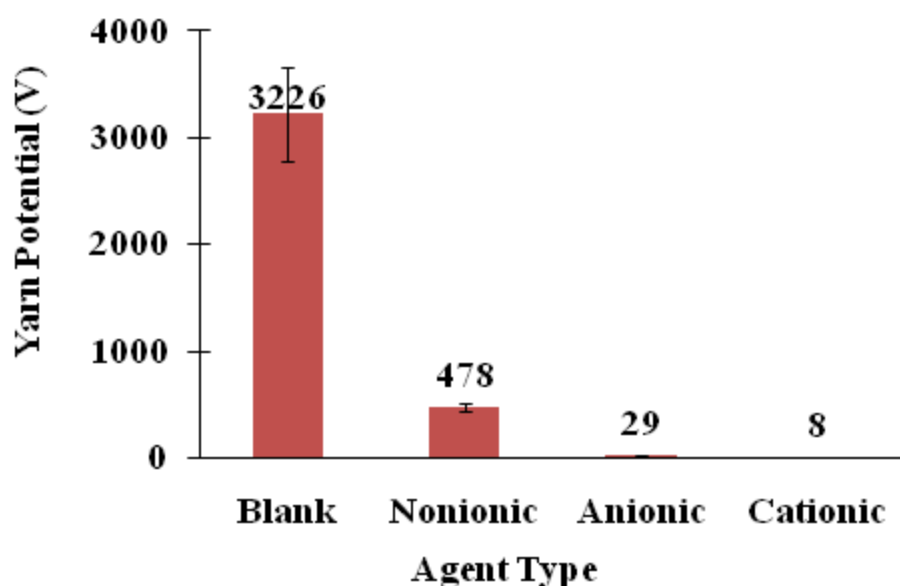


Figure 7.9 Surface charge potential of nylon yarns by moving over a chrome pin (surface concentration of active finish: 7 mg/m^2 , nylon yarns: 200 denier/60 filaments, yarn speed: 300 m/min, yarn input tension: 20 gf, charging pin size: 2 cm in diameter, contact angle: 90°) (Goulston Technologies, Inc.)

Although different devices were used for investigating the antistatic effect of those three agents and test conditions were significantly different (speed, surface area, etc.), the same overall tendency was observed. In both of the contact and frictional electrification, the nonionic treatment gave significant reduction in static generation and the ionic materials generated little or no charge.

The resistance of the finish free nylon yarn is measured as 10^{14} ohm. The resistance of nylon yarns coated by those three finishes at the concentration of 7 mg/m^2 was as follows:

- 10^{12} ohm for yarns treated by the nonionic solution
- $10^{9.5}$ ohm for yarns treated with the anionic solution
- 10^{12} ohm for yarns treated by the cationic solution

From this result, we can see that the anionic antistatic agent give a significant improvement in the conductivity of the nylon yarns. The cationic treatments give small

improvement in conductivity. This could be associated with the commercial use observation that cationic materials strongly absorb to the surface of nylon. This gives an ionic coating on the surface, but with little ionic mobility, and thus small decrease in resistance. However, all experiments results showed the cationic agent reduced charge generation as effectively, or even better than the anionic treatment (Figures 8 and 11). This suggests different antistatic mechanism for the cationic and the anionic solutions. For the surface coated with the anionic solution, the surface's resistivity was reduced and the improved charge conductivity may well have been a significant component of the static control mechanism. For the surface treatment based on the cationic agent, the surface's resistance is the same as the nonionic treatment. This suggests that the reduction in charge by the cationic treatment must be based on controlling the charge generation. The surface of the substrate nylon has been modified by absorption of the cationic material. This change modifies the charge generation process at the nylon surface, reducing the amount of charge generated by rubbing against the metal pin. Such effect needs to be investigated further to confirm the overall behaviour.

7.4 Conclusions

The PP and nylon flat surfaces were treated by three different finishes, nonionic, cationic, and anionic, at four levels of solution concentration (0.025%, 0.05%, 0.075%, and 0.1%). The electrostatic properties of the PP and nylon surfaces with/without treatment were investigated by contact tests and rubbing tests.

The contact tests revealed that charge accumulated on PP surfaces after contacts/separations against stainless steel decreased as the applied solution concentration increased. The antistatic effect of the cationic finish was better than that of the anionic finish, and both of them were better than that of the nonionic finish. No charge was observed on nylon surfaces.

The rubbing tests showed that charge accumulated on nylon surfaces after rubbing against stainless steel decreased as the applied nonionic solution concentration increased.

There was no charge generated on nylon surfaces at any applied concentration of cationic and anionic finishes.

Tribo-electrification was also investigated on nylon yarns moving across a chrome pin. The experiments indicated all the three agents reduce or eliminate static charge generation at an applied level of 7 mg/m², and the antistatic effect of the cationic agent was the best.

Several areas for future investigations were identified:

- In frictional charging of nylon, there appears to be two types of charge, one controlled by traditional lubricant system and the other, more stable with time, and not impacted by the presence of the lubricant treatment.
- Although the charge conductivity of nylon treated by the cationic agent was similar to that treated by the nonionic agent (resistivity was 10¹² ohm for both yarns), the cationic agent appears to be absorbed to the polymer surface and changes the propensity of nylon to generate charge. This is obviously an interesting behavior and warrants further investigation.

References

Holme, I., McIntyre, J.E., and Shen, Z.J. (1998). Electrostatic charging of textiles. *Textile Progress*, 28(1), p. 1-85.

Kan, C.W. and Yuen, C.W.M. (2008). Static properties and moisture content properties of polyester fabrics modified by plasma treatment and chemical finishing. *Nuclear Instruments and Methods in Physics Research B*. 266(1), p. 127-132.

Kowalski, J.M. and Wroblewska, M. (2006). Premises for practical valuation of the anti-electrostatic properties of protective garments. *Fibres and Textiles in Eastern Europe*, 14(5), p. 23-28.

Lo, L.Y., Li, Y., Yeung, K.W., and Yuen, C.W.M. (2007). Indicating the development stage of nanotechnology in the textile and clothing industry. *International Journal of Nanotechnology*, 4(6), p. 667-679.

Seyam, A.M., Cai, Y., and Oxenham, W. (2009). Devices for measuring electrostatic generation and dissipation on the surfaces of polymeric materials. *Journal of Textile Institute*. 100(4), p. 338-349.

Seyam, A.M., Liu, L., Hassan, Y.E., Abid, S.A., and Oxenham, W. (2008). Static generation and dissipation of textile fabrics and films. Proceedings of the Textile Institute 86th World Conference, Hong Kong.

8 OVERALL CONCLUSIONS

In this work, three testing systems, linear system, rubbing system, and contact system, were used to study contact and frictional electrification on polymeric surfaces. The advanced devices and precisely controlled experiments allow a comprehensive study of electrostatic behavior of polymeric surfaces. Four sets of studies were designed and carried out:

- Frictional electrification between yarn and pin (Chapter 4),
- Frictional electrification between parallel polymeric plates (Chapter 5),
- Contact electrification between polymeric plates (Chapter 6),
- Frictional and contact electrification on polymeric surfaces (plates and yarns) treated by antistatic finishes (Chapter 7).

The conclusions of each study have been given at the end of each Chapter. Here is a comparison and summary of results from the four studies:

In both contact and frictional electrification, it is found that charge increased as the number of contacts or rubbing cycles increased. The reasons for charge accumulation are discussed in section 5.3.2. After repeating cycles of rubbing, the magnitude of charge reaches the saturation after 40-50 cycles of rubbing for nylon. However, it reaches the saturation after only 2-3 cycles of rubbing for PP and PTFE. This could be explained by the difference of their charge dissipation properties. The saturation value is reached when the charge generation and dissipation get a balance. It was found that charge decays exponentially on nylon and the charge retained on nylon is about 60% or less after 30 seconds, but the charge does not decay on PP or PTFE during 30 seconds of observation. The reasons for why different polymers have different charge dissipation properties were given in section 5.4.1. One of the reasons is that charge can spread along the nylon surface, but cannot move on the other two surfaces.

The frictional electrification on both polymeric plates and yarns indicate that, the magnitude of charge generated on PP was less than that on nylon. On one hand, this could be due to the fact that polar groups exist in the chemical structure of nylon, which can provide electrons or ions to contribute to the charge transferring. On the other hand, this might be also related to the high crystallinity of PP. As a result of high crystallinity,

fewer chemical segments, which could provide electrons or ions, appear on the PP surface.

Both frictional and contact electrification show that, charge increased as the contact force increased. This could be explained by the increase of contact area between two contacted surfaces. In addition, more chemical segments could be broken under a high contact force, which would provide more electrons or ions to contribute to the charge transferring, therefore, promote charge generation.

The frictional charging is more complicated than the contact electrification because the former one is influenced by the rubbing speed. It is shown that more charge was generated due to rubbing than repeating contacts/separations. In regard to the effect of rubbing speed, it is clearly shown that charge increases as the relative rubbing speed increases from 400 mm/sec to 1600 mm/sec. However, the effect of rubbing speed was not obvious in slow rubbing motion (27 ~ 94 mm/sec).

The studies of charge generated on finish free polymeric surfaces provide the reference for whether a polymer requires antistatic finish treatment to reduce/eliminate the electrostatic problems during processing or consumer using. The experiments of contact and frictional electrification on nylon and PP treated by three types of finishes indicated that: ionic finishes perform better than nonionic finish; cationic finish works better than anionic finish and the charge was controlled based on different mechanism for cationic and anionic treated nylon.

In conclusion, this work provides a better understanding of the electrostatic behaviours of commonly used textile materials, nylon, PP, PET, and PTFE. The effect of different parameters on the charge generation and dissipation of these materials were investigated and analyzed. Based on these studies, suggestions were given to industry for eliminating static generated in textile processing, such as using rotating rollers instead of fixed guiders. Furthermore, to eliminate the charge, antistatic finishes were applied on top of the polymers. The effects of different finishes with suitable level of applied concentration of finish are suggested.

APPENDICES

A. Experiment procedure of linear test

Experiment Preparation:

1. Clean the friction pin with alcohol
2. Wind the yarn on CTT
3. Open the LJStream software for recording the voltage

Set the parameters as follows:

- a. Set the back panel parameters as:

Chanel	Voltage	Connector
A	$Y=v*1000$	A12
B	$Y=v*1000$	A10

- b. Set the data collection rate as:

Yarn Speed (meter/min)	Data Collection Rate (points/sec)
50	50
100	100
300	300

- c. Select a file to save the data

Zero-check Probe and Set Its Position:

4. Turn on the voltmeters
5. Remove the yarn to the back of the metal ground plate
6. Move the probe close to the metal ground plate (as close as possible but without touch)
7. Turn the “balance” button till it shows 0 on the voltmeter panel

8. Move the probe far from the metal ground plate (as far as possible on the probe holder)
9. Turn the “zero” button till it shows 0 on the voltmeter panel
10. Repeat procedure 5 to 9 till it always shows 0
11. Make sure the distance from the yarn to the metal ground plate is kept as 6 mm, and the distance from the end of the probe to the yarn is **3 mm**.

Test:

12. Hand in the speed of yarn on CTT panel
13. Check the required speed of friction pin
14. Start the CTT
15. Set the tension on the left side of the CTT
16. Turn on the motor at required speed level for the friction pin
17. Use the Tachometer to measure the real rotating speed of the friction pin
18. Adjust the speed of the friction pin till the reading of Tachometer is the required speed
19. Keep them running for about 5 second till it is stable.
20. Click the button on potential measurement panel on the computer to star recording the potential detected on two probes
21. Click “Stop” on the front panel of CTT after certain time (about 5 seconds at 300 m/min, 15 seconds at 100 m/min, and 30 seconds at 50 m/min)
22. Stop data recording
23. Repeat step 13 to 24 for next run
24. Turn off the gas supply outside the environmental room after finish all the tests

Apply Probe Adapter:

1. Measure the yarn potential without the adapter, record the data shown on the voltmeter panel
2. Take the probe off from the holder
3. Fix the adapter onto the end of the probe
4. Put the probe back onto the holder
5. Measure the same position of the yarn
6. If it does not show 1/10 of the value got before applying adapter, then take the probe off again, and modify the position of the adaptor until it can read the same value (if the value shows higher than that without adapter, then pull the adaptor a little bit tighter to the end of the probe, vice versa.)

Safety Information

1. Cover the back end of the probe surface by insulate tape
2. Do not touch the probe by hand when the voltmeter is on (you may get a shock!)
3. Do not put any conductor close to the end of the probe
4. Avoid the cable of the probes crossing or close to any EMF source

B. Experiment procedure of rubbing test

1. Set up distance from the end of the probe to the sample surface to be constant as 3 mm
2. Raise up the rubbing head
3. Discharge the rubbing sample until the initial surface potential is close to zero
4. Push the probe and rubber to the very beginning position
5. Hand in the parameters of movement on computer based on the information below:

Software motor configuration: 2000 steps/r

Stepper motor property: $7.5^\circ/\text{step} = 0.008 \text{ inch}/\text{step} = 0.2032 \text{ mm}/\text{step}$

Calculation between software parameter setup to motor real movement:

e.g. when speed is 7 r/min, that is $7/60 \text{ (r/s)} \times 2000 \text{ steps/r} \times 0.2032 \text{ mm}/\text{step} = 47.4 \text{ mm}$

e.g. when acceleration is 25 r/s^2 , that is $25 \text{ r/s}^2 \times 2000 \text{ steps/r} \times 0.2032 \text{ mm}/\text{step} = 10150 \text{ mm/s}^2$

Speed			Acceleration			Stroke Length		Ideal probe eye-to-rubbing head edge distance	
								25mm width head	10 width head
r/min	mm/s		rps ²	mm/s ²		steps	mm	mm	mm
3	20.3	vibrate	0.4	162	smooth	120	24.4	N/A	7.2
4	27.1	smooth	0.5	203	smooth	200	40.6	7.8	15.3
5	33.8	vibrate	0.6	244	smooth	250	50.8	12.9	20.4
6	40.6	smooth	0.8	325	smooth	270	54.8	14.9	22.4
7	47.4	smooth	1	406	smooth				
8	54.1	smooth	2	812	smooth				
9	60.9	smooth	4	1624	smooth				
10	67.7	smooth	5	2030	smooth				
11	74.4	smooth	10	4060	smooth				
12	81.2	smooth	20	8120	smooth				
13	88.0	smooth	25	10150	smooth				
14	94.7	smooth	50	20300	smooth				
15	101.5	vibrate	100	40600	smooth				

6. Put required load on top of the rubbing head
7. Release the rubbing head to contact the rubbing plate
8. Turn on the stepper motor.
9. Turn on the voltmeter.
10. Start the movement
11. Stop the movement when the probe is above center of the rubbing area, after finishing required number of rubbing cycles
12. Turn off the motor
13. Keep reading the surface potential of rubbing plate for 30 seconds
14. Stop reading
15. Turn off the voltmeter
16. Check the surface potential data

C. Experimental procedure of contact test

The contact test procedure consists of the sample initial charge checking, the sample and the electrometer setting, the contact movement controlling, and the contact force monitoring. The electrometer is controlled by the “ExceLINX”. The contact movement is programmed by the “LabVIEW”, and the contact force is recorded by the “LJstream”.

Sample Initial Charge Checking:

1. Put a clean contact head sample onto the end of the movable rod using clean metal tweezers
2. Clean the contact head using the neutralizing gas
3. Keep the contact head outside the Faraday tube
4. Turn on “Zero check” function of the electrometer and start it
5. Turn off the “Zero check” function of the electrometer and start it
6. Move the contact head into the Faraday tube by pushing the movable rod manually
7. Check the charge shown on the electrometer when the contact head is inside the Faraday tube
8. Stop the electrometer
9. Move the contact head outside the Faraday tube by pulling the movable rod manually
10. Repeat step 2 to 9 until no charge measured in step 7
11. Mount a clean contact plate onto the plate holder
12. Clean the contact plate using the neutralizing gas
13. Check the plate surface potential using a probe (Figure 4-14)
14. Repeat step 12 and 13 until the potential measured is zero

Electrometer and Sample Setting:

15. Check the configuration parameters in the “ExceLINX” software (example shown in Figure L-1). For the data collection rate, “Rate=0.5” means the data collection rate is about 1 point/sec and “Rate=10” means the data collection rate is about 0.5 point/sec.
16. “Zero check” the electrometer when the contact head (no charge measured) is outside the Faraday tube

17. Move the contact head into the Faraday tube by pushing the movable rod manually
18. Mount the contact plate holder steadily onto the supporting table
19. Make sure no cable entangle or touch each other

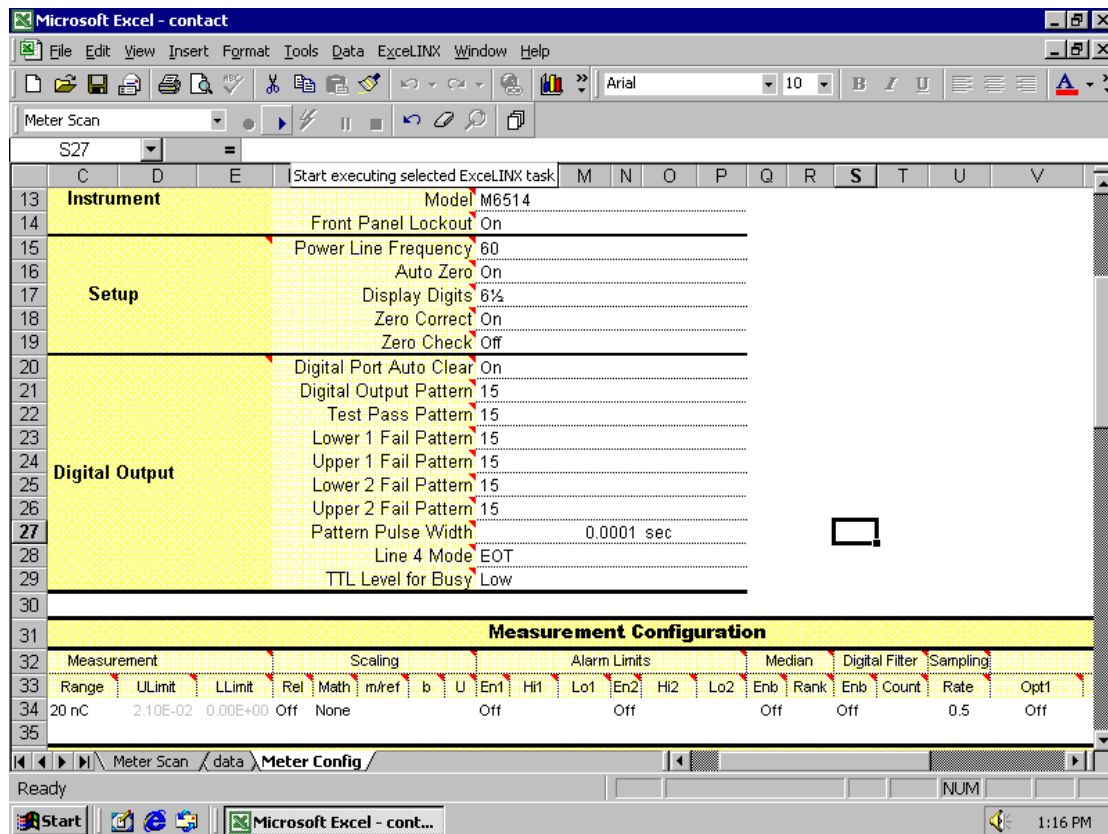


Figure 0-1 Meter configuration in ExceLINX

Motion Control Programming:

20. Initialize PCI-7344 card every time before use
21. The motion control panel on the "LabVIEW" is shown in Figure K-2. Check the parameters setting: axis: #4, velocity: from 5 to 15 rpm, set a target position, for example 5 steps (0.2 mm/step), and do not choose the "cycle mode"
22. Turn on the stepper motor
23. Start the motion
24. Turn off the stepper motor
25. Set the target position to be 0 and click the start button without turn on the motor, so

that the “present position” on the computer goes back to 0, but the truly position stays at 5, so that the stepper motor will not be bumped directly in the movement

26. Set the target position, for example 120 and choose the cycle mode

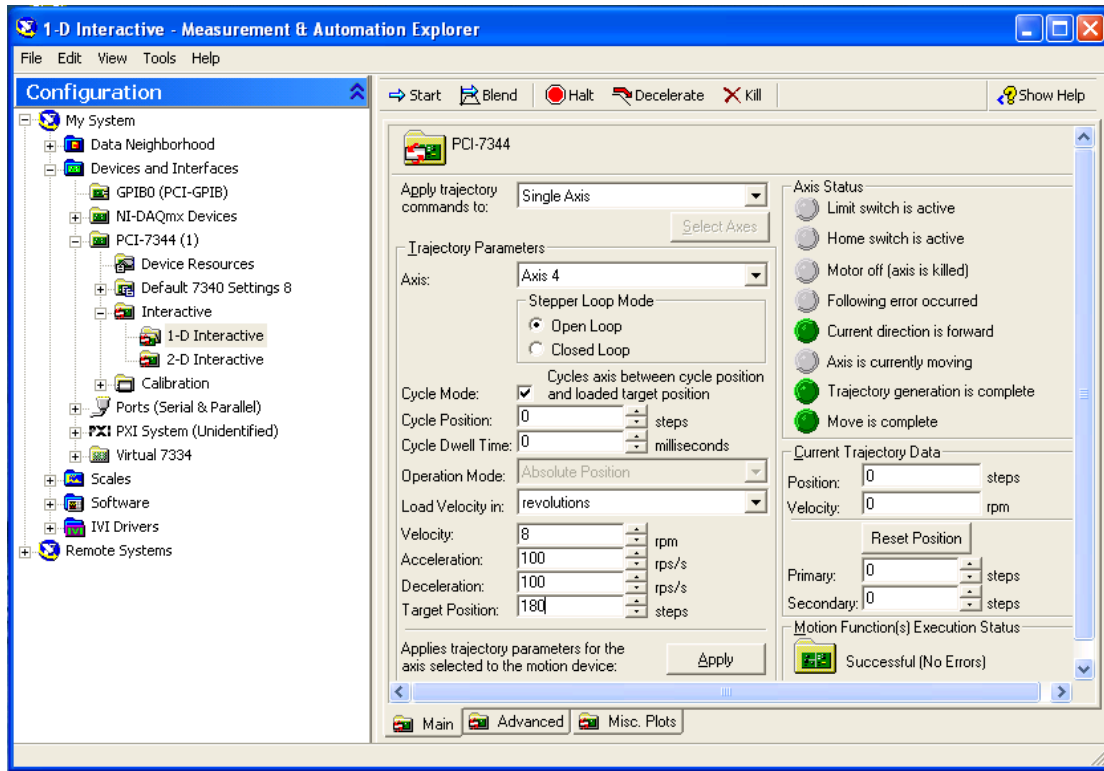


Figure 0-2 Parameters for controlling contact motion

Contact Force Monitoring

27. The interface of the “LJstream” is shown in Figure K-3. Check the parameters setting shown in Figure K-4 (channel B: AI6, channel C: AI7, channel D: AI(6-7), gain for channel D: 20(+/-1V))

28. Choose a file to save the data of contact force and click “write to file” before test

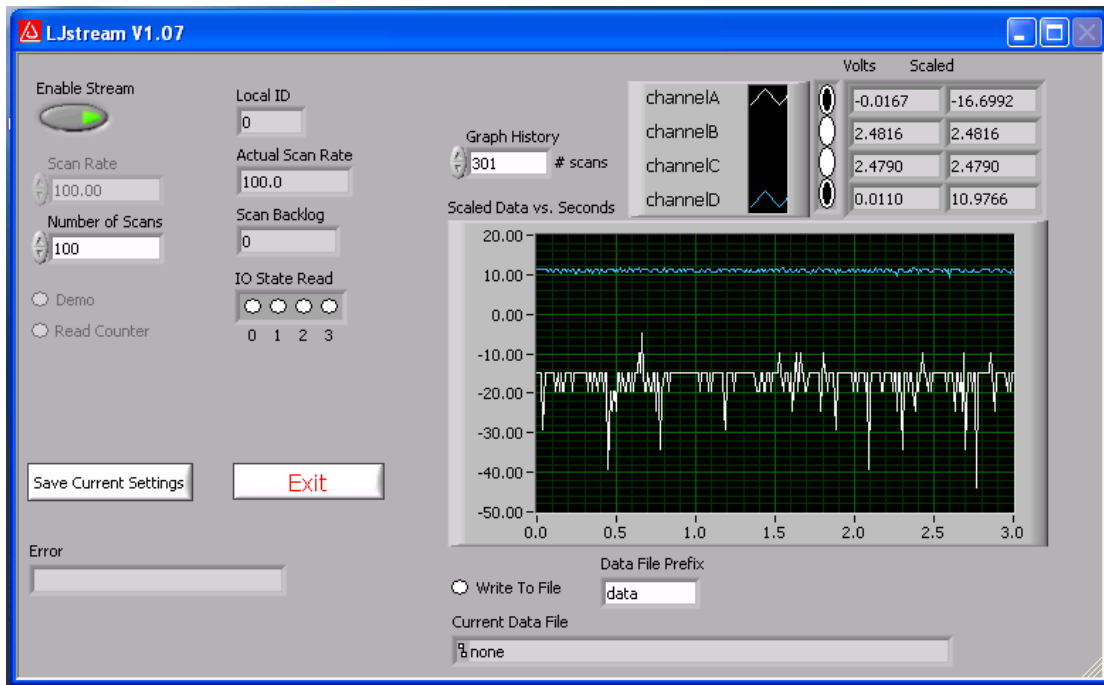


Figure 0-3 Working status of LJstream

The LJstream Channel Config dialog box is divided into two main sections: "Analog Input Configuration" and "Test Data".

Analog Input Configuration:

Channel Name	Scaling Equation	AI#	Gain
1st Channel Name: channelA	Scaling Equation: $y=1000*v;$	AI#: 0 SE (+/-10V)	Gain: 1 (+/-20V)
2nd Channel Name: channelB	Scaling Equation: $y=v;$	AI#: 6 SE (+/-10V)	Gain: 1 (+/-20V)
3rd Channel Name: channelC	Scaling Equation: $y=v;$	AI#: 7 SE (+/-10V)	Gain: 1 (+/-20V)
4th Channel Name: channelD	Scaling Equation: $y=1000*v;$	AI#: 6-7 Diff	Gain: 20 (+/-1V)

Test Data:

v	y
0.542	532.227
2.476	2.490
2.480	2.480
0.011	0.011

Manual Entry / Sampled Data: A radio button is currently selected for "Manual Entry".

Instructions:

- The input voltage is "v".
- The scaled output value is "y".
- Each equation must have a semicolon at the end.
- If your equation has an error, the output will be zero.
- You can select text and use Ctrl-c to copy and Ctrl-v to paste.

Buttons: "Save & Exit" and "Cancel".

Figure 0-4 Parameter for recording the contact force

Test:

29. Start the electrometer through the “ExceLINK”
30. Start the contact force monitoring through the “LJstream”
31. Turn on the stepper motor
32. Start the contact movement through the “LabVIEW”
33. After required number of cycles or until the electrometer reading reaches the 2500 reading buffer (“*” symbol disappears), stop the contact movement through the “LabVIEW”
34. Turn off the stepper motor
35. Stop the electrometer measurement through the “ExceLINK”
36. Stop the force recording through the “LJstream”
37. Wait about 3 minute for the data transferring from the electrometer to the computer through the “ ExceLINX”
38. Check the measured charge signal
39. Check the detected contact force signal
40. Move the contact plate holder away from the supporting table
41. Take the contact head off the rod

D. Raw data of Chapter 4: Frictional electrification of yarn and pin

Raw data of experimental design I:

Pin Diameter = 25.4 mm

Vy=50m/min

Run Sequence #	15	4	7	8	23	9	16	11	19
Relative Speed (Vy-Vp) m/min	-150	-100	-50	-25	0	25	50	100	150
Pin Surface Speed (Vp), m/min	200	150	100	75	50	25	0	-50	-100
Pin Rotational Speed, rev/min	2508	1881	1254	940	627	313	0	-627	-1254

Measurement Responses:

Potential-I Average, V	-358	-374	-267	-219	-24	-385	-516	-716	-728
Potential-I Average, V (absolute value)	358	374	267	219	24	385	516	716	728
STDEV, V	35	27	22	20	4	34	35	52	48
Potential-II Average, V	-453	-457	-322	-269	-46	-472	-625	-899	-967
STDEV, V	40	29	22	20	6	37	40	63	62
Tout, cN	11	13	19	25	51	97	116	127	133
STDEV, cN	5.4	5.1	5.3	4.1	4.0	11.8	8.7	28.0	25.0
Pin Rotational Frequency, Hz	41.8	31.4	20.9	15.7	10.5	5.2	0.0	10.5	20.9
Vibration Amplitude, dB	-65.7	-83.5	-83.8	-84.2	-85.8	-88.2	N/A	-85.8	-92.7
STDEV, dB	0.3	6.7	7.6	8.6	6.1	8.3	N/A	6.1	8.7

Calculated Responses:

Contact Force (Normal Force), cN	30.7	31.7	34.6	37.5	50.7	73.5	83.0	88.5	91.7
Friction Force (Tangential Force), cN	33.5	31.8	26.7	21.7	1.1	40.7	57.2	66.7	72.2
Coefficient of Friction	1.4	1.3	0.9	0.7	0.0	0.6	0.8	0.9	0.9
Vibration Force, cN	0.052	0.007	0.006	0.006	0.005	0.004	N/A	0.005	0.002

Raw data of experimental design I continued:

Pin Diameter = 25.4 mm

Vy=100m/min

Run Sequence #	26	1	18	27	25	14	20	24	12
Relative Speed (Vy-Vp) m/min	-150	-100	-50	-25	0	25	50	100	150
Pin Surface Speed (Vp), m/min	250	200	150	125	100	75	50	0	-50
Pin Rotational Speed, rev/min	3135	2508	1881	1567	1254	940	627	0	-627

Measurement Responses:

Potential-I Average, V	-270	-242	-234	-152	-46	-267	-332	-444	-513
Potential-I Average, V (absolute value)	270	242	234	152	46	267	332	444	513
STDEV, V	20	20	16	12	4	16	17	30	26
Potential-II Average, V	-352	-310	-291	-209	-76	-337	-424	-570	-667
STDEV, V	27	24	16	15	5	17	22	38	34
Tout, cN	6	9	18	23	50	91	105	110	128
STDEV, cN	2.8	2.9	3.3	2.8	2.4	5.5	8.0	8.6	14.5
Pin Rotational Frequency, Hz	52.2	41.8	31.4	26.1	20.9	15.7	10.5	0.0	10.5
Vibration Amplitude, dB	-58.6	-58.6	-82.5	-91.7	-92.7	-86.8	-91.8	N/A	-84.9
STDEV, dB	0.3	0.3	7.0	7.6	9.3	8.4	7.7	N/A	5.6

Calculated Responses:

Contact Force (Normal Force), cN	28.2	29.7	34.0	36.4	49.8	70.3	77.5	79.8	88.9
Friction Force (Tangential Force), cN	37.8	35.2	27.7	23.6	0.4	35.1	47.6	51.6	67.5
Coefficient of Friction	2.0	1.6	1.0	0.8	0.0	0.6	0.7	0.7	0.9
Vibration Force, cN	0.118	0.118	0.007	0.003	0.002	0.005	0.003	N/A	0.006

Raw data of experimental design I continued:

Pin Diameter = 25.4 mm

Vy=150m/min

Run Sequence #	22	3	5	17	13	10	2	21
Relative Speed (Vy-Vp) m/min	-150	-100	-50	-25	0	25	50	100
Pin Surface Speed (Vp), m/min	300	250	200	175	150	125	100	50
Pin Rotational Speed, rev/min	3761	3135	2508	2194	1881	1567	1254	627

Measurement Responses:

Potential-I Average, V	-265	-359	-285	-191	-76	-385	-581	-597
Potential-I Average, V (absolute value)	265	359	285	191	76	385	581	597
STDEV, V	17	18	17	11	6	34	27	23
Potential-II Average, V	-335	-443	-347	-239	-113	-472	-690	-644
STDEV, V	22	19	18	11	7	37	29	53
Tout, cN	6	13	20	26	50	97	103	120
STDEV, cN	2.1	2.0	2.2	1.9	2.0	11.8	5.5	11.7
Pin Rotational Frequency, Hz	62.7	52.2	41.8	36.6	31.4	26.1	20.9	10.5
Vibration Amplitude, dB	-59.5	-59.5	-64.4	-74.6	-85.3	-82.5	-85.1	-91.7
STDEV, dB	0.3	0.3	1.2	3.8	6.3	7.0	6.9	7.6

Calculated Responses:

Contact Force (Normal Force), cN	28.2	31.6	34.8	38.0	50.2	73.5	76.3	84.8
Friction Force (Tangential Force), cN	37.8	32.0	26.3	20.8	0.3	40.7	45.6	60.3
Coefficient of Friction	2.0	1.3	0.9	0.6	0.0	0.6	0.7	0.8
Vibration Force, cN	0.106	0.106	0.060	0.019	0.005	0.007	0.006	0.003

Raw data of experimental design I continued:

Pin Diameter = 6.35 mm

Vy=50m/min

Run Sequence #	12	13	1	2	3	4	5	17
Relative Speed (Vy-Vp) m/min	-100	-50	-25	0	25	50	100	150
Pin Surface Speed (Vp), m/min	150	100	75	50	25	0	-50	-100
Pin Rotational Speed, rev/min	7523	5015	3761	2508	1254	0	-2508	-5015

Measurement Responses:

Potential-I Average, V	-499	-284	-231	-42	-338	-540	-1120	-1212
STDEV, V	54	31	25	6	38	83	176	229
Potential-II Average, V	-542	-309	-270	-17	-379	-565	-1235	-1306
STDEV, V	51	32	28	8	46	95	212	247
Tout, cN	29.8	35.2	37.0	48.7	70.0	74.7	82.4	86.6
STDEV, V	2.2	2.0	1.8	3.9	3.9	5.2	9.0	11.0
Pin Rotational Frequency, Hz	125	84	63	42	21	0	42	84
Vibration Amplitude, dB	-60.2	-61.5	-70.6	-76.9	-81.8	N/A	-82.1	-61.3
STDEV, dB	3	0	3	7	8	N/A	5	0

Calculated Responses:

Contact Force (Normal Force), cN	39.9	42.6	43.5	49.4	60.0	62.3	66.2	68.3
Friction Force (Tangential Force), cN	17.5	12.8	11.3	1.1	17.4	21.4	28.1	31.7
Coefficient of Friction	0.49	0.34	0.29	0.02	0.32	0.38	0.48	0.52
Vibration Force, cN	0.098	0.084	0.029	0.014	0.008	N/A	0.008	0.086

Raw data of experimental design I continued:

Pin Diameter = 6.35 mm

Vy=100m/min

Run Sequence #	7	8	9	10	11	14	15	7
Relative Speed (Vy-Vp) m/min	-50	-25	0	25	50	100	150	-50
Pin Surface Speed (Vp), m/min	150	125	100	75	50	0	-50	150
Pin Rotational Speed, rev/min	7523	6269	5015	3761	2508	0	-2508	7523

Measurement Responses:

Potential-I Average, V	-449	-397	-78	-468	-780	-1286	-1438	-449
STDEV, V	35	31	8	35	81	140	160	35
Potential-II Average, V	-491	-438	-75	-471	-915	-1467	-1722	-491
STDEV, V	39	35	12	36	99	177	195	39
Tout, cN	36.7	39.1	49.7	69.7	79.6	80.0	84.0	36.7
STDEV, V	2.6	2.6	2.1	2.4	3.5	3.3	3.9	2.6
Pin Rotational Frequency, Hz	125	105	81	63	42	0	42	125
Vibration Amplitude, dB	-60.2	-64.4	-63.2	-73.8	-72.3	N/A	-82.1	-60.2
STDEV, dB	3	2	0	5	6	N/A	5	3

Calculated Responses:

Contact Force (Normal Force), cN	43.4	44.6	49.8	59.8	64.8	65.0	67.0	43.4
Friction Force (Tangential Force), cN	11.5	9.4	0.3	17.1	25.6	26.0	29.4	11.5
Coefficient of Friction	0.30	0.23	0.01	0.32	0.44	0.45	0.50	0.30
Vibration Force, cN	0.098	0.060	0.069	0.020	0.024	N/A	0.008	0.098

Raw data of experimental design I continued:

Pin Diameter = 6.35 mm

Vy=150m/min

Run Sequence #	19	17	20	18	21	16	19	17
Relative Speed (Vy-Vp) m/min	-25	0	25	50	100	150	-25	0
Pin Surface Speed (Vp), m/min	175	150	125	100	50	0	175	150
Pin Rotational Speed, rev/min	8777	7523	6269	5015	2508	0	8777	7523

Measurement Responses:

Potential-I Average, V	-576	-87	-600	-915	-1171	-1552	-576	-87
STDEV, V	32	7	33	88	111	147	32	7
Potential-II Average, V	-601	-73	-612	-1062	-1359	-1749	-601	-73
STDEV, V	34	9	40	95	138	185	34	9
Tout, cN	40.6	47.4	69.6	80.1	82.8	82.4	40.6	47.4
STDEV, V	1.6	1.8	2.1	2.7	3.0	2.8	1.6	1.8
Pin Rotational Frequency, Hz	146	125	105	84	42	0	146	125
Vibration Amplitude, dB	-57.2	-60.2	-56.6	-62.0	-75.3	N/A	-57.2	-60.2
STDEV, dB	2	3	0	0	5	N/A	2	3

Calculated Responses:

Contact Force (Normal Force), cN	45.3	48.7	59.8	65.1	66.4	66.2	45.3	48.7
Friction Force (Tangential Force), cN	8.1	2.3	17.0	26.1	28.4	28.0	8.1	2.3
Coefficient of Friction	0.20	0.05	0.32	0.45	0.48	0.48	0.20	0.05
Vibration Force, cN	0.138	0.098	0.148	0.080	0.017	N/A	0.138	0.098

Raw data of experimental design II:

Yarn Type: Nylon							
Random Run Sequence #	6	5	1	3	2	7	4
Relative Speed (Vy-Vp), m/min	-100	-50	-25	0	25	50	100
Pin Surface Speed (Vp), m/min	200	150	125	100	75	50	0
Pin Rotational Speed, rev/min	2508	1881	1567	1254	940	627	0
Measurement Responses:							
Potential-I Average, V	5978	4588	3680	2329	4937	5785	9489
STDEV, V	874	706	579	516	756	987	278
Potential-II Average, V	7672	5752	4487	2844	6135	7243	12234
STDEV, V	1226	888	685	625	917	1259	404
Tout, cN	14.7	15.4	15.3	22.4	31.4	32	32.6
STDEV, cN	1	1.1	1	2.2	1.5	1.7	1.4
Motor Rotational Frequency, Hz	41.8	31.3	26.1	20.9	15.7	10.4	0.0
Motor Vibration Amplitude, dB	-91.2	-91.1	-90.8	-93.6	-90.4	-90.6	N/A
STDEV, dB	4.3	4.0	3.2	7.8	1.7	2.3	N/A
Calculated Responses:							
Contact Force (Normal Force), cN	19.4	19.7	19.7	23.2	27.7	28.0	28.3
Frictional Force (Tangential Force), cN	8.1	7.4	7.5	1.4	6.4	6.9	7.4
Coefficient of Friction	0.468	0.424	0.430	0.066	0.257	0.275	0.293
Vibration Force, cN	0.00276	0.00279	0.00287	0.00208	0.00300	0.00293	

Raw data of experimental design II continued:

Yarn Type: PET							
Random Run Sequence #	8	14	11	9	10	13	12
Relative Speed (Vy-Vp), m/min	-100	-50	-25	0	25	50	100
Pin Surface Speed (Vp), m/min	200	150	125	100	75	50	0
Pin Rotational Speed, rev/min	2508	1881	1567	1254	940	627	0
Measurement Responses:							
Potential-I Average, V	-3557	-3474	-3448	-3285	-3637	-3745	-3732
STDEV, V	886	466	415	410	519	444	579
Potential-II Average, V	-4915	-3761	-4165	-3940	-4436	-4544	-4695
STDEV, V	976	590	523	536	626	550	730
Tout, cN	14.3	14.7	15.3	23.8	34.6	35.7	36.3
STDEV, cN	1.5	1.1	1.2	3.2	2.8	2.8	2.3
Motor Rotational Frequency, Hz	41.8	31.3	26.1	20.9	15.7	10.4	0.0
Motor Vibration Amplitude, dB	-91.1737	-91.1027	-91.92	-90.7423	-90.5165	-90.5412	N/A
STDEV, dB	4.3	4.0	5.5	2.7	1.9	2.2	N/A
Calculated Responses:							
Contact Force (Normal Force), cN	19.2	19.4	19.7	23.9	29.3	29.9	30.2
Frictional Force (Tangential Force), cN	8.4	8.1	7.5	0.2	9.2	10.1	10.7
Coefficient of Friction	0.495	0.468	0.430	0.008	0.349	0.379	0.395
Vibration Force, cN	0.00276	0.00279	0.00254	0.00290	0.00298	0.00297	N/A

Raw data of experimental design II continued:

Yarn Type: PP							
Random Run Sequence #	19	15	17	16	21	20	18
Relative Speed (Vy-Vp), m/min	-100	-50	-25	0	25	50	100
Pin Surface Speed (Vp), m/min	200	150	125	100	75	50	0
Pin Rotational Speed, rev/min	2508	1881	1567	1254	940	627	0
Measurement Responses:							
Potential-I Average, V	-817	-794	-716	-706	-829	-976	-1238
STDEV, V	359	438	337	356	353	336	327
Potential-II Average, V	-881	-848	-765	-759	-920	-1138	-1469
STDEV, V	465	510	389	412	412	398	381
Tout, cN	12.8	12.7	12.8	23.1	40.4	40.48196	40.8
STDEV, cN	0.9	0.9	0.8	3.6	2.2	1.984275	1.4
Motor Rotational Frequency, Hz	41.8	31.3	26.1	20.9	15.7	10.4	0.0
Motor Vibration Amplitude, dB	-91.1737	-92.4983	-90.9521	-91.62	-90.444	-90.4423	N/A
STDEV, dB	4.3	6.8	3.9	5.3	1.7	1.9	N/A
Calculated Responses:							
Contact Force (Normal Force), cN	18.4	18.4	18.4	23.6	32.2	32.2	32.4
Frictional Force (Tangential Force), cN	9.7	9.8	9.7	0.8	14.2	14.3	14.5
Coefficient of Friction	0.601	0.608	0.601	0.037	0.498	0.499	0.507
Vibration Force, cN	0.00276	0.00237	0.00283	0.00262	0.00300	0.00301	N/A

E. Raw data of Chapter 5: Frictional electrification of polymeric plates

Raw data of Experimental design I

Rubbing plate:	Nylon				PTFE				PP			
Contact force, N:	0.4	1	1.5	2	0.4	1	1.5	2	0.4	1	1.5	2
First cycle average, V	67	61	132	73	236	329	464	413	21	29	42	70
STDEV, V	49	74	94	34	27	73	40	105	3	5	8	15
50 cycle average, V	223	233	257	273	447	579	693	680	31	80	120	143
STDEV, V	92	89	79	30	6	32	15	37	8	6	8	28
Charge retained after 30 seconds, V	111	133	132	111	447	579	693	680	31	80	120	143
STDEV, V	51	54	54	20	6	32	15	37	8	6	8	28
Normalized charge retained, %	49	57	51	40	100	100	100	100	100	100	100	100
STDEV, %	5	3	11	3	0	0	0	0	0	0	0	0

Raw data of Experimental design II

Rubbing plate:	Nylon				PTFE				PP			
Speed, mm/s	0	27	47	95	0	27	47	95	0	27	47	95
First cycle average, V	0	80	61	85	0	394	329	371	0	32	29	37
STDEV, V	0	18	74	34	0	10	73	25	0	6	5	6
50 cycle average, V	73	239	233	257	60	578	579	581	61	83	80	86
STDEV, V	6	5	89	31	10	44	32	48	32	0	6	3
Charge retained after 30 seconds, V	47	116	133	130	60	578	579	581	61	83	80	86
STDEV, V	10	23	54	14	10	44	32	48	32	0	6	3
Normalized charge retained, %	64	48	57	51	100	100	100	100	100	100	100	100
STDEV, %	10	11	3	1	0	27	47	95	0	27	47	95

Raw data of Experimental design III

Average Potential, V					STDEV				
Head:					Head				
Plate:		Nylon	PTFE	PP	Plate:		Nylon	PTFE	PP
	SS	49	-300	-38		SS	39	69	22
1st cycle	Nylon	0	-50	-37	1st cycle	Nylon	0	18	10
	PP	10	-34.67	-10		PP	17	14	17
	PTFE	15	0	49		PTFE	5	0	40
Nylon					Nylon				
PTFE					PTFE				
PP					PP				
	SS	274	-548	-38		SS	81	85	28
50th	Nylon	10	-212	-104	50th	Nylon	0	110	16
cycle	PP	10	-69	-18	cycle	PP	0	25	31
	PTFE	58	0	80		PTFE	8	0	38

F. Raw data of Chapter 6: Contact electrification of polymeric plates

Raw data of Experimental design I

FirstCharge (pC)	Charge after 50 contacts (pC)	Charge after 100 contact (pC)	Charge after 120 contact (pC)	Temp. (°C)	R.H. (%)	Force (N)
-67.4	-99.25	-112.87	-115.91	21	43	17.1
-122.3	-173.82	-192.31	-196.8	21	55	17.1
-50.8	-79.01	-88.62	-91.46	21	65	17.1
-47.4	-74.73	-86.82	-91.21	25	43	17.1
-72.2	-90.89	-94.79	-96.22	25	55	17.1
-54.4	-80.77	-86.65	-87.79	25	65	17.1
-56.6	-81.7	-91.79	-94.47	30	43	17.1
-72.1	-183.9	-195.33	-197.84	30	55	17.1
-51.3	-102.9	-124.67	-125.58	30	65	17.1
-51.5	-97.98	-104.42	-105.03	21	43	14.5
-75.3	-97.39	-102.72	-104.12	21	55	14.5
-46.9	-63.04	-66.87	-68.38	21	65	14.5
-54.7	-78.12	-78.12	-88.32	25	43	14.5
-50.8	-77.14	-77.14	-86.2	25	55	14.5
-51.7	-82.67	-82.67	-89.71	25	65	14.5
-44.4	-73.72	-73.72	-85.36	30	43	14.5
-62.1	-96.85	-96.85	-109.37	30	55	14.5
-64.6	-93.02	-93.02	-98.6	30	65	14.5
-48	-81.52	-89.74	-92.7	21	43	11.2
-48.5	-75.89	-87.76	-90.11	21	55	11.2
-38.8	-57.74	-59.49	-59.38	21	65	11.2
-36.4	-60.02	-62.54	-63.72	25	43	11.2
-46.6	-67.07	-70.51	-70.32	25	55	11.2
-56.5	-75.06	-76.83	-77.1	25	65	11.2
-37.1	-59.07	-61.05	-61.56	30	43	11.2
-59.3	-90.23	-95.94	-97.53	30	55	11.2
-57.5	-89.42	-96.51	-98.18	30	65	11.2

Raw data of Experimental design II

50 contact charge, pC

Head	Plate	30°C, 43%	30°C, 55%	30°C, 65%	21°C, 43%	21°C, 55%	21°C, 65%
	Nylon	-73.7	-96.9	-93.0	-98.0	-97.4	-63.6
Teflon	PP	-3.1	-0.7	-15.5	-84.6	-2.9	-42.6
	Metal	-64.3	-41.2	-12.0	-61.3	-7.9	-55.1
	Teflon	10.6	0.0	5.4	15.9	15.3	0.0
Nylon	PP	12.2	0.0	7.9	0.5	0.0	0.0
	Metal	0.0	0.0	0.0	2.2	0.0	0.0
	Teflon	93.4	74.9	83.0	49.7	40.0	7.7
PP	Nylon	-148.6	-90.8	-93.8	-56.8	-77.9	-68.0
	Metal	-67.3	-33.2	-37.0	-46.4	-5.7	-2.6

First contact charge, pC

Head	Plate	30°C, 43%	30°C, 55%	30°C, 65%	21°C, 43%	21°C, 55%	21°C, 65%
	Nylon	-44.4	-62.1	-64.6	-51.5	-75.3	-46.9
Teflon	PP	-14.2	-23.4	-21.8	-6.5	-20.1	-38.2
	Metal	-24.4	-43.6	-6.3	-27.7	-7.9	-23.9
	Teflon	8.7	0.0	4.2	15.9	15.3	0.0
Nylon	PP	7.6	0.0	7.3	0.8	0.0	0.0
	Metal	0.0	0.0	0.0	1.1	0.0	0.0
	Teflon	28.7	23.8	17.8	17.8	17.5	1.9
PP	Nylon	-53.0	-80.4	-37.2	-26.4	-27.1	-29.2
	Metal	-7.9	-17.4	-16.7	-22.3	-5.1	-2.6

G. Raw data of Chapter 7: Electrification of polymeric surfaces treated by antistatic finishes

Raw data of Experimental Design I

Charge on PP contact head after contacting again stainless steel

	Concentration	Charge after the first contact	Charge after 40 cycles of contact
Agent A (nonionic)	0	-53	-230
	0.025	-25.2	-221.1
	0.05	-32.7	-192.6
	0.075	-25.2	-158.2
	0.1	-18.7	-70.26
Agent B (Anionic)	0	-53	-230
	0.025	-21.7	-158.4
	0.05	-28.3	-86.8
	0.075	-12.5	-54.6
	0.1	-7.7	-33.6
Agent C (Cationic)	0	-53	-230
	0.025	-11	-45
	0.05	-20.5	-29.47
	0.075	-8.5	-37.1
	0.1	-8	-32

Raw data of Experimental Design II

Surface potential of nylon plate with nonionic agent after rubbing against stainless steel

Solution Concentration	Potential after 50 cycles of rubbing (V)	Potential after first cycle of rubbing (V)
0	430	200
0.025	246	80
0.05	148	40
0.075	30	10
0.1	0	0
0.0125	0	0

Raw data of Linear Test in Goulston Technologies, Inc.

Sample	m/min	Friction Force (g)	Voltage, V	
Finish Free Blank	20	27±1	2805±294	2805
	50	47±4	3251±567	3251
	100	51±2	3385±382	3385
	200	52±2	3345±396	3345
	300	58±7	3226±442	3226
377-10A	20	50±5	-276±57	276
	50	123±13	-431±50	431
	100	158±17	-546±57	546
	200	174±20	-535±46	535
	300	172±18	-478±43	478
377-10B	20	87±7	-10±5	10
	50	125±25	-15±3	15
	100	168±17	-23±3	23
	200	181±17	33±5	33
	300	176±16	29±4	29
377-10C	20	104±15	-1±2	1
	50	169±22	-4±2	4
	100	193±25	22±4	22
	200	199±27	-36±6	36
	300	198±21	-8±2	8

Note: Finishes applied @0.5% to finish free 200-denier Nylon.
Pretension = 20 grams
Fiber to Metal: Three 3/4" chrome pins, 90° wrap angle, 5 RMS value